NCAR/CT–38

Physical Mechanisms Responsible for the Major Synoptic Systems in the Eastern Canadian Arctic in the Winter and Summer of 1973

Ellsworth Frank LeDrew

NCAR Cooperative Thesis No. 38
INSTAAR Occasional Paper No. 22
University of Colorado and
National Center for Atmospheric Research

1976

The National Center for Atmospheric Research (NCAR)
is operated by the nonprofit University Corporation
for Atmospheric Research (UCAR) under the sponsorship
of the National Science Foundation.

Physical Mechanisms Responsible for the Major Synoptic Systems in the Eastern Canadian Arctic in the Winter and Summer of 1973

Ellsworth Frank LeDrew

A thesis submitted to the Graduate School of the University of Colorado in partial fulfillment of the requirements for the degree of Doctor of Philosophy, Department of Geography, based on research conducted in cooperation with the scientific staff of the Climate Project, National Center for Atmospheric Research, Boulder, Colorado.

Mr. LeDrew received his B.A. degree from the University of Toronto in 1972 and his M.A. degree from the University of Colorado in 1974.

NCAR Cooperative Thesis No. 38
INSTAAR Occasional Paper No. 22
University of Colorado and
National Center for Atmospheric Research
1976

ABSTRACT

In this study the physical processes producing the major centers of synoptic activity in the eastern Canadian Arctic are examined. We choose the total vertical velocity at 85 centibars as an indicator of the intensity of the synoptic activity. A diagnostic three-dimensional atmospheric model from which the total vertical velocity from six physical processes may be computed is designed and validated. These processes are: the differential advection of vorticity, the thickness advection, the release of latent heat, the effects of the surface enthalpy flux, and the influence of friction and orography at the surface. By partitionment of this diagnostic model (the omega equation) into the component vertical velocities the magnitude and relative importance of each process may be determined.

The significance of each physical mechanism is examined at 48 hour intervals throughout the history of a mid-latitude depression system which enters the region as a developing cyclone on July 13, 1973 and leaves on July 22 as a stagnant vortex. The relationships between the large scale flow (the advected properties) and the local influences at various stages of

development and decay are of interest. Also discussed is the effect of this synoptic system on the local thermal regime. An important ice melt event occurred during this interval along the eastern Baffin Island coast.

For the winter and summer seasons of 1973 the major synoptic systems in the area are identified by pattern (eigenvector) classification of the 85 centibar total vertical velocity field. For each synoptic feature the average physical processes responsible for the vertical circulation are determined by empirical comparison of patterns in each component field with the pattern of the synoptic feature, and by comparison of magnitudes of the total and component vertical velocities at the center of the feature throughout time. The physical linkages proposed by considerations of these two independent tests are verified by subjective analysis of individual cases. Seasonal trends of these mechanistic linkages are also discussed.

ACKNOWLEDGMENTS

This research was supported by Grant Number GV 28218 to Dr. R. G. Barry from the Office of Polar Programs in the National Science Foundation. The generous support of the computing facilities of both the National Center for Atmospheric Research and the University of Colorado is gratefully acknowledged.

I am indebted to Dr. R. G. Barry of the Institute of Arctic and Alpine Research and Dr. T. Sasamori of the National Center for Atmospheric Research for their interest and instructive assistance during this study. The critical review of the manuscript by Dr. T. N. Caine is appreciated. Mrs. M. Eccles abstracted the National Meteorological Center data for the computational grid from the complex data tape files. Her assistance was invaluable. However, all computer programming beyond this is the author's responsibility.

A special note of appreciation goes to my wife, Veronika, for her understanding and patience throughout my graduate studies.

TABLE OF CONTENTS

TABLE OF CONTENTS (continued)

TABLE OF CONTENTS (continued)

LIST OF TABLES

LIST OF TABLES (continued)

LIST OF FIGURES

LIST OF FIGURES (continued)

CHAPTER ONE

INTRODUCTION

Statement of the Problem

In studies of synoptic systems interest is often focused on the changing nature and intensity of the physical mechanisms, changes which are responsible for the evolution of an atmospheric vortex. One common measure of the strength of synoptic activity at a given stage in this evolution is the vertical velocity within the system. The relative contribution by each physical process to the total vertical circulation may be determined with numerical techniques derived through considerations of atmospheric dynamics.

In this study the physical mechanisms responsible for major synoptic features in the eastern Canadian Arctic are examined for the winter and summer seasons of 1973. The data for analysis are mid-tropospheric vertical velocities calculated with a diagnostic atmospheric model. From these derived data the magnitudes and relative importance of each process are estimated. The seasonal variability of the mechanistic linkages involved in the circulation of the synoptic systems and the intensity of these systems is emphasized.

Background for the Study

There are six major physical processes involved in the vertical circulation: advection of vorticity and thickness, and local effects of latent heat release, surface temperature, orography and friction.

For a cyclonic system Bjerknes and Holmboe (1944) have related uplift and the concomitant surface pressure fall to upper level divergence along the east limb of a trough in the hemispheric flow. At this location there is positive advection of relative vorticity from the region of maximum cyclonic curvature at the base of the wave. The ascent may be enhanced or subdued by lower level positive or negative thickness (thermal) advection along a baroclinic zone (Petterssen, 1955).

The significance of these two advective terms may be altered by processes of local origin. During winter, when there is a large surface to air temperature difference over an unfrozen water surface, Petterssen and Calabrese (1959) noted that a strong positive enthalpy flux with low level convergence has a dominating influence on cyclonic activity in the Great Lakes region. This has been confirmed in numerical modelling efforts by Danard and Rao (1972) who calculated a 7 mb pressure fall with a $6C^{o}$ temperature excess of the Great Lakes. This has dramatic effects on the regional climate, largely in the form of increased precipitation (Lansing, 1965; Lavoie, 1972). Sutcliffe (1951) attributed the anchoring of a trough in the hemispheric circulation to the thermal effect of the open

Hudson Bay.

Also of importance in the vertical circulation is the buoyancy due to latent heat release in a precipitation belt. This can be shown to have a prolonging influence on a depression system (Rao, 1966). The diabatic heating offsets the inhibiting adiabatic cooling within the uplift sector.

Bryson and Kuhn (1961) stress the frictional influence on low level convergence in littoral regions which is related to the land-sea differential of frictional drag. In a numerical study Lavoie (1972) found frictional ascent to extend 50 km inland from the Lake Erie shore.

Forced orographic uplift and descent will interact with these processes on a local scale. In the large scale flow, however, it is considered the dominating influence on cyclogenesis in the lee of mountain barriers (Charney and Eliassen, 1949). The vertical stretching and generation of cyclonic vorticity downstream of the Rocky Mountains is the suggested origin of the 'Alberta' and 'Colorado' lows (Chang, 1972).

During the history of a synoptic system the change of the total vertical velocity is a function of the change in intensity of each process and the change in the relative imbalance of all six in combination. Often the stage of a system may be defined with respect to the dominance of one or more of these advective and local mechanisms (Krishnamurti, 1968b).

In the Arctic the identification of these mechanisms in synoptic processes has not yet received the same attention that it has for the more fully documented mid-latitude features. It is not for a lack of synoptic situations to study in a region where the day to day variability is of more significance than the mean map (Hare and Orvig, 1958). Rather it is related to the acknowledged lack of experience in dealing with an area for which adequate aerological data has become available only within the last two decades. Before 1952 surface pressure maps were drawn with the assumption of the existence of a polar anticyclone (Reed and Kunkel, 1960).

Many of the Arctic analyses are based on subjective examination using principles derived for mid-latitude situations or inference from statistical association in the available data. There are still many uncertainties. For example, Dzerdzevskii (1945) and Vowinckel and Orvig (1970) believe that strong thermal contrasts of ice covered land and sea favour summer baroclinic development but Reed and Kunkel (1960) suggest that this is over simplified and orographic influences must be considered. Hare (1968), however, notes that mid-tropospheric features are uniform and simple so that these complex thermal effects must be restricted to a shallow surface layer. Reed and Kunkel (1960) identified a frequency maximum of cyclonic activity in Baffin Bay while Petterssen (1950) found a similar feature in south Davis Strait. Reed and Kunkel attribute the difference to revised and more

reliable data but still acknowledge that general conclusions are impossible from their small sample in light of the great year to year variability of Arctic systems.

A clear physical understanding of the mechanistic linkages involved in Arctic synoptic processes is necessary. On the basis of synoptic experience, the Baffin Bay cyclone center may be interpreted at times as an orographic effect superimposed on the flow in a trough around Greenland or the result of topographic obstruction and in situ decay of the advective processes of mature mid-latitude systems deflected up Davis Strait by strong North Atlantic blocking (Hare and Orvig, 1958). There is a similar frequency maximum of low pressure over southwest Baffin Island which Reed and Kunkel (1960) believe is a meeting point for depression tracks from west Canada and Colorado. This was subjective interpretation based on the proximity of the mean positions of the respective fronts in this region, positions which have since been redefined using revised techniques (Bryson, 1966; Barry, 1967). The only studies using dynamical models have been related to the thermal effects on baroclinic disturbances by the temperature gradient over the North Atlantic (Mansfield, 1974) and the contribution of strong surface heating to vorticity generation during a few case examples of 'explosive' cyclogenesis in the Gulf of Alaska (Winston, 1955).

There are relatively few quantitative data on which to base a complete analysis of synoptic dynamics in the Arctic. The difficulty is that the pertinent data - the vertical velocity for example - are not observed directly but are calculated from theoretical models. The data that are available for the Canadian Arctic are based on empirical approximations to these models and hand analysis of charts for one season only (Fogarasi, 1972).

Organization of the Presentation

A theoretical model of atmospheric dynamics is used to generate vertical velocity data in the eastern Canadian Arctic. From these data the intensity and relative contribution to the total circulation is examined for each of the advected and local physical processes. The purpose is to determine the dynamical explanation for the major synoptic features in this region and any seasonal changes or biases in the mechanistic linkages.

The study is subdivided according to the following topics.

In Chapter Two a three-dimensional diagnostic model of the atmosphere is presented. Using the model the total vertical velocity due to each advective and local process may be calculated from grid point aerological data. The physical interpretations of the terms and limitations of the parameterizations are discussed.

In Chapter Three a verification of the model is presented.

A convenient performance indicator is the precipitation predicted by the model which is compared with reliable observations for sixteen cases of cyclonic disturbance in the mid-west United States.

In Chapter Four a detailed analysis of the history of a single synoptic system in the eastern Canadian Arctic is discussed. Magnitudes and contributions of each physical process are presented for case examples and probable dynamical relationships at various stages of the system are suggested. This detailed study provides a foundation for the interpretation of empirical analysis of the model generated data in the following chapter.

In Chapter Five the data for a 234 day sample including the winter and summer seasons of 1973 are examined empirically. Mean centers of significant synoptic activity are identified through the use of pattern recognition techniques. The important physical mechanisms for each center are determined and verified using two independent statistical tests. The results are compared subjectively with those of the detailed analysis in Chapter Four for selected cases.

In Chapter Six the results are summarized. Modifications and improvements to the technique and experimental design are suggested.

CHAPTER TWO

MODEL AND COMPUTATIONAL DESIGN

Introduction

To be a complete diagnostic tool for the study of advective and local effects on synoptic behavior a model must include realistic linkages between these three sources of influence identified in the introduction:

1) advection of vorticity and thickness (temperature)
2) diabatic heating or cooling
3) orographic deformation of the surface flow and frictional convergence or divergence.

The relative importance of each source must be determined by analysis of synoptic cases.

The advective processes have been studied extensively on the synoptic scale (disturbance wavelength of 10^3 km). Techniques for the calculation of the associated vertical velocities vary from empirical vorticity tendency expressions at one or two levels (Penner, 1963; Harley, 1964, 1965; Fogarasi, 1972), the complete time dependent vorticity equation (Winston, 1955), or the more tractable steady state 'omega' equation (Petterssen et al, 1962; Pedersen, 1963; Baumhefner, 1968; Krishnamurti, 1968a and b; Stuart, 1964, 1974). The advantage of the omega equation is that only space derivatives are calculated; the time derivatives of the vorticity tendency

models and attendant computational stability criteria need not be considered. In addition, the omega equation is a physical model devoid of parameterization when applied to item one (above) although in actual practice some assumptions are made on the basis of scale analysis. Whereas empirical vorticity models must have different coefficients at various levels, and are therefore usually restricted to only one or two atmospheric layers, the omega equation has complete physical integrity in three-dimensions and a perturbation at any location may be propagated throughout the system with complete fidelity.

A furthur advantage in the choice of a steady state model is that data restrictions may be relaxed. Filtering of the input fields through objective analysis to reduce instrument errors and remove high order oscillations, which is a requirement in prognostic models in order that spurious error growth is damped, is not necessary (Smith, 1973).

For the computation of mid-tropospheric vertical velocities on the synoptic scale the three-dimensional omega equation has been reasonably successful (Stuart, 1970). If influences of categories two and three (above) are to be included, however, some terms must be parameterized or incorporated in the computational scheme by appropriate boundary conditions. The degrees of freedom and computational complexities are increased and, consequently, there are fewer studies which include the complete dynamics of synoptic processes. One scheme to include all three factors of influence has been proposed by

Krishnamurti (1968a).

A difficulty inherent in the omega equation is the lack of verification statistics. There is not any observed field with which to compare the only output - the vertical velocity. Model reliability may be evaluated only by comparison with other independent models (Smith, 1971) or by subjective examination of indicators, such as the spatial relation between the sign of vertical motion and cloud and moisture distribution (Baumhefner, 1968). Therefore the omega equation is used primarily as a diagnostic rather than as a prognostic model. Comparative statistics and not absolute magnitudes are of primary interest.

In this section the diagnostic omega equation is presented with the necessary parameterization to permit a complete study of the physical relationships in an Arctic synoptic system. The computational design and data source is also discussed.

The Omega Equation

The derivation of the omega equation is based on a combination of the thermodynamic energy equation and the quasi-geostrophic vorticity equation manipulated such that all time derivatives of these two expressions are removed (cf. Holton, 1972).

The thermodynamic energy equation may be written as:

$$\frac{\partial}{\partial t}\{-\partial\Phi/\partial p\} = -V_g \cdot \nabla\{-\partial\Phi/\partial p\} + \sigma\omega + \frac{R\,H}{p\,C_p} \qquad (2.1)$$

A B C D

where the symbols are identified in Appendix one and the del operator (∇) is in the two horizontal dimensions only. V_g is the geostrophic velocity and ω(omega) is defined as:

$$\omega \simeq -\rho g w \qquad (2.2)$$

Thus a negative ω indicates a positive vertical velocity (w). The static stability parameter σ is defined as:

$$\sigma = \frac{RT}{p\theta}\frac{\partial\theta}{\partial p} \qquad (2.3)$$

with units of $m^2\ cb^{-2}\ s^{-2}$. We use the hydrostatic approximation so that:

$$\frac{RT}{p} = \alpha = \frac{\partial\Phi}{\partial p} \qquad (2.4)$$

For a hydrostatic atmosphere $\frac{\partial\Phi}{\partial p}$ is proportional to the temperature as $\partial p \to 0$. Term A of 2.1 is therefore proportional to the local rate of temperature change on an isobaric surface (Holton, 1972). The first term on the right hand side (B) is then proportional to the geostrophic temperature advection on an isobaric surface. The last two terms are, respectively, the adiabatic (C) and diabatic (D) heating terms contributing to the thickness change (A). Thus we have two of the three sources of interest, but in a time dependent form. Term A must be removed.

The quasi-geostrophic vorticity equation may be written as:

$$\frac{\partial \zeta}{\partial t} = -V_g \cdot \nabla\{\zeta + f\} + f_o \frac{\partial \omega}{\partial p} \qquad (2.5)$$

E F G

where the geostrophic vorticity is:

$$\zeta = \nabla^2 \Phi / f_o \qquad (2.6)$$

and f_o is the Coriolis parameter for the region. The beta-plane approximation is used so that the variation of f with latitude is constant.

The interpretation of the terms of the quasi-geostrophic vorticity equation are as follows (Holton, 1972):

E the local rate of change of relative vorticity

F the horizontal advection of absolute vorticity

G the divergence term

From case study analysis (Krishnamurti, 1968b) we know that the other terms of the vorticity equation (which include the vertical advection of vorticity and the twisting or tilting term) may be neglected without serious consequence. On the synoptic scale they have a tendency to cancel one another.

The vertical derivative of ω in G is defined by the continuity expression:

$$\nabla \cdot V = -\frac{\partial \omega}{\partial p} \qquad (2.7)$$

Note that the horizontal velocity in 2.7 is not approximated

by the geostrophic value as is done in term F of 2.5 hence the name quasi-geostrophic. If this approximation were made there would not be any divergence and corresponding vertical motion as it is the small departure from geostrophic flow which accounts for mass divergence or convergence (Holton, 1972).

The continuity expression (2.7) has been used to compute the vertical velocities directly through kinematic analysis (Lateef, 1967; Fankhauser, 1969, 1975; Kung, 1972; O'Brien, 1970; Smith, 1971). With suitable error correction routines (e.g. O'Brien, 1970) this method can yield reasonable results from the horizontal velocity field only. However, since the vertical velocity is only a function of small departures from geostrophic balance, small data errors can have significant effects on the result. For example, a 10 per cent accuracy of the divergence requires a one per cent accuracy of the wind observations (Thompson, 1969). The final error may be of greater magnitude than the divergence itself. The wind data in the Arctic are not of sufficient accuracy to permit a kinematic approach (Baumhefner, pers. comm. 1975).

To remove the time dependent terms we take the horizontal Laplacian of 2.1, equating $\chi = \partial\Phi/\partial t$;

$$\nabla^2 \partial\chi/\partial p = -\nabla^2\{V_g \cdot \nabla(\partial\Phi/\partial p)\} - \sigma\nabla^2\omega - \frac{R}{p\,C_p}\nabla^2 H \qquad (2.8)$$

Equation 2.5 is differentiated with respect to pressure:

$$\frac{\partial\{\nabla^2\chi\}}{\partial p} = -f_o \frac{\partial}{\partial p}\{V_g \cdot \nabla(\frac{1}{f_o}\nabla^2\Phi + f)\} + f_o^2 \frac{\partial^2\omega}{\partial p^2} \qquad (2.9)$$

Subtracting 2.8 from 2.9 to remove χ yields the final form of the steady state omega equation for isobaric co-ordinates:

$$\{\sigma\nabla^2 + f_o^2\frac{\partial^2}{\partial p^2}\}\omega = f_o\frac{\partial}{\partial p}\{V_g \cdot \nabla(\frac{1}{f_o}\nabla^2\Phi + f)\} - \nabla^2\{V_g \cdot \nabla\frac{\partial\Phi}{\partial p}\}$$

H I J

$$-\frac{R}{p\,C_p}\nabla^2 H_E - \frac{R}{p\,C_p}\nabla^2 H_{LP} \qquad (2.10)$$

K L

This expression is a Poisson equation and is solved for ω using relaxation techniques. The major input is the geopotential field (Φ) and 2.10 is often solved only using terms I and J. The diabatic terms require parameterization for heating due to surface thermal effects (H_E) and latent heat release (H_{LP}). The terms of 2.10 are additive for the solution of omega and K and L may be combined as a total diabatic effect.

Each term on the right hand side of 2.10 may be solved individually for omega (Krishnamurti, 1968b, Petterssen et al, 1962) to assess the relative contribution of each energy source. It is, therfore, useful to determine the physical meaning of each (cf. Holton, 1972, McPherson et al, 1969).

For illustrative purposes consider a short wave baroclinic system (Figure 1) in mid-latitudes. Term I ot 2.10 is the differential vorticity advection. For southerly flow in a wave, which at 50 cb is situated over a surface low, the relative

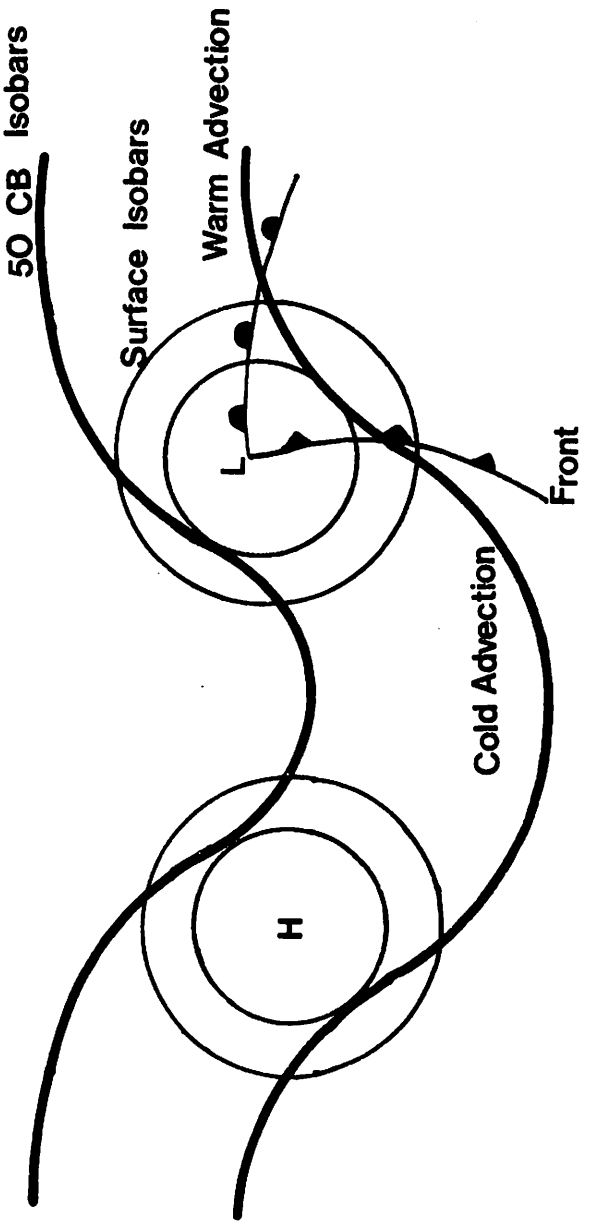

FIGURE I IDEALIZED BAROCLINIC WAVE (after Holton, 1972)

vorticity advection is positive (export of vorticity from the cyclonic curvature). At the surface low vorticity advection is small and differential vorticity advection is positive resulting in negative omega (a rising motion field) over the low. If a hydrostatic atmosphere is to be maintained within the cyclonic system as the air cools through adiabatic expansion of ascent the geopotential height must fall. This falling geopotential is consistent with increasing vorticity at upper levels (cf. equation 2.6). Once positive horizontal advection dominates within the low, the hydrostatic atmosphere cannot be maintained unless development (falling geopotential and positive vorticity advection) ceases. At the pre-occlusion stage vorticity advection is reduced and thickness advection dominates the vertical circulation (Krishnamurti, 1968b).

Term J is directly proportional to the thickness advection. Recalling that $\partial\Phi/\partial p$ may be referred to as temperature in a hydrostatic atmosphere, J would be positive for warm air advection in a baroclinic zone (increasing thickness advection). In the absence of vorticity advectional diabatic effects omega is negative (a rising circulation). Such is the case in Figure 1 ahead of the surface warm front under the 50 cb wave. Here, increasing thickness advection builds the ridge by increasing the geopotential height. To maintain geostrophic balance the anticyclonic vorticity must increase. This is accomplished by increased upper level divergence with resultant mid-tropospheric ascent. Note that this increases the differential vorticity

advection over the low which has the effect of increasing the low level cyclonic circulation and furthur deforming the isotherms under the ridge. With the isobaric configuration of Figure 1 and this positive reinforcement of thickness and vorticity advection, the system is at the self-development stage. The only inhibition is adiabatic cooling within areas of ascent and possibly diabatic effects as the system moves over colder surfaces.

The diabatic terms (K and L) represent the heating/cooling due to convergence/divergence of the surface enthalpy flux and the buoyancy effect of latent heat release during precipitation. Note that it is the Laplacian of these terms - the topography of the horizontal field - that is important, not the absolute magnitudes. From case studies (Chapter Four) it is shown that there may be ascent with cooling due to divergence of the surface enthalpy flux because the cooling at neighbouring grid points is more intense.

Since the Laplacian of the heating function is used, radiative heating under clear skies for the computational area can be neglected. Spatial differences would occur in a cloudy atmosphere. To estimate the significance of the change of longwave cooling under a cloud compared to neighbouring clear grid points a sensitivity analysis is performed. Soundings for Clyde on Baffin Island for 1968 were selected and the 85 cb cooling by longwave divergence was calculated using the routine of Sasamori (1968) for clear days (cooling of -3×10^{-5} kj kg^{-1}

s^{-1}) and days with complete overcast above 85 cb (-1×10^{-5} kj kg^{-1} s^{-1}). Omega was calculated for a grid with this cooling rate at one grid point (representing a cloudy atmosphere) and the former rate at the surrounding points (representing clear skies). The motion at the central point due to the lower cooling under a cloud cover is estimated to be -2×10^{-8} cb s^{-1}. A representative total vertical velocity for this region during July (Chapter Four) is -5×10^{-5} cb s^{-1}. By comparison, the vertical motion due to a latent heat release of 7×10^{-5} kj kg^{-1} s^{-1} at the same point with no release at the surrounding points (a figure characteristic of stable upglide precipitation, from Krishnamurti, 1968a) is -8×10^{-8} cb s^{-1}. The difference is not negligible and radiative effects would provide additional uplift in precipitation areas. Following Krishnamurti (1968a), however, the radiative effects are ignored since the required computations are complex and time consuming when applied to a large matrix of data.

The Frictional, Topographic and Diabatic Parameterizations

In the three-dimensional omega equation presented above, frictional drag and orographic uplift are not considered explicitly. Friction could be considered as an internal term, but it would be necessary to compute horizontal derivatives near 90 cb which is a layer not included in the NMC data set used for this study. These two effects are parameterized in terms of the vertical velocity at the top of the Ekman layer (assumed to be

the 100 cb observation) and incorporated into the computations as the surface boundary criteria.

For the Ekman layer frictional pumping the formulation of Charney and Eliassen (1949) is used:

$$\omega_e = \frac{-p_e F \zeta}{2f_o} \tag{2.11}$$

where the subscript e refers to the assumed height of the Ekman layer. F may be called a 'friction' coefficient. Derome and Winn-Nielsen (1971) have found a value of $F = 4 \times 10^{-6}\ s^{-1}$ for oceans and $F = 8 \times 10^{-6}\ s^{-1}$ for continents to yield reasonable results. These values are adopted in this study.

The topographic forcing is expressed as (Knighting, 1969; Derome and Wiin-Nielsen, 1971):

$$\omega_e = V_e \cdot \nabla p_e \tag{2.12}$$

which is added to 2.11 to give the total vertical motion field at the surface due to mechanical deformation. The topography at each grid point is converted to pressure equivalent heights through the hydrostatic approximation. The result is a smoothed topography where gradients are the average of those between points. The intense uplift due to local steep topographic slopes will not be represented in these calculations which are of synoptic scale.

A great deal of parameterization is required for the diabatic effects and the selection of models and coefficients may be open to criticism. For the surface diabatic heating the instantaneous enthalpy flux (F_E) is computed from a bulk

transfer formulation:

$$F_E = C_h V_g C_p \rho (T_e - T_s) \qquad (2.13)$$

where V_g is the geostrophic velocity at the top of the Ekman layer, T_e is the temperature at that point and T_s is the surface temperature. C_h is the bulk transfer coefficient applicable at the top of the Ekman layer. C_p is the specific heat of air.

The bulk transfer relation is open to many objections, largely because such a wide range of coefficients have appeared in the literature for seemingly similar conditions (Robinson, 1966; Roll, 1965; Hicks, 1972). Hicks (1972) has observed small but significant variations in the value of the coefficient with fetch, wind speed and stability. For meso-scale experiments, however, the bulk transfer formulations are used extensively (e.g. Anthes et al, 1971).

In this study two broad classes are defined for the selection of the coefficient value: stable, neutral and unstable (defined as $T_e > T_s$, $T_e \simeq T_s$, and $T_e < T_s$ respectively), and land or sea surface. Csanady (1972) has suggested, from theoretical arguments and observational evidence, a value of C_h at the top of the Ekman layer approximately in the range of 2×10^{-3} at neutrality, 3×10^{-3} for an unstable regime and 1×10^{-3} for a stable regime over land. For the north Alaskan coast region Walters (1975) found that the 10 m value over water is approximately one half of that over land. In the absence of more precise measurements for the arctic at present these values and ratios are used in this study.

This instantaneous flux is assumed to approach zero at 85 cb, the first observational level next to the surface. Therefore, the total heating or cooling is restricted to this first layer. This assumption is reasonable for the commonly stable stratification in the Arctic with a surface inversion; the deepest extends to one km (Vowinckel and Orvig, 1970). For the unstable situation we assume the enthalpy flux to be of such small intensity that it does not penetrate the 85 cb level. This seems to be an acceptable approximation in the Arctic since deep low level cumulus convection is almost entirely absent and of cyclonic origin when observed (Vowinckel and Orvig, 1970). Complex funcitons relating the intensity of surface diabatic heating to the vertical rate of decrease have been presented for similar studies (Asani and Mishra, 1975) but evaluation of the coefficients has been restricted to tropical and subtropical convective situations. There is no comparable observational evidence for the Arctic. However, for intense small scale subtropical synoptic systems with wavelengths of less than 10^3 km, these authors have found the heating function to vanish at 85 cb.

The instantaneous surface flux (positive or negative) is assumed to be completely dissipated within this first layer:

$$H_E = g \frac{\partial F_E}{\partial p}$$

$$= g \frac{(F_E - 0)}{(100 - 85)} \qquad (2.14)$$

The heating function (H_E) to be used in term K of 2.10 is applied at the 85 cb level to compute the contribution to the vertical motion by the surface thermal effects. It should be applied at a level intermediate to 100 and 85 cb since it is an average for that level, but there are no NMC data to complete the balance of 2.10 and the approximation at 85 cb is necessary. Krishnamurti (1968a) also applied this heating function at the level where the surface flux is assumed to vanish.

The diabatic heating due to latent heat release is calcualted at each level following Kuo (1965). One scheme is employed for widespread stable upglide and another for situations of conditional instability. The conditional instability for a layer is defined as:

$$\frac{\partial \theta_e}{\partial z} < 0 \qquad (2.15)$$

where θ_e is the equivalent potential temperature:

$$\theta_e \simeq \theta \exp(Lq_s/C_pT) \qquad (2.16)$$

If there is vertical motion when the atmospheric layer is stable and relative humidity is in excess of 70 per cent (Krishnamurti and Moxim, 1971, adopted 80 per cent but this value is revised in Chapter Three), the latent heat release is calculated from:

$$H_{LP} = -L \frac{\partial q_s}{\partial p} \qquad (2.17)$$

where q_s is the saturation specific humidity and L is the latent heat of condensation ($L = 2.5 \times 10^6\ m^2\ s^{-2}$). This relationship was proposed for all forms of large scale ascent in nearly saturated air. Kuo assumes that all products of

precipitation fall out of an air parcel and are not stored. For this case the heating rate is:

$$-L(dq_s/dt) = -L(\partial q_s/\partial t + V \cdot \nabla q_s + \omega \partial q_s/\partial p) \quad (2.18)$$

If this change occurs only during ascent we may neglect the horizontal components and if we assume steady state at a grid point $\partial q_s/\partial t$ vanishes. We than have equation 2.17.

Conditional instability may be present over frontal shear zones and this expression (2.17) would underestimate the local convective precipitation (Krishnamurti and Moxim, 1971). The second scheme of Kuo, originally applied to tropical storms, is included for completeness.

If the atmosphere is conditionally unstable, moisture convergence (negative divergence, D) is tested:

$$D = \nabla \cdot (V_g \, q) \quad (2.19)$$

If there is convergence, precipitation is possible with ascent and the latent heat release is calculated from:

$$H_{LP} = \frac{a \, C_p \, (T_s - T)}{\Delta t} \quad (2.20)$$

where T_s is the temperature of the cloud at saturation and Δt is the estimated time of convective formation and decay so that the heat generated is completely mixed with the surroundings. We assume this interval to be 3600 seconds (Kuo, 1965). a is the cloud cover which may be computed directly, although a constant of six tenths is assumed for frontal systems in this study to simplify the computations.

The term $a\,C_p\,(T_s - T)$ has been derived by considering the total mixing of a single cumulus tower with the environment after time Δt (Kuo, 1965). If the fractional cover of cumulus is a, the environmental air temperature is T and the temperature of the cloud at saturation is T_s, then the mean air temperature after mixing of the energy is T^*:

$$T^* = (1 - a)T + aT_s \tag{2.21}$$

$$= T + a(T_s - T) \tag{2.22}$$

The increase in temperature due to mixing of the release latent heat is $a(T_s - T)$ and the heating is $a\,C_p(T_s - T)$.

It should be noted that, at present, there are conceptual difficulties with the formulation of extratropical convective development (Tracton, 1975). The intensity of development is generally underforecast in official prognoses (Leary, 1971). The assumptions used in the procedure outlined above may not be entirely valid and the calculations are only expedient approximations to reality. The omega model and the parameterizations are tested in Chapter Three.

Additional Computations

To examine the contribution to synoptic behavior by each source of influence it is necessary to compute indicators that may be associated exclusively with each source. Two indicators that may be so partitioned are the heating rates and vertical velocities. Since the advective terms do not apply at the surface and the surface heating effects vanish above 85 cb,

we must restrict our analysis to that level.

The heating due to latent heat release and the surface thermal effects has been discussed. The other heat sources (neglecting radiation) are advective, both vertical (adiabatic expansion or compression) and horizontal.

The local temperature change following a parcel is:

$$\frac{dT}{dt} = \frac{\partial T}{\partial t} + V\cdot\nabla T + w\frac{\partial T}{\partial z} \qquad (2.23)$$

From the first law of thermodynamics:

$$H = C_p \frac{dT}{dt} - \alpha\frac{dp}{dt} \qquad (2.24)$$

where H is the non-adiabatic heating of the moving air parcel. Combining we find:

$$H = C_p \left(\frac{\partial T}{\partial t} + V\cdot\nabla T + w\frac{\partial T}{\partial z}\right) - \alpha\frac{dp}{dt} \qquad (2.25)$$

Defining $\frac{dp}{dt}$ in Cartesian co-ordinates we have:

$$H = C_p \left(\frac{\partial T}{\partial t} + V\cdot\nabla T + w\frac{\partial T}{\partial z}\right) - \alpha\frac{\partial p}{\partial t} + \alpha V\cdot\nabla p + \alpha w\frac{\partial p}{\partial z} \qquad (2.26)$$

If we restrict the analysis to isobaric surfaces the local pressure change term $(\alpha\frac{\partial p}{\partial t})$ may be neglected and the cross isobaric flow of the horizontal wind $(\alpha V\cdot\nabla p)$ is normally small (Haltiner and Martin, 1957). We now have:

$$H_E + H_{LP} + H_R = C_p \left(\frac{\partial T}{\partial t} + V\cdot\nabla T + w\left\{\frac{\partial T}{\partial z} + \frac{\alpha}{C_p}\frac{\partial p}{\partial z}\right\}\right) \qquad (2.27)$$

A B C D

The local rate of heating (B) is thus a function of the three

diabatic heating sources (A: enthalpy flux, release of latent heat, and radiative effects), the horizontal advection of temperature (C) and the vertical advection (D). The two components of the thermal advection (C and D) are computed for comparison with local energy sources. Note that all heating functions except the surface heating apply to 85 cb. The surface heating is an average for the layer below 85 cb.

Since each term on the right hand side of the omega equation (2.10) may be solved individually for omega we may determine the contribution towards the total vertical motion by differential vorticity advection (w_V), thickness or thermal advection (w_{TH}), latent heat release (w_{LP}), and surface diabatic heating (w_H). Unfortunately, this partitionment is valid only if the boundary conditions are zero. For non-homogeneous boundaries each term, when solved individually for omega, is forced by the same magnitude during the relaxation computations as the total equation and the total is no longer a sum of the components. Consequently, when the advected and local influences on the vertical circulation are discussed the model generated data do not include orographic or frictional effects; these are included only in the total vertical velocity.

The Computational Scheme

The computational design for the solution of the omega equation is now discussed. Routines are not described in the literature and the computer programme is designed specifically for this study (Appendix Two).

The omega equation is a Poisson equation in three-dimensions of the form:

$$\nabla^2 u = F \qquad (2.28)$$

where u is the unknown and F is a previously determined group of forcing functions that may be considered as a constant for each case under consideration. The del operator is in three dimensions with pressure as the vertical co-ordinate and distance as the horizontal co-ordinate. For the omega equation the left hand side of 2.28 also includes constants, however this does not alter the computational scheme.

The Poisson equation is solved through relaxation techniques. Initially, guesses of u are made at all points within a three-dimensional grid and the equation is solved for each point using these values at neighbouring points. The result is a new three-dimensional field of u which is used as input for the next series of calculations over the grid. The iteration process is repeated until the difference between two successive iterations for the sum of all grid points falls below a specified tolerance level. This level is two orders of magnitude smaller than the expected values for this study. This may be interpreted as the accuracy of the solution of this

part of the calculations.

The scheme used is the Gauss-Siedel (Liebmann) relaxation method. The two-dimensional form given in Carnahan et al (1969) is modified for the three-dimensional case. All derivatives are forward differences. Boundary values of $\omega=0$ are specified at the top and sides of the matrix. The vertical motion due to orographic and frictional effects is the lower boundary condition. An 8 x 8 data grid in the horizontal dimension is expanded to a 10 x 10 grid by linear extrapolation of the data towards the edge. The model generated data for analysis is the central 6 x 6 grid so that the influence of the major 'edge' effects due to zero boundary values of omega are reduced. These effects are not entirely removed and may extend five grid points towards the center from the outer (10 x 10) margins (Baumhefner, pers. comm. 1975). However, the disadvantages of the greatly increased size of data storage requirements and number of computations is considered to outweigh the accuracy advantages of increasing the computational area for the present study. Error estimates of the zero boundary assumption are made in Chapter Three.

The solution of the omega equation is non-linear in that the latent heat release function includes an estimate of omega (cf. equations 2.10 and 2.17). Omega is first computed without the latent heat release term. This term is then calculated using this initial estimate of omega and the final omega field is calculated with the latent heat release included.

Data Input

The data are from the National Meteorological Center (NMC) analysis. Rawinsonde data were interpolated by this group to give estimated data on a nearly equidistant grid of 350 km along the horizontal interval with six constant pressure surfaces in the vertical (100, 85, 70, 50, 30 and 10 centibars). The data selected for this study represent a 64 point grid centered on Baffin Island (Figure 2). In three-dimensions omega is computed at 384 points and after removal of edge effects 216 points are suitable for analysis.

Other grid configurations are possible; for example spherical polar co-ordinates with equal distances along each meridian and latitude circle have been used in atmospheric models. Spherical polar co-ordinates have the effect of artificially increasing the resolution near the poles with the result that higher order circulation oscillations are resolved near the poles than near the equator (Schmidt, 1975). Moreover a non-homogeneous framework requires a complex modification of the relaxation scheme. For time dependent models Schmidt (1975) notes that both configurations have inherent errors but "for physical reasons, the atmosphere works mass or area wise, not polar co-ordinate angle wise". For these reasons, a homogeneous grid is used.

Although the basic omega equation requires only fields of geopotential height, the following data are needed for the surface boundary conditions and diabatic parameterizations:

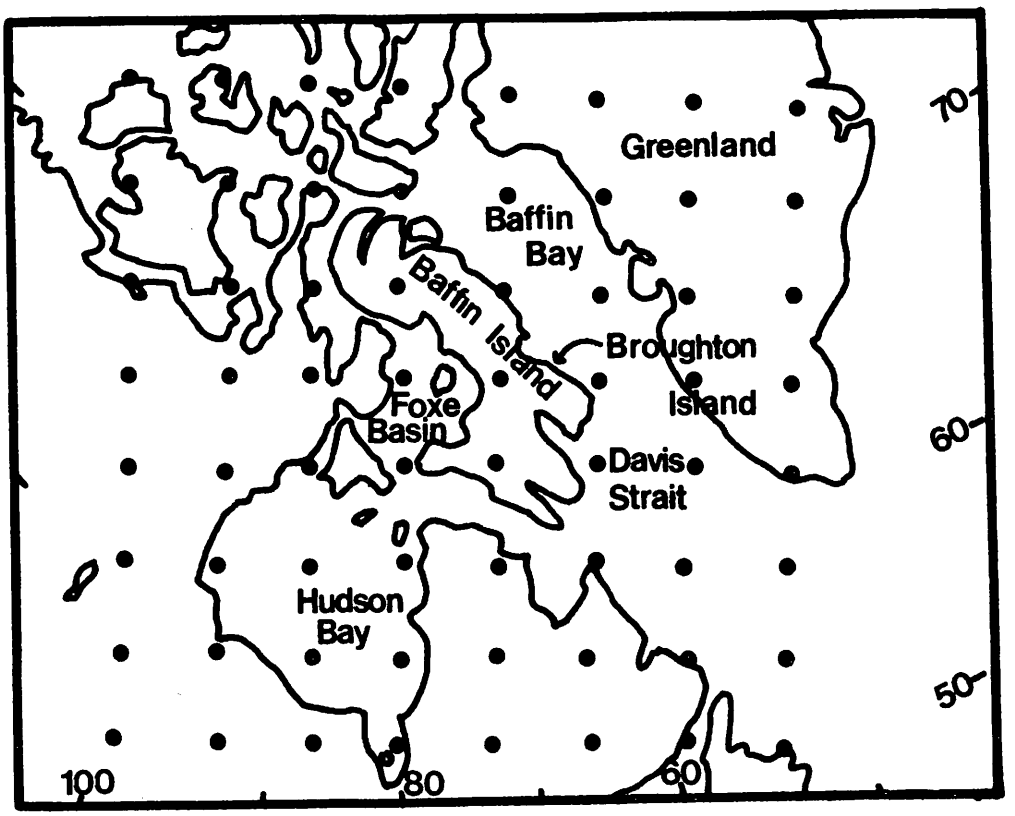

Figure 2 EIGHT BY EIGHT DATA GRID

relative humidity, temperature and sea surface temperature. This latter data set, derived from satellite radiation data, is not always available for the 1973 period and is not available at all before 1973. In addition surface winds are unavailable; these are approximated from the 100 cb pressure pattern through geostrophic considerations and the resultant wind vector is rotated 20 degrees towards low pressure to include, in a gross manner, frictional modification to the geostrophic flow at this level.

The actual pressure level for the top of the Ekman layer is not known and will vary with the synoptic situation and topographic height. It is assumed to be 100 cb for all calculations. This is a necessary approximation if the computations are to remain in pressure co-ordinates. In prognostic models, where the resulting error may amplify with time, it is common to use sigma co-ordinates which relate a pressure level to the observed surface pressure in non-dimensional terms (Holton, 1972). The necessary revision is not warranted on the present grid scale for a diagnostic study when comparative effects, not actual magnitudes, are of major importance.

The Climatic Characteristics of the Sample Period

On account of the great amount of computer time required for this type of study, and the exploratory nature of the experimental design, only a limited sample is examined. The computer expense

involves not only the model computations and subsequent analysis but also the abstraction of the aerological data for the limited area model from the large file of world data tapes from the National Meteorological Center. If the data for this study are to be limited to one magnetic tape an eight month sample is a practical limit. Upon confirmation of the suitability of the techniques adopted for this study a more extensive sample involving several source tapes may be considered.

The sample year of 1973 was selected for practical reasons. As mentioned above, for one parameterization the radiometric surface temperatures are required. These data are not available before 1973 in the NMC grid analysis used in this study. When this investigation was started, NMC data were unavailable after 1973.

It is generally recognized that there is a great inter-annual variability in the Arctic circulation (Namias, 1958; Reed and Kunkel, 1960). Even the five year data base of Reed and Kunkel does not correspond at all locations with a fifteen year 'normal' pressure distribution. The results of the 234 day sample of 1973 must be interpreted in terms of the restrictions of this variability.

There are not any long term statistics comparable to the results of the diagnostic model used in this study; however, an indication of the climatic representation of the sample period is possible from an examination of the 70 cb pressure field, surface synoptic data, and the sea ice extent.

Departures of the 70 cb pressure field from monthly means are published in the MONTHLY WEATHER REVIEW (Vol. 101, numbers 4 to 11) for the period of interest. These monthly departures for Davis Strait and Foxe Basin are in Table I.

TABLE I

1973 MONTHLY DEPARTURES OF THE 70 CB SURFACE IN DECAMETERS

	J	F	M	A	M	J	J	A
Davis Strait	-9	-5	-6	+3	0	-3	-3	+3
Foxe Basin	-4	-6	-6	0	0	0	+4	+6

The departures are not the same in both locations during the sample. In July the difference is seven decameters. It is apparent that there has been a change in the regional circulation from the normal throughout most of the period of analysis. To put these figures in perspective, note that the standard deviation of the 85 cb surface in the eastern Canadian Arctic on July 15, 1973 (Appendix Three, this case is examined in detail in Chapter Four) was seven decameters when there was a steep pressure gradient between a southerly low over Quebec and a Greenland ridge. Standard Deviations for other days in this synoptic episode varied from three to eight decameters. Although the two data sets are not strictly comparable, it seems that

the departures, and differences in departures between the two locations, are of significant magnitude so that the circulation of the sample cannot be considered to be truly representative of the long term mean. The effects of the non-normal circulation on the interpretation of the vertical velocity field are unknown.

Monthly averages of surface synoptic data and departures from the 30 year normal are published in MONTHLY CLIMATIC DATA FOR THE WORLD (U.S. Department of Commerce, Environmental Data Service, Asheville, N.C., Vol. 26, No. 1 to 8). These data are reproduced in Table II for Frobisher and Hall Beach (stations which correspond closely to the Davis Strait and Foxe Basin locations of Table I). The monthly areas of sea ice extent outside the minimum area of cover observed during the 1966 to 1974 interval (from Sanderson, 1975) are presented in Table III for 1972, 1973 and 1974 for the eastern Canadian Arctic.

At Frobisher temperatures were below normal throughout most of the sample. The eight month precipitation total was 24 mm above normal. For Hall Beach temperatures were below normal during the winter and above normal in the summer, and the total precipitation was 47 mm below normal. Corresponding to the anomalous circulation regime, there is not a consistent deviation of synoptic observations over the region of interest.

The maximum winter extent of sea ice in the Davis Strait Labrador Sea area (Table III) for the 1966 - 1974 period occurred during 1972. In 1973 there was a return towards decrease extent although the monthly values were above the 1966 to 1974 mean - an

TABLE II

MONTHLY AVERAGES AND 1973 DEPARTURES OF SYNOPTIC DATA

FOR FROBISHER AND HALL BEACH

	J	F	M	A	M	J	J	A
HALL BEACH								
Temperature (°C)								
Normal	-33.9	-34.1	-29.7	-22.2	-9.5	2.6	6.8	6.0
Departure	-3.2	-1.3	-1.4	-2.1	0.2	2.0	0.7	1.5
Vapour Pressure (mb)								
Normal	0.3	0.3	0.5	1.1	3.1	6.5	7.8	7.8
Departure	na	na	na	0	0	0.9	0.1	0.3
Precipitation (mm)								
Normal	4	6	8	13	4	7	8	31
Departure	-4	-4	13	3	-13	-1	-31	-10
FROBISHER								
Temperature (°C)								
Normal	-29.1	-29.8	-25.6	-14.3	-3.3	3.6	7.3	8.0
Departure	-2.6	-4.3	-5.1	-0.6	-0.2	0	-0.6	1.1
Vapour Pressure (mb)								
Normal	0.5	0.4	0.8	2.1	4.1	5.9	7.8	7.9
Departure	-0.4	-0.6	-0.2	0.2	0.1	-0.2	-0.1	0
Precipitation (mm)								
Normal	19	9	38	61	24	37	63	20
Departure	-3	-18	19	40	5	4	10	-33
Per cent of the long term mean of sunshine	162	150	102	83	105	136	53	213

TABLE III

SEA ICE EXTENT IN THE EASTERN CANADIAN ARCTIC OUTSIDE THE MINIMUM AREA OBSERVED DURING THE 1966 to 1974 INTERVAL

areas are $km^2 \times 10^6$	MONTH		
	F	M	A
1972	0.90	0.85	0.45
1973	0.65	0.60	0.35
1974	0.55	0.55	0.25
1966 to 1974 mean	0.55	0.45	0.33

Data are from R.M. Sanderson (1975)

observation consistent with the below normal winter temperatures in the region. Dickson et al (1975) found a pressure fall of 9.6 mb between 1966-70 and 1971-74 over Greenland. They attributed the weakening of northerlies over north Europe and the succession of mild winters to this circulation change. Similar arguments would indicate a weakening of southerly flow in the eastern Canadian Arctic to the west of this feature with a corresponding reduction in warm air advection. The 1972 maximum of sea ice extent was related to an anomalous northwesterly wind component in the Canadian Arctic (Sanderson, 1975).

We may conclude that 1973 cannot be considered a representative year. The circulation regime, synoptic observations and sea ice extent (which affects sea surface temperatures and thus the enthalpy fluxes) were anomalous. 1972 was an extreme period in terms of ice extent while 1973 represented a recovery, but still there were below normal temperatures along the east Baffin Island coast.

CHAPTER THREE

MODEL VALIDATION

Introduction

The atmospheric model described in Chapter Two is designed as a diagnostic tool. The output is used to assess the relative importance of the various processes which generate the vertical circulation. A by-product - precipitation - is an important feature of the atmospheric hydrological balance. For interpretation of the derived data it is useful to have some level of confidence for their magnitudes and the spatial configuration.

On account of the diagnostic rather than prognostic nature of the omega equation, verification of the performance has not received much attention in the literature. Danard (1964) adjusted the parameters in his form of the omega model by comparison of the vertical motion field with results of kinematic analysis, despite the errors inherent in the latter technique (cf. previous chapter). Smith (1971) made a similar comparison but first assessed the kinematic technique qualitatively through correspondence of the calculated field with the circulation expected for particular synoptic features. Baumhefner (1968) related the sign of vertical motion to the spatial pattern of moisture convergence and cloudiness. The forecast precipitation field (assuming air to be saturated in all regions of ascent) was compared with observed patterns by

Stuart (1970) who found that his assumptions led to underestimates of an order of magnitude. He concluded that the methodology was not suitable for regions where sub-grid convective storms may be important precipitation mechanisms. Stuart suggested that a diabatic heating term incorporating latent heat release is required to yield higher omega values and therefore larger precipitation rates. Using the latent heat scheme employed in this study, Krishnamurti and Moxim (1971) found that computed intensities and distributions compared favourably with observations in a qualitative manner for a single case of a mid-latitude disturbance.

These studies represent the present state of validation of the omega equation. Most workers have avoided the difficulty of not having an observational field for comparison by examining the product of a sub-model - precipitation. The common ground to all is the qualitative nature of the discussion and the limited number of cases examined.

Following the studies cited the performance of the omega equation is evaluated by a qualitative examination of the precipitation field. Several cyclonic disturbances are modelled so that the resultant data base is large enough for a simple quantitative comparison of the forecast and observed fields of precipitation. The cases are restricted to instances of frontal upglide precipitation processes as these types are more amenable to systematic comparison with classical concepts than non frontal occurrences. In addition, magnitudes are larger

and there are more clearly defined cases for analysis.

It is possible that poor correspondence of the observed and predicted precipitation fields may be the result of errors in the latent heat parameterization, not in the omega formulation directly. As an independent check, grid average precipitation is also forecast from an independent statistical model (Sasamori, 1975). The input fields are identical to the latent heat model. Thus, the suitability of the latent heat formulation alone may be determined.

For the eastern Canadian Arctic, only five of the NMC grid points are near observation stations with precipitation data (Clyde, Hall Beach, Churchill, Baker Lake and Egedesminde). To provide an adequate data base for statistical analysis a great number of storms passing over these stations would have to be examined. A study of spatial patterns would be inconclusive. As an alternative, the target area is shifted to the mid-west United States. The precipitation network is more dense and there is a station within reasonable distance of each of the thirty-six grid points. Therefore, a large sample may be accrued from computations for relatively few storms. However, independence of the sample data is sacrificed and the statistical tests must be limited.

The grid area is illustrated in the first map of Figure 3. The northeast border is the Great Lakes. The Western Cordillera is not included and problems of precipitation measurements in mountain area (Hutchinson, 1968, 1970) need not be considered.

However, the orographic effects of the mountains are included as boundary conditions for the western two rows of the 10 x 10 computational grid.

Sixteen days representing stages of eight cyclonic disturbances from the spring of 1973 are examined. These storms are characterized by intense precipitation due to frontal passage through the target area with a pronounced trough aloft (Figure 3). The validation therefore pertains to the vertical motion field resulting from the advection of vorticity and thickness during cyclogenesis.

Limitations of the Validation Data

The observed precipitation data are from the DAILY WEATHER MAPS of the United States Department of Commerce. The observation nearest each grid point is recorded.

There is considerable error associated with this manner of data abstraction. Despite the dense station network, subjective interpolation between stations was required in some cases. In addition, we assume the observed data to represent a smooth pattern that would correspond to the large scale grid point calculations when, in fact, a station record may be biased considerably by local, sub-grid scale, convective storms. Bosart (1973) notes that much of the east coast winter precipitation is the localized intensive type of convective uplift with the storm system operating on the scale of a few

hours. From radar observations Browning et al (1973) found that a cellular structure with widths of less than 100 km is a major feature of frontal systems with intensities of 1 - 4 mm hr^{-1} within cells and less than 0.5 mm hr^{-1} between. The records used in this study are 24 hr totals ending at 100 EST whereas the calculations are instantaneous values multiplied through time to yield 24 hr totals. A point by point comparison would be valid only if the storm were stationary and precipitation rates constant through the 24 hr observation period. In reality, the storm has travelled eastward and the records reflect the integration of several stages of the disturbance.

The representation of the precipitation records themselves may be suspect. Allis et al (1963) note that "The true areal precipitation is unknown". Using five years of data, Hendrick and Comer (1970) illustrate precipitation differences of 3 cm per day within an eight kilometer radius for a small watershed network. Within one kilometer the difference may be 2 cm. The authors noted that spatial variability changes with storm size, direction of moisture influx and season. The instrumentation may also be a source of error, with the catch changing with windspeed (Wilson, 1954) and exposure (Green, 1970). For two similar gauges 3 m apart, Court (1960) recorded a difference of 50 per cent of the smaller catch. For annual averages the differences may be smoothed (Allis et al, 1963), but for individual storms these uncertainties must be considered.

There is not any a priori reason to expect a station record to correspond to a calculation at a grid point several kilometers away. In the empirical analysis, we must anticipate considerable error in point by point comparisons.

Synoptic Analysis

To illustrate the synoptic characteristics of precipitation predicted by the model for situations of cold polar outbreaks four cases in the mid west United States are selected. The 50 cb flow (700 EST), surface frontal positions and the extent of 24 hr precipitation are shown in Figure 3. Also shown are computer drawn isohyets of calculated precipitation, expressed as inches per day for ease of comparison with the official records. The fronts are clearly within the grid area for these cases. For the examples not shown the grid encompasses only the leading edge or decaying tail of a frontal complex.

According to the classical theory of atmospheric kinematics (Bjerknes and Holmboe, 1944; Sutcliffe, 1947; Petterssen, 1955) the difference between subgeostrophic flow in the cyclonically curved base of an upper level trough (region of generation of positive vorticity) and the supergeostrophic flow in the anticyclonically curved crest of this wave results in diffluence or divergence along the east - poleward - limb of the trough (ca. 50 cb). This divergence in the zone of positive vorticity advection is associated with lower level convergence and vertical uplift in order that mass continuity be preserved (cf. discussion

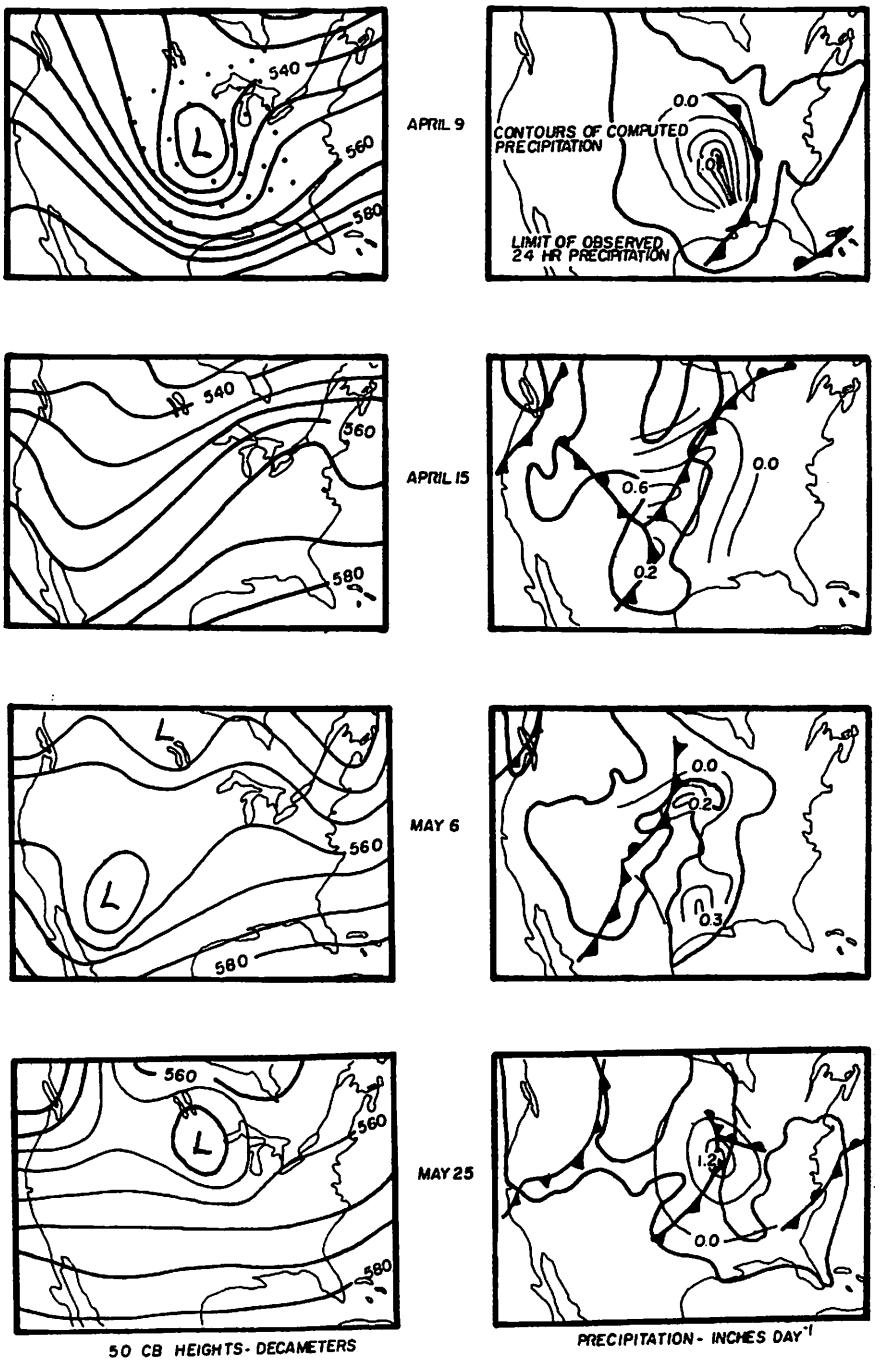

FIGURE 3 MODEL VALIDATION

of Figure 1, Chapter Two). The attendant precipitation is usually along the east side of the resulting cyclonic vortex at the surface (Palmen and Newton, 1969, pp 265).

The actual structure of this precipitation belt has been investigated using radar data by Browning et al (1973) and Harold (1973). They found that the belt is organized into bands with widths of less than 100 km which develop close to the surface warm front, move through it and then dissipate at the leading edge. The large scale flow is likened to a 'conveyor belt' with the moist warm air intrustion being forced over the warm front by the advancing cold front. This explains the foreward movement of the precipitation bands with the warm 'upglide' front. This band structure is the result of small scale convection superimposed on the widespread ascent. The source of the convectional instability is unknown. These studies emphasize that the synoptic scale flow is responsible for the areal distribution of precipitation but does not necessarily enhance the intensity which may be linked more strongly to the cellular meso scale (<100 km) dynamics. For a severe east coast precipitation event in 1956 Stringer (1973, pp 455) cites nine contributing aerological factors in addition to the 'classical' frontal influences of forced uplift. Some characteristic spatial relationships are evident, however, in the examples studied for the mid west United States even though these small scale features cannot be expected to be resolved with the present grid interval.

For a case study of the energetics of a mid-winter storm in the United States, Danard (1964) computed precipitation rates from the vertical motion field. The rates increased to a maximum along the cold front and then decreased in a smooth bell shaped distribution. Such a computed form is found for the cases illustrated, in particular for May 25.

These isohyet patterns also exhibit a characteristic elliptical shape, with the major axis roughly orientated along the frontal surface. From a statistical study of 30 year precipitation records, Caffey (1965) noted that this elongated configuration and frontal alignment is a significant feature of cyclonic precipitation in the plains region.

The relationships between the polar front jet and precipitation has been examined for seven intense storms in the central United States by Smith and Younkin (1972). Their cases correspond closely with those of this study with a deep southward intrusion of polar air over the mid-west and strong cyclonic curvature of the 50 cb wind field. For all cases they found a well defined elliptical isohyet pattern with dimensions similar to those of Figure 3 (1300 km along the major axis, 350 km along the minor axis). This pattern was aligned along the northward limb of the jet wave with the maximum intensity slightly to the east of the maximum flow. The magnitudes, as well as position, were similar to those of this study.

As mentioned above, the general 50 cb pattern over the areas of precipitation is northward flow which implies

positive vorticity advection (a decrease of relative vorticity towards the wave crest) and upper level divergence. For individual cases this simple explanation may be complicated by other factors.

On April 9 (Figure 3) the trough is centered over the central portion of the grid with positive vorticity advection in the east over the surface front. The extreme curvature of this wave results in large precipitation amounts (one inch per day maximum). Precipitation declines to zero to the west and northwest. Commonly, in cold air outbreaks vertical shrinking is found on the southern and western edges of the intrusion (Palmen and Newton, 1969, pp 292) with the strongest descent in the southernmost sector. Thus, the predicted reduction of precipitation is expected.

On April 15 the curvature is weaker and the vorticity export extends over the entire plains area. The surface front is occluded. Ascent is weaker and widespread. The isohyet pattern is roughly orientated with the flow, along the frontal surface, and maximum rates are relatively low - 0.6 inches per day (1.5 cm dy^{-1}) as compared with one inch per day (2.5 cm dy^{-1}) on April 9.

The May 6 pattern of flow is similar, except that the 50 cb geopotential gradients are lower with the result that the maximum of precipitation is only 0.2 inches per day (0.5 cm dy^{-1}) along the cold frontal surface. A second non-frontal maximum in the south of the grid is related to upper level

diffluence as the flow approached a weak local ridge south of the Great Lakes. This feature is evident in the observed limit of 24 hour precipitation over east Texas.

On May 25 flow over the southern United States is predominantly zonal, however there is marked convolution west of the Great Lakes with a local cut off low which represents the decay of a polar outbreak. Strong vorticity export to the east from the tight vortex is combined with strong diffluent flow to produce an intense local precipitation maximum of 1.2 inches per day (3.1 cm dy^{-1}) over Lake Michigan. This is situated at the apex of an occluding system. There is a steep gradient of precipitation towards the south and west where the flow is zonal and weak.

Empirical Analysis

In this section the forecast precipitation field is compared with the observed data at each grid point to determine the reliability of the computed magnitudes. Rigorous statistical testing is impossible due to the limitations of the observed data and the fact that the predicted data are not completely independent. In this section we can only infer the source and range of error in the model.

In an exploratory test seven cyclonic disturbances were modelled assuming precipitation to occur in all regions of uplift with relative humidity in excess of an arbitrary level of 80 per cent, a level adopted by Krishnamurti and Moxim

(1971). The forecast field (not shown) was restricted in area and grid averages were an order of magnitude less than the observed field. Although the error is similar to that noted by Stuart (1970), the scheme employed here is more realistic and, despite the aforementioned errors inherent in such a comparison, the correspondence should be closer. The calculations were repeated with a cut-off level of 70 per cent relative humidity. Since relative humidity does not enter into the calculations, the magnitudes at each point where precipitation was previously predicted does not change, but the number of points where precipitation is forecast increases. For these revised tests the mean of all grid points is increased by an order of magnitude to within 5×10^{-2} cm dy^{-1} of the observed mean. For the entire sample of sixteen cases the means of the observed and predicted fields are 4.1 and 2.8 cm dy^{-1}, respectively, for a total of 576 grid points. The corresponding standard deviations are 7.4 and 5.8. In light of the large standard deviations of both the forecast and observed fields the small difference of means is accountable. The data for the individual cases are in Figure 4 and Table IV.

The nature of the discrepancy may be investigated furthur with the aid of a frequency table (Table V). To allow for considerable error latitude the data are arranged in intervals of 1.2 cm dy^{-1} (0.5 in dy^{-1}) with a separate category for zero or trace values (less than 0.1 in dy^{-1} or 0.3 cm dy^{-1}). A Chi-square statistic is not applicable since the table would be

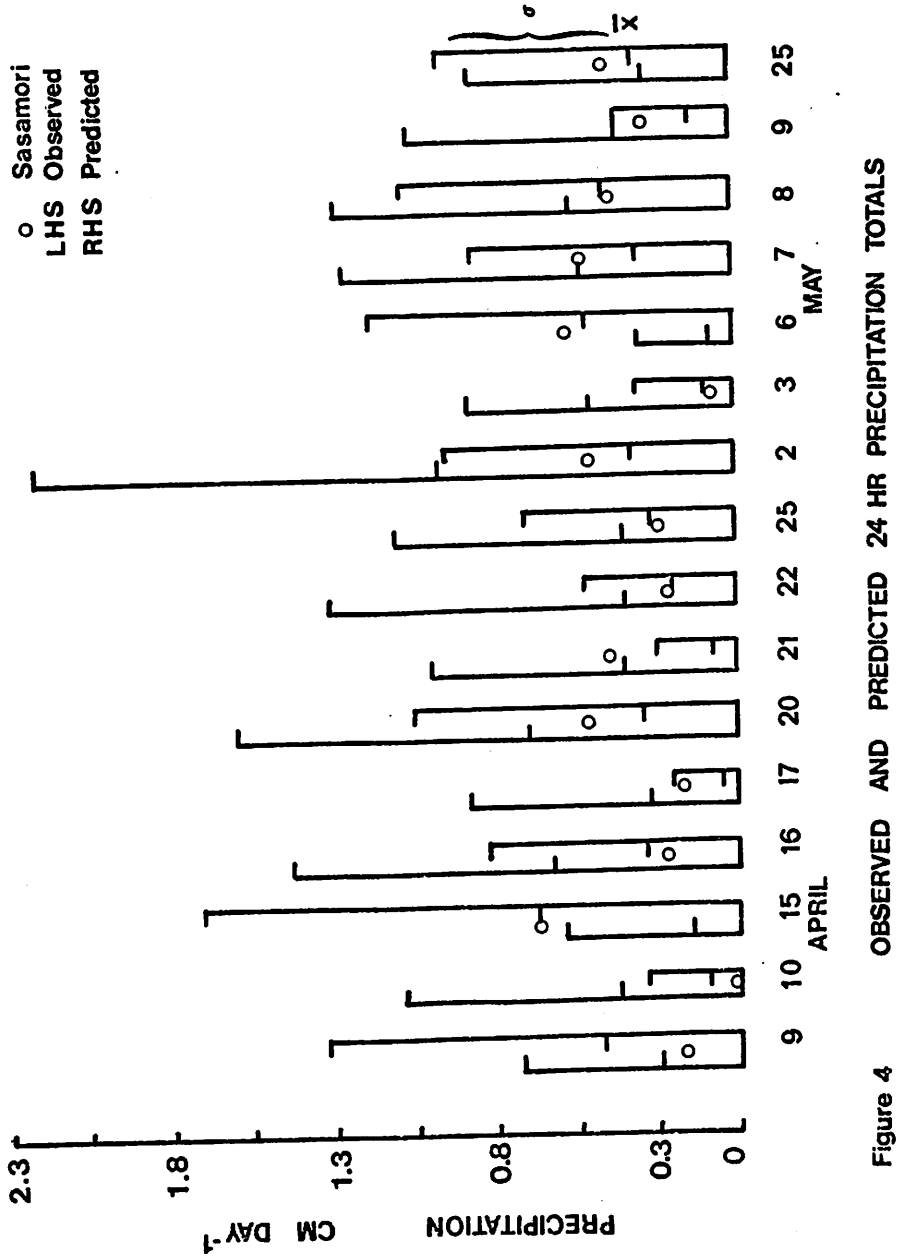

Figure 4 OBSERVED AND PREDICTED 24 HR PRECIPITATION TOTALS

TABLE IV

PRECIPITATION DATA FOR MODEL VALIDATION

Date 1973		Precipitation cm dy^{-1}					85 cb Vertical Velocity cm s^{-1}	
		Observed		Predicted		Sasamori		
		X	SD	X	SD	X	X	SD
April	9	2.5	4.3	4.3	8.3	1.8	1.6	4.2
	10	3.8	6.8	1.0	2.0	0	-1.0	2.0
	15	1.5	4.1	6.4	9.9	6.3	1.6	3.2
	16	5.8	8.1	2.7	4.8	2.3	0.2	2.0
	17	2.8	5.3	0.5	1.0	1.8	0.0	1.1
	20	6.6	9.1	3.1	6.8	4.8	1.1	3.2
	21	3.6	5.8	0.7	1.8	4.1	0.5	1.8
	22	3.6	9.4	2.0	2.3	2.3	0.2	1.4
	25	3.6	6.8	2.8	3.8	2.5	0.3	1.3
May	2	9.4	12.9	3.3	5.8	4.5	0.8	2.2
	3	4.6	5.6	0.8	2.3	0.8	-0.6	1.8
	6	0.7	2.0	4.5	7.1	5.3	1.1	2.2
	7	4.8	7.4	3.1	5.6	4.8	0.5	2.1
	8	5.1	7.4	4.1	6.4	3.8	0.3	2.1
	9	3.5	6.6	1.3	2.3	3.1	0.2	1.4
	25	2.8	5.3	3.1	6.1	4.1	0.3	1.9
Statistics for the entire sample								
		4.1	7.4	2.8	5.8	3.1		

X grid point mean
SD grid point standard deviation

TABLE V

FREQUENCY OF PRECIPITATION AMOUNTS

Data are based on daily totals of precipitation.

Total sample size is 576 grid points. 208 points are out of range.

Class units are cm dy^{-1}

		Predicted					Total
		0.	0.3	1.2	2.5	3.8	5.0	
Observed	0.	129	49	8	3	1	187
	0.3	68	27	9	1	0	105
	1.2	40	18	27	1	0	66
	2.5	5	3	1	0	0	9
	3.8	1	0	0	0	0	1
	5.0						
Total		240	97	25	5	1	368

overcollapsed to get a minimum of five in all categories.

Rates in excess of 5 cm dy^{-1} are rejected. These probably represent intense localized convective storms. There are not any such cases in the forecast field but in the observed data there are 208 rejections. In the predicted population there is a distinct bias towards rates of less than 1.2 cm dy^{-1} with few values in excess of this. These characteristics are anticipated since small precipitation totals are associated with slow wide spread ascent, for which the model is suitably designed, while large rates are usually associated with intense local storms which may not be resolved by the grid (Bosart, 1973). There is also a high predictive capability for points of zero or trace precipitation. Of 187 points of observations in this category the model is correct for 129.

As an independent measure of the suitability of the latent heat parameterization precipitation is also forecast from the statistical model described by Sasamori (1975). The input fields are identical except that grid averages and standard deviations of omega are used instead of point values. The prediction is an average over the grid. The only constants to be set are the time scale describing the mean growth rates of cloud droplets and crystals and the lifetime of vertical motion of an individual air parcel. These constants are taken as specified by Sasamori which yield reasonable estimates of the annual global precipitation rate. The data are included in Table IV and Figure 4.

For the sixteen storms the mean of the Sasamori estimates is 3.1 cm dy^{-1} which is slightly greater than that of the model used in this study. The case by case comparison (Figure 4) illustrates the near coincidence of forecast of the two mutually exclusive parameterizations. The Sasamori forecast is always within one standard deviation of the forecast of this study and the means of both are within one standard deviation of the observed mean (except for April 15 and May 6). We may be reasonably confident that the model used in this study gives realistic results and that an analysis of the vertical motion of the omega equation in terms of the precipitation distribution and intensity is valid.

Error Analysis of the Zero Boundary Assumption

Seven of these storm examples will serve to illustrate the probable range of error that may be traced to the assumption of zero omega at the lateral boundaries of the computational grid (cf. Chapter Two). For each example (April 9, 10, 15, 16, 17, 20 and 21) omega was computed assuming zero boundaries and those values of omega at the interior grid points adjacent to these boundaries were used as revised boundary values for a second computation of the omega field. These values are not true values of the boundaries consistent with the input data since they have been initially affected by the zero boundary assumption; however, this revision is conceptually more realistic than the adoption of zero values. For all seven cases the initial mean 85 cb vertical

velocity for the 36 grid points is 0.29 cm s^{-1}. For the revised boundaries the mean is 0.31 cm s^{-1}. The corresponding mean precipitation values are 2.5 and 2.8 cm dy^{-1}. Obviously the effect of the revised boundaries will be different for a case with the major synoptic feature in the center of the grid with near zero vertical motions at the boundaries as compared to a case when the major feature with strong vertical velocities is near the boundary, but for these seven cases with features both at the center and at the edge this simple test suggests that the effect of the revised boundaries is only marginal when grid point averages of the central 36 point matrix are considered. A more rigorous, but more complex, test would be to compute an omega field for a very large data matrix, perhaps on a hemispheric scale. Omega could then be recomputed for a small section of this matrix, where edge contamination is non existent in the hemispheric scale analysis, with zero boundaries to estimate the true effect of this approximation.

Summary

For validation purposes, we assume that the pattern and magnitude of precipitation is a faithful indicator of the overall behavior of the omega equation. Comparison of the precipitation (latent heat) sub-model used in this study and an independent statistical model (Sasamori, 1975) using identical input data confirms this assumption. Major discrepancies in the forecast and observed precipitation fields should be traced

directly to the omega equation, or to the observational data.

Synoptic considerations indicate that forecast isohyetal patterns conform to those expected from observational studies of similar storm systems in size, intensity, orientation and configuration. Precipitation is predicted where vertical uplift is expected from subjective examination of 50 cb flow features. Conversely, where we anticipate nearly zero or negative uplift, precipitation is not forecast. The location of latent heat release is in accord with the broad scale circulation regime.

The empirical analysis is hampered by the inadequacy of the observational data for the purpose of this study. This could be reduced partially by using 3 hr records at the time of forecast, but uncertainty due to instrumental and spatial sampling errors would remain. Overall the forecast compares favourably with observations in variability and relative magnitudes providing a 70 rather than 80 per cent relative humidity cut off for precipitation computation is used. Despite the incorporation of a conditional instability parameterization in the precipitation sub-model, intense rates are not well reproduced, probably due to the coarse resolution of the data set and local nature of these convective storms. Weak, widespread upglide types of rainfall in stable stratification are well predicted.

We may conclude that the magnitudes and spatial patterns

of the omega calculations are both reasonable and acceptable. For cyclonic disturbances the model may be used to forecast instantaneous precipitation with reasonable confidence. The reliability for non-frontal processes is less certain.

CHAPTER FOUR

A CASE STUDY OF A DEPRESSION SYSTEM IN THE EASTERN CANADIAN ARCTIC

Introduction

As noted in Chapter One the physical explanations for the Arctic synoptic systems identified on mean pressure maps (Namias, 1958; Keegan, 1958; Reed and Kunkel, 1960; O'Connor, 1961) have been largely speculative. Interpretations were based on synoptic experience and statistical associations. Prognostic models have been used successfully to simulate actual circulations in the Arctic (Winston, 1955; Namias, 1958), however, these numerical techniques have not been employed in a diagnostic sense to examine the dynamics involved in a specific circulation feature.

In this chapter the steady state diagnostic model described and tested in chapters Two and Three is applied during the course of a single synoptic event in the eastern Canadian Arctic. For this July event the relative significance and magnitude of each of the various mechanisms of advected and local origin is determined at different stages of development, stabilization and decay. The system is characteristic of the summer circulation. A mid-latitude depression is deflected up Davis Strait by strong North Atlantic blocking. This route is one of the principal storm tracks found on the mean (1951-1970) July maps (Reiten, 1974). Although the results of this detailed

case analysis cannot be considered to have general application, they can, however, provide a point of reference for the interpretation of features found in the empirical analysis of a large sample of model generated data in Chapter Five. Also included in this detailed study is a discussion of the effects of the synoptic system on the regional thermal regime.

Synoptic Background for the Case Study

Hare and Orvig (1958) have characterized the Arctic circulation in terms of ceaseless change. Standing circulations do not exist during the summer when persistence of small scale features rarely exceeds a day or two (Wilson, 1958). Day to day variability is more significant than the mean condition.

This vigorous variability is clearly illustrated in the 1973 summer synoptic record for Broughton Island (Figure 5, radiation data are from Jacobs, 1974). For the case study the thirteen day interval from July 13 through 25 is chosen. There is a steady pressure decrease from a maximum on the 13th but the rapid initial cooling followed by a slow warming to a maximum on the 23rd seems interesting since commonly the low pressure is associated with immediate advection of southerly warm air. Records of ice thickness (R.L. Weaver, pers. comm., 1975) indicate a major ice melt of 25 cm within 48 hours at Broughton Island during the delayed warming interval beginning on the 19th.

In terms of atmospheric energetics this synoptic episode

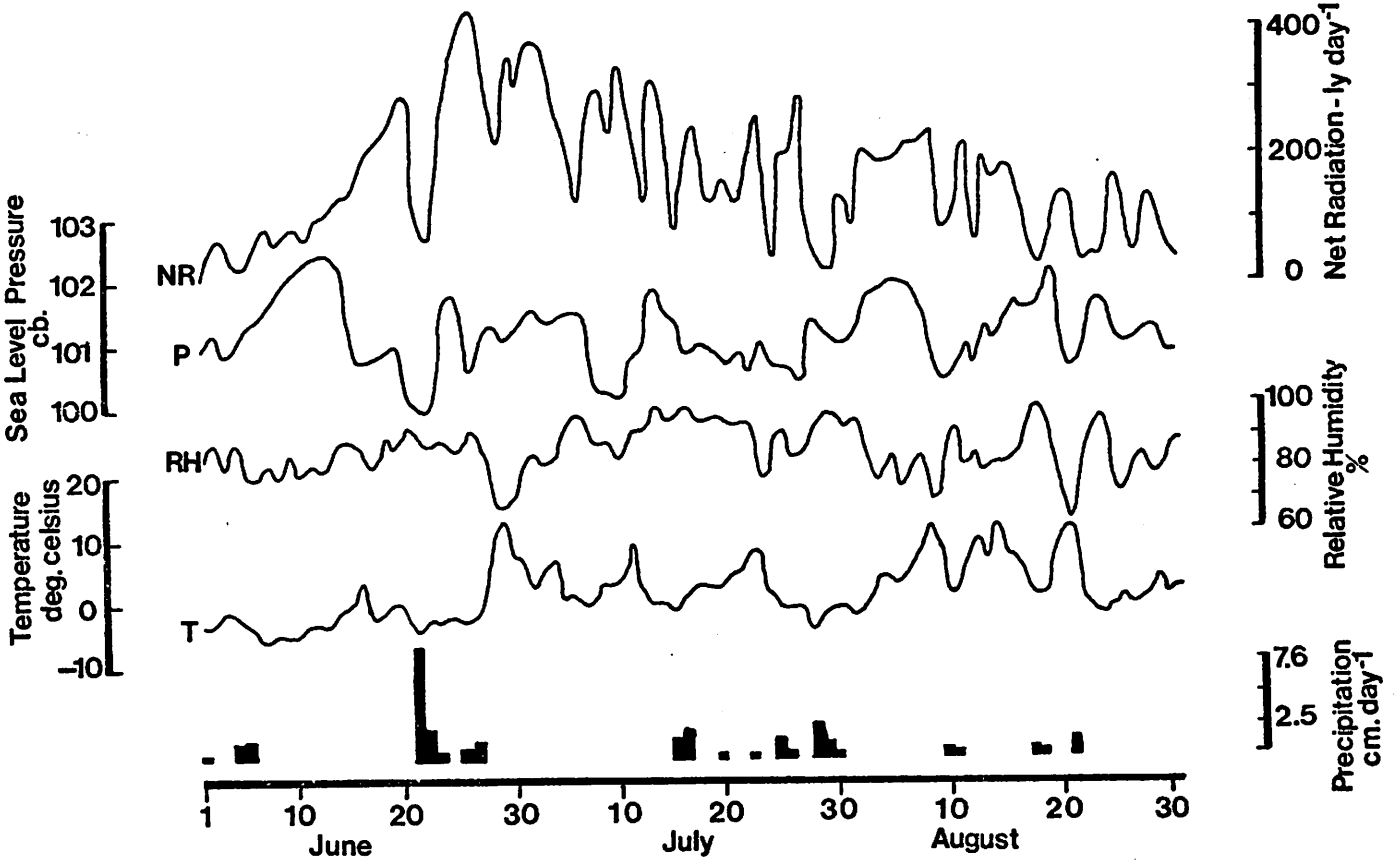

Figure 5 SURFACE SYNOPTIC DATA : BROUGHTON ISLAND , 1973

seems worthy of detailed analysis. Jacobs (INSTAAR memorandum) found the July 14-19 period to be important with respect to surface energy budgets. According to Barry's (1974) subjective scheme the July 19 regional circulation may be classified as a 'SW low' type with a low to the southwest of Baffin Island at the surface, a ridge over northern Baffin Bay, and southeasterly flow over Davis Strait.

Records from the Broughton Island station log (R.L. Weaver, pers. comm. 1975) indicate persistent low level fog with visibility restricted to less than 1 km and intermittent rain until July 22 when there was a general clearing. The ice surface quality degraded as the rain saturated the upper levels and melt holes expanded. Accurate figures for the surface albedo are in preparation by Weaver but there was a noticeable reduction in surface reflectance during this synoptic event.

The period selected for detailed analysis comes immediately after an abrupt transition from quiescent zonal flow of the Westerlies to a convoluted meridional transport, a circulation which remained until August 3. The trigger for this meridional flow was a low which originated over the Gulf of Alaska on July 1 and remained anchored there until July 11. It then weakened and may be traced on the maps as a small convolution in the zonal circulation which drifted eastward until it approached a major trough over Hudson Bay. On July 12 this convolution deepened over Keewatin as a closed low. The trough has also deepened and formed a closed low over the central

St. Lawrence region. The large scale circulation has now developed into a deep broad trough encompassing the two systems. It is this dual depression formation which enters the Arctic along the east limb of the trough bringing the initial pressure drop to the Baffin Island area.

On July 12 the surface pressure pattern in the eastern Canadian Arctic is similar to the Thule low configuration which Keegan (1958) identified as being characteristic of the winter meridional circulation. There is an elongated trough over eastern Canada with a shallow surface low west of Thule. This is associated with a slow moving primary cyclone to the southeast of Greenland with closed isotherms in mid-troposphere. This leads a wave train over Canada with the above mentioned secondary low over the St. Lawrence region bringing southerly air into the Davis Strait sector.

This is the surface situation at the beginning of the episode of meridional flow and at the beginning of the period chosen for detailed numerical analysis. The subsequent movement of the southerly depression is illustrated in Figure 6 for the 85 cb level (the level chosen for analysis). The low moves northward with a maximum depth on July 15. It becomes anchored over south Baffin Island until July 19 when it drifts east, with the height of the center stabilized, and leaves the grid area to the south of Greenland. During the first days of this interval the NMC charts indicate a deep depression system (120 decameters -dm- on July 12) in the central Polar Basin.

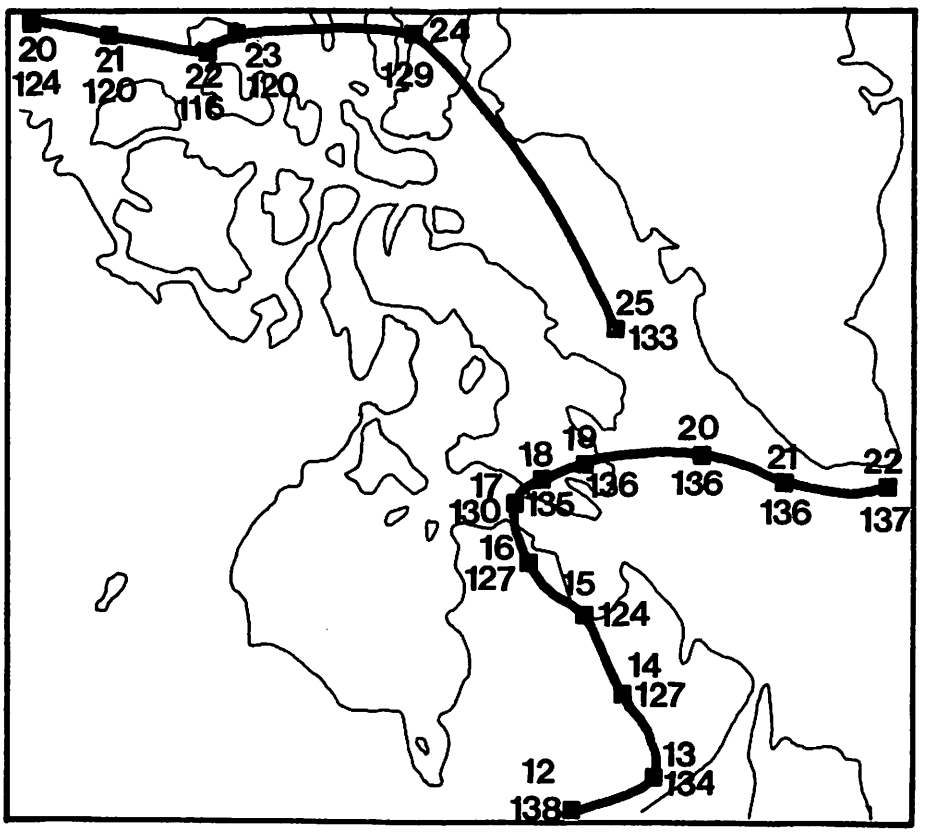

22 DATE : JULY 1973

137 HEIGHT OF CENTER - DECAMETERS

Figure 6 - 85 CB DEPRESSION CENTERS

As this circulation weakens it enters the discussion area from the northwest and drifts southward along the west coast of Greenland. This is a major cyclonic track during July (Namias, 1958) prompted by the thermal contrast along the Polar Basin and resultant baroclinicity. Even though the analysis period includes the entire history of an instrusion of a southerly system through the grid area, it also includes the influence of a northern synoptic system which will be shown to have an appreciable effect of the Baffin Island thermal regime.

The north steering of depressions over eastern Canada is evident on mean maps and there is a local maximum of cyclonic activity in Baffin Bay (Keegan, 1958) but here they tend to stagnate and fill (Reed, 1958). Although this trend may be seen on Figure 6 there is also a definite revitalization of the vortex as it leaves the region. Only after passing east of Greenland does it fill and decay to any extent.

Synoptic Analysis

This section is a detailed examination of the model generated data for the period July 13-25, 1973. The primary purpose of this analysis is to identify the relative importance of advected and local energy sources and sinks in the behavior of a synoptic system within the grid area. Here we include orographic and frictional effects at the surface as a local energy effect in terms of the cyclone circulation.

On account of the enormous amount of data computed from the model some restrictions are necessary in the discussion with the realization that pertinent information may be overlooked. The maps presented (Figures 7 through 14) are only for the 85 cb level and therefore the interpretations are limited to lower tropospheric activity. This is a compromise so that both surface influences and features of the broad scale circulation may be included. Where appropriate, important factors from other levels are discussed verbally. To simplify the presentation furthur, data at 48 hr intervals only are presented in map form although regional averages at 24 hr intervals are tabulated (Appendix Three). For each day discussed the following data are contoured: 85 cb heights, 85 cb total vertical velocity (w_T), 85 cb vertical velocity due to vorticity advection (w_V) thickness advection (w_{TH}) and surface thermal effects (w_H), 85 cb thermal advection, total precipitation and total vapour flux divergence. The 85 cb temperature fields are in Figure 15.

A restriction on interpretation should be clarified. Unlike the vorticity tendency equation the omega equation is not a development model; it describes steady state fields. Explanations for development and advective processes must be conservative since they are based on a subjective examination of a sequence of maps, not on a prognosis from one map to the next. Temporal trends are not clear from one map in isolation.

On July 13 the southern depression system is in two centers, one over the Gulf of St. Lawrence (134 decameters at 85 cb) and a more vigorous vortex over southern Keewatin (131 dm). The curvature of the 50 cb flow suggests steering towards the northeast. A weak localized high over Baffin Island separates this system from a deep low (122 dm) over the Polar Basin. The steep gradient of the Polar depression extends to the northern sector of Baffin Island.

The strongest uplift (Figure 7) is in the southeast quadrant of the grid; in advance of the St. Lawrence low. At 50 cb the vorticity advection along the east side of the deep trough containing the two southerly depression centers is approximately 2×10^{-9} s^{-2} and ascent due to differential vorticity advection (w_V) is strong (1.8 cm s^{-1}). Positive thickness advection resulting from the import of relatively warm air (advective heating of 1×10^{-4} kj kg^{-1} s^{-1} in this sector) contributes additional uplift (w_{TH} approaches 1 cm s^{-1}). There is a total vapour flux convergence of 0.2 mm cm^{-2} hr^{-1} (negative divergence) and this uplift promotes intense precipitation and additional ascent of 0.2 to 0.5 cm s^{-1} due to latent heat release. These factors are augmented by strong cyclonic frictional convergence (1 cm s^{-1} at the surface) and topographic uplift from onshore flow over the Torngat mountains (2 cm s^{-1} at the surface). This latter factor acts to anchor the 85 cb total vertical velocity maximum (w_T is

CONTOUR INTERVAL: LOWER RIGHT HAND CORNER
ZERO CONTOUR: HEAVY LINE

85 CB HEIGHT CONTOURS-DECAMETERS

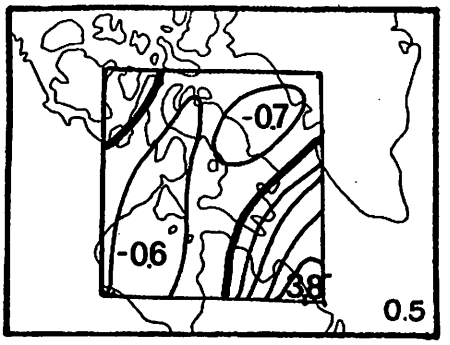

85 CB VERTICAL VELOCITY - CM. SEC.$^{-1}$ TOTAL

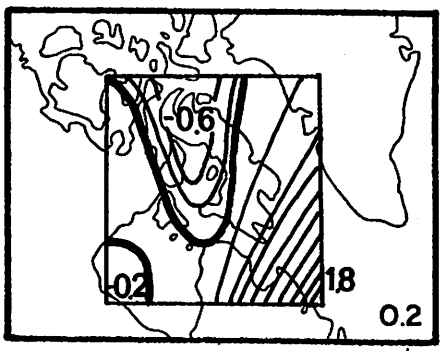

85 CB VERTICAL VELOCITY - CM. SEC.$^{-1}$ VORTICITY ADVECTION

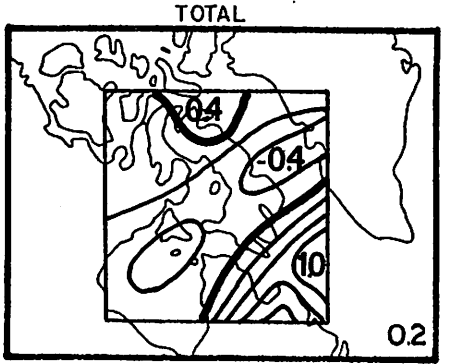

85 CB VERTICAL VELOCITY - CM. SEC.$^{-1}$ THICKNESS ADVECTION

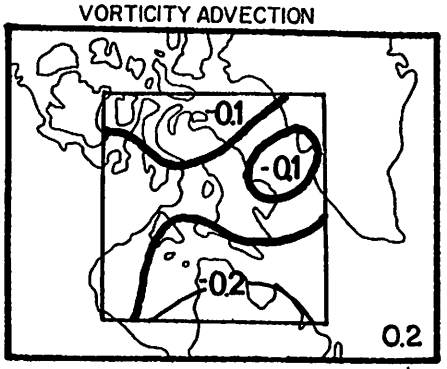

85 CB VERTICAL VELOCITY - CM. SEC.$^{-1}$ SURFACE ENTHALPY FLUX

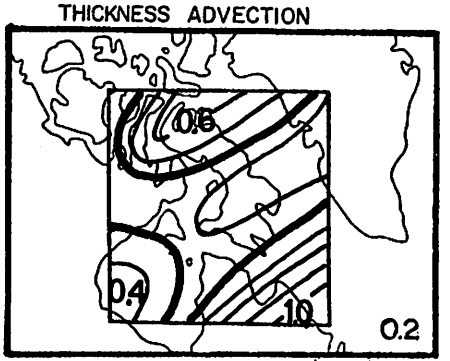

THERMAL ADVECTION - KJ. KG.$^{-1}$ SEC.$^{-1}$ $\times 10^{-4}$

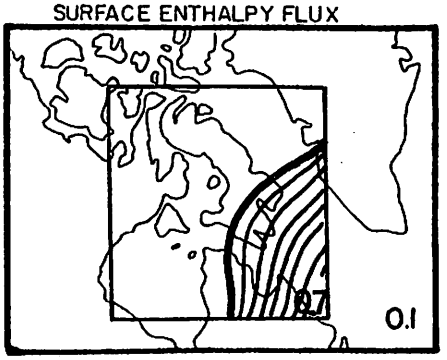

PRECIPITATION - MM HR^{-1}

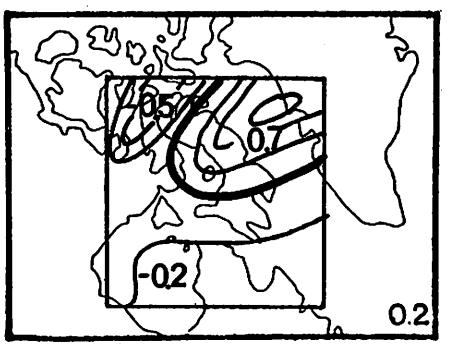

VAPOUR FLUX DIVERGENCE MM CM^{-2} HR^{-1}

FIGURE 7 SYNOPTIC ANALYSIS JULY 13 1973

4 cm s^{-1}) at this shore region. At this stage, the system exhibits the classical signs of a developing mid-latitude wave cyclone, as described by Krishnamurti (1968b). Ahead of the vortex, in the direction of the 50 cb flow, vorticity and thickness advection as well as latent heat release act in conjunction to remove mass and promote a pressure fall with attendant development of the depression.

Over the entire grid area the surface enthalpy flux is negative. The resulting cooling is a maximum in zones of maximum warm air advection - in advance of the system - since there is a maximum air-surface temperature contrast. Since it is the spatial pattern of the surface flux that determines the vertical motion related to it (w_H) there is subsidence to the south (w_H is -0.1 cm s^{-1}) acting in mild opposition to the thickness advection, while to the north there is ascent where the cooling is a relative minimum (w_H is +0.1 cm s^{-1} over central Baffin Island).

The isotherm pattern (Figure 15) is of interest since, in later maps, a cold dome forms which eventually coincides with the isobaric pattern. The result is an example of the classic cold low described by Reed (1958) and Scherhag(1957). At this map time there is a decaying primary depression to the southeast of Greenland. The northwesterly flow along the west coast of Greenland coupled with the southwesterly flow along the east side of the St. Lawrence low sets up a strong deformation field over southern Davis Strait and the Labrador Sea. With this

circulation the axis of dilation is roughly orientated northeast - southwest (cf. Palmen and Newton, 1969, pp 240) and a tongue of cold air is drawn southward over Baffin Bay. The zero degree isotherm is along the east coast of Baffin Island. The cyclonic flow from the Polar low is crossing into this tongue bringing warm air advection to the northern region (0.5×10^{-4} kj kg^{-1} s^{-1}) which acts to shift the northern sector of the tongue east. In the central Baffin Island area the circulation of the St. Lawrence depression acts in opposition, deepening the tongue to the southwest. The interaction of these three vortices set the isotherm-isobar configuration for the development of the cold low.

By July 15 the two southern depression centers have coalesced into a deep low of 124 dm over Ungava Bay. The isobaric gradient has intensified and extends into the area of northern Baffin Island where it joins the Polar Basin low; the 147 dm isoline encircles both systems. This map (Figure 8, cf. also Figure 6) represents the maturation of the system, the center weakens noticably in the next map. The synoptic sequence thus illustrates fully the decay of a mid-latitude system as it enters the Arctic.

The strongest ascent due to differential vorticity advection (w_v = 0.6 cm s^{-1}) is weaker than on the previous map and is situated to the northeast of the vortex center over Davis Strait. The 50 cb vorticity advection is 1×10^{-9} s^{-2} here. Although the location relative to the low is similar to that of the

CONTOUR INTERVAL: LOWER RIGHTHAND CORNER
ZERO CONTOUR: HEAVY LINE

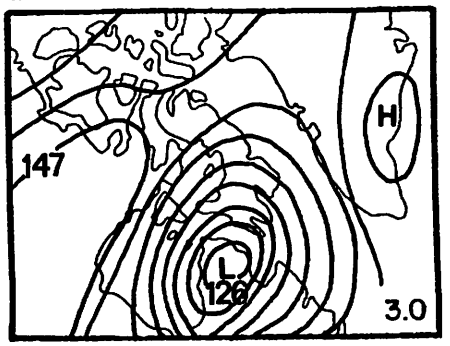

85 CB HEIGHT CONTOURS-DECAMETERS

85 CB VERTICAL VELOCITY - CM. SEC.$^{-1}$ TOTAL

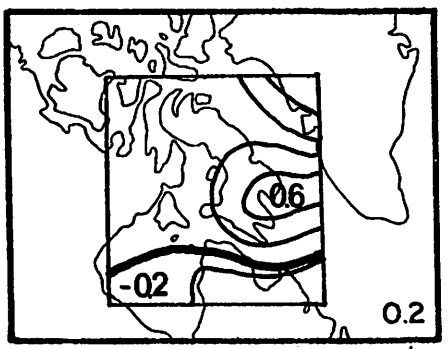

85 CB VERTICAL VELOCITY - CM. SEC.$^{-1}$ VORTICITY ADVECTION

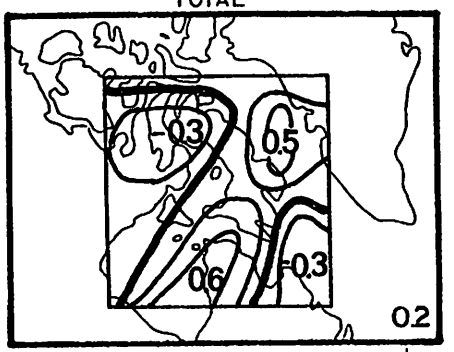

85 CB VERTICAL VELOCITY - CM SEC.$^{-1}$ THICKNESS ADVECTION

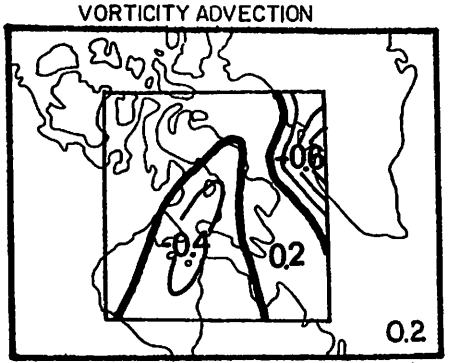

85 CB VERTICAL VELOCITY - CM. SEC.$^{-1}$ SURFACE ENTHALPY FLUX

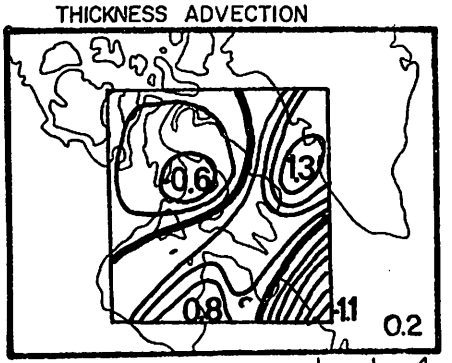

THERMAL ADVECTION - KJ. KG.$^{-1}$ SEC.$^{-1}$ x 10^{-4}

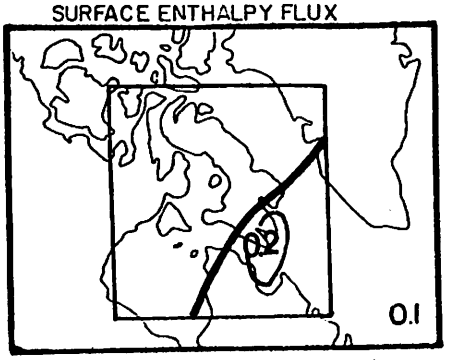

PRECIPITATION - MM HR^{-1}

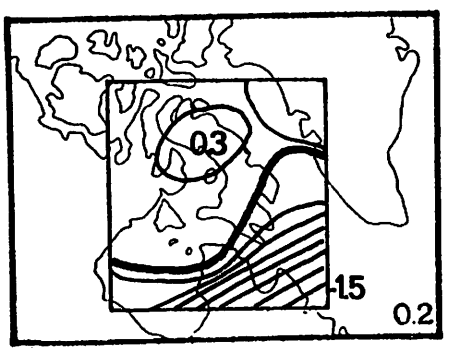

VAPOUR FLUX DIVERGENCE MM CM^{-2} HR^{-1}

FIGURE 8 SYNOPTIC ANALYSIS JULY 15 1973

13th, the magnitude of the maximum vorticity advection has decreased by one-half.

The patterns of vorticity and thickness advection are no longer coincident and, within the depression, thickness advection dominates the vertical circulation. This is characteristic of the peak of development for mid-latitude systems (Krishnamurti, 1968b). Deformation of the temperature pattern has extended into Hudson Bay and the zero degree isotherm forms a closed dome immediately to the west of the depression center. The result is warm air advection (approximately 0.8×10^{-4} kj kg^{-1} s^{-1}) to the north and west of the system with ascent of 0.6 cm s^{-1}, effectively overriding the descent due to differential vorticity advection. Where w_V is a maximum to the northeast w_{TH} is zero or slightly negative.

As the patterns of w_V and w_{TH} move out of phase local effects assume dominance. The maximum total ascent (1.5 cm s^{-1}) is to the north of the low over southeast Baffin Island. Since w_V and w_{TH} are both zero here, this is directly related to orographic precipitation effects and frictional and topographic uplift.

For this particular case the surface vertical velocities due to frictional and topographic factors are illustrated in Figure 9. The onshore southeasterly flow results in an orographic uplift of 1 cm s^{-1} over southern Baffin Island.

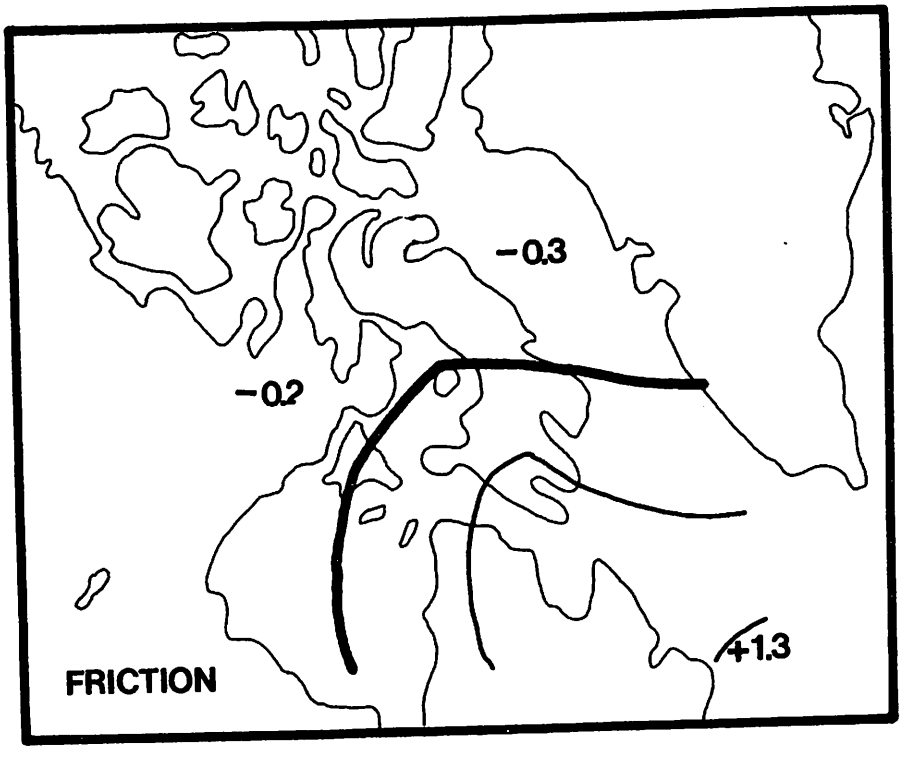

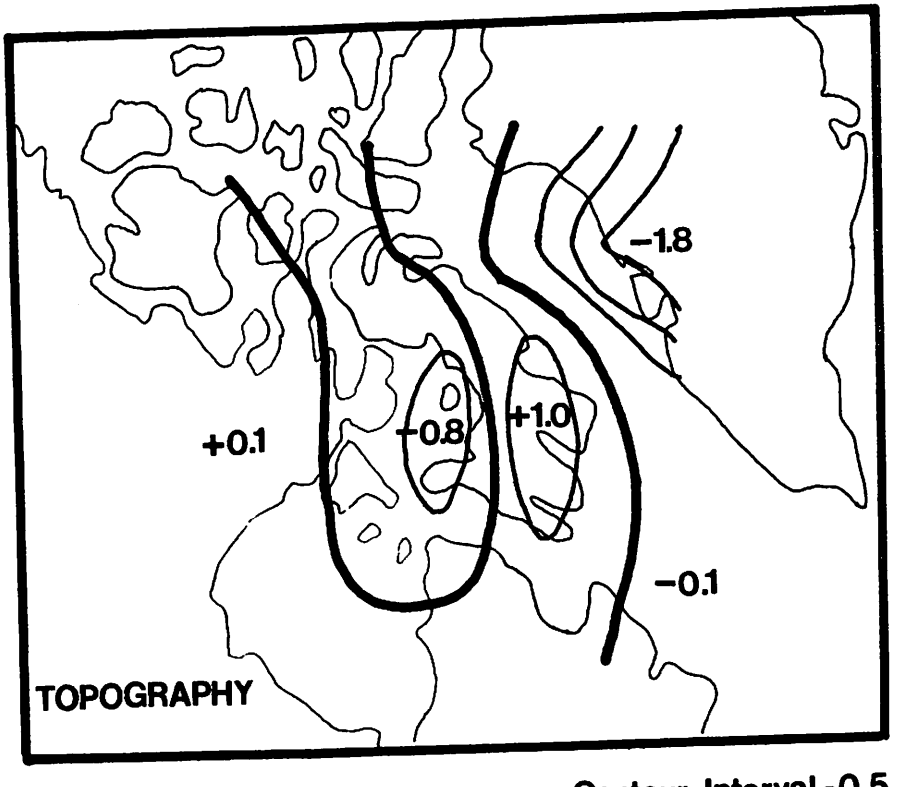

JULY 15 1973 Contour Interval - 0.5

SURFACE VERTICAL VELOCITY COMPONENTS cm sec^{-1}

Fig. 9

Over Foxe Basin, the lee side, descent is of the order of -0.8 cm s^{-1} and uplift is 0.1 cm s^{-1} over Keewatin. Note the marked influence of the Greenland ice cap (-1.8 cm s^{-1}) even though flow is more alongshore than offshore. Offshore descents may reach -4 cm s^{-1} on other dates. Frictional cross-isobaric convergence within the low vortex approaches 1.5 cm s^{-1}. A slight curvature of the isoline over southern Baffin Island due to onshore convergence and differential drag is noticable. Elsewhere there is moderate descent of the order of -0.3 cm s^{-1} due to frictional divergence.

Precipitation and latent heat release in the surface (100 to 85 cb) layer is significant in response to the orographic and frictional ascent. Heat release of 3×10^{-5} kj kg^{-1} s^{-1} is calculated over southern Baffin Island which results in additional ascent of 1 cm s^{-1} at 85 cb. As before, the net vapour flux divergence is negative in this northeast sector of the depression (-1.5 mm cm^{-2} hr^{-1}).

The surface enthalpy flux results in a cooling except over Baffin Island where the warm surface coupled with negative temperature advection promotes a heating of 4×10^{-5} kj kg^{-1} s^{-1} at 85 cb with a strong local ascent approaching 0.7 cm s^{-1} over the east coast. Note that this augments local topographic, frictional and latent heat effects in this sector. Elsewhere the advective pattern is the predominant control on w_H. Generally w_H and w_{TH} are in opposition. The two are nearly equal in magnitude over Davis Strait and the Labrador Sea

while over Foxe Basin and Hudson Bay, in the region of the cold dome, thickness advection has a much greater effect.

Part of the cold dome is off the grid and a complete examination of the internal energy exchanges is not possible until the next example.

This map illustrates the maturation of a mid-latitude low in the subarctic. Vorticity and thickness advection patterns are out of phase with the latter dominating the vertical motion field within the depression. Considering only these two parameters at 85 cb the vertical motion in the vortex center would be near zero. The surface frictional convergence and uplift of 0.5 cm s^{-1} would rapidly fill the system in the lower troposphere leading to decay. Any displacement would be a response to the steering of the large scale flow. However there is strong ascent and concomitant pressure fall to the north related to local effects.

The importance of these local controls is apparent on July 17 (Figure 10) when the depression center has moved northward to south Baffin Island. It has weakened to 130 dm and the regional scope of the cyclonic circulation is much more restricted as compared to July 15. The Polar low remains unchanged.

The decay of the system is reflected in the advective terms. The pressure pattern is almost in phase in the vertical (other pressure levels are not shown) such that there is very little differential vorticity advection over the system center.

CONTOUR INTERVAL: LOWER RIGHTHAND CORNER
ZERO CONTOUR: HEAVY LINE

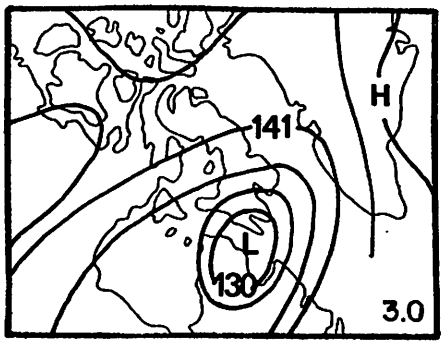

85 CB HEIGHT CONTOURS-DECAMETERS

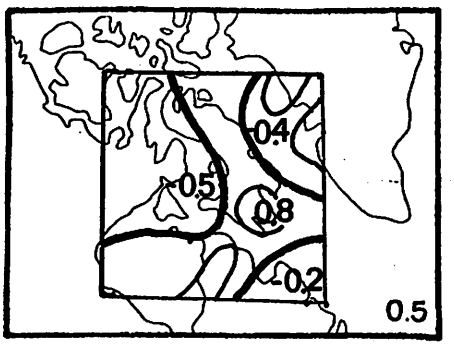

85 CB VERTICAL VELOCITY - CM. SEC.$^{-1}$
TOTAL

85 CB VERTICAL VELOCITY - CM. SEC.$^{-1}$
VORTICITY ADVECTION

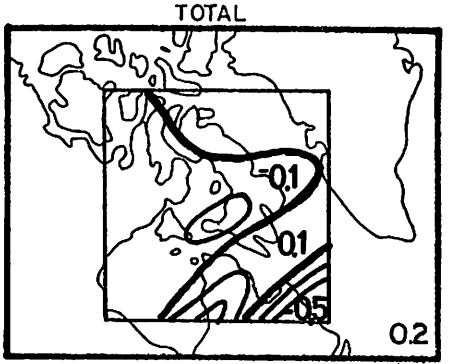

85 CB VERTICAL VELOCITY - CM. SEC.$^{-1}$
THICKNESS ADVECTION

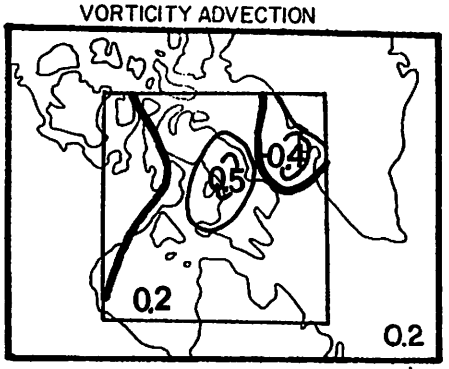

85 CB VERTICAL VELOCITY - CM. SEC.$^{-1}$
SURFACE ENTHALPY FLUX

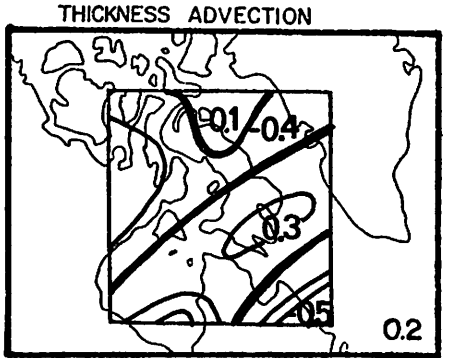

THERMAL ADVECTION - KJ. KG.$^{-1}$ SEC.$^{-1}$ $\times 10^{-4}$

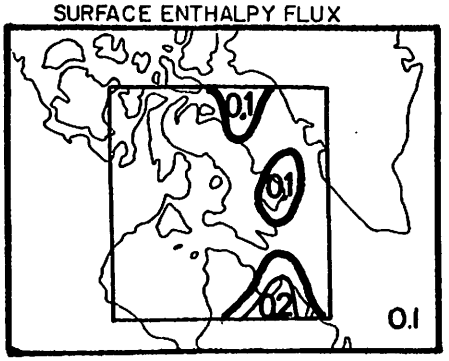

PRECIPITATION - MM HR^{-1}

VAPOUR FLUX DIVERGENCE
MM CM^{-2} HR^{-1}

FIGURE 10 SYNOPTIC ANALYSIS JULY 17 1973

w_V is almost zero here. To the northeast of the system the 50 cb vorticity advection is still positive but has been reduced to 1 x 10^{-10} s^{-1} (this may be suspect on account of NMC analysis errors over Greenland) as the circulation weakens and vorticity generation and export of the depression falls.

The isobaric and isotherm patterns at 85 cb are almost coincident. The geostrophic thickness advection results in a vertical circulation of less than $\pm$ 0.1 cm s^{-1} within the low and acts to oppose the equally small vorticity effect. Only in the northeast sector does one factor, the differential vorticity advection, predominate, but this uplift is cancelled by orographic descent. The advective fields have a negligible net influence on the synoptic system.

The low is stabilized, however, by strong net ascent (0.8 cm s^{-1}) within the vortex, with the result that the system remains anchored here for three days. Again, this may be attributed entirely to local effects. Over the Hall Peninsula region surface orographic uplift is 0.3 cm s^{-1}, there is a strong onshore frictional convergence of 0.6 cm s^{-1}, the release of latent heat (1 x 10^{-5} kj kg^{-1} s^{-1}) contributes o.1 cm s^{-1} at 85 cb and the enthalpy heating by the warm land surface under the cold dome contributes an additional 0.5 cm s^{-1}.

The near coincidence of the isothermal (Figure 15) and isobaric patterns is a classic indicator of an occluding

system (Palmen and Newton, 1969) and also defines a cold low which can be first discerned at this stage for this example. The zero line of horizontal advection runs through the closed zero degree isotherm which encompasses two computational grid points, one to the northwest and one to the southeast of the cold dome over southeast Baffin Island. With the circulation of July 17 there is warm air advection on the upstream (southeast) side of 5×10^{-6} kj kg^{-1} s^{-1} and cooling of -4×10^{-6} kj kg^{-1} s^{-1} on the downstream (northwest)side. However, there is a reverse trend due to the surface enthalpy flux with a heating of 2×10^{-5} kj kg^{-1} s^{-1} over land to the northwest and a cooling of -1×10^{-5} kj kg^{-1} s^{-1} over Davis Strait. Over land there is a latent heat release of 2×10^{-5}kj kg^{-1} s^{-1} and over water to the southeast it is 1×10^{-5} kj kg^{-1} s^{-1}. Corresponding cooling rates by vertical advection (adiabatic expansion) are -3×10^{-5} and -1×10^{-5} kj kg^{-1} s^{-1} - the orographic influence is evident. Noting the restrictions of the coarse grid resolution and approximate nature of the parameterizations we can estimate the total 85 cb energy exchange within the cold low to $+6 \times 10^{-6}$ kj kg^{-1} s^{-1} to the northwest and -5×10^{-6} kj kg^{-1} s^{-1} to the southeast. Thus, there is a net intensification of the cold dome to the southeast which may be traced to the dominance of adiabatic expansion over advective heating. This dominance of vertical expansion was also noted by Reed and Tank (1956) and Scherhag (1957). The 85 cb cooling in this sector is approximately -0.4 C^{o} dy^{-1}. However, the

decay to the northwest is traced to the failure of the combined effects of adiabatic expansion and advective cooling to exceed heating by the surface enthalpy flux and precipitation. The heating is approximately 0.5 C^{o} dy^{-1}.

By July 19 (Figure 11) the depression center has shifted slightly toward the northeast - still influenced by the strong localized ascent over Baffin Island. It is no longer a closed low but forms part of a southeast trough extension of the Polar Basin low which is over the Queen Elizabeth Islands.

With this slight displacement, the flow over Baffin Island is from the northwest and there is orographic descent of -0.2 cm s^{-1} at the surface over the east coast. The cold dome is displaced slightly eastwards, as anticipated from the energy exchange considerations on July 17, and as a result there is a broad region of negative thickness advection within the depression with a maximum that coincides with the orographic descent to produce a region of net subsidence at 85 cb within the low. On the west coast of Greenland southerly air is flowing into the cold dome (+2 x 10^{-5} kj kg^{-1} s^{-1}) with a moderate positive w_{TH} of 0.3 cm s^{-1}. This adds to the positive vorticity advection along the east side of the trough (1 x 10^{-9} s^{-2} at 50 cb, the increase from the previous day probably reflects the combined circulation of the Polar and Baffin Island low around the trough) which contributes an ascent of 0.5 cm s^{-1}. As a result, there is precipitation and latent heat release (4 x 10^{-5} kj kg^{-1} s^{-1}). The total uplift approaches 1.3

CONTOUR INTERVAL LOWER RIGHTHAND CORNER
ZERO CONTOUR: HEAVY LINE

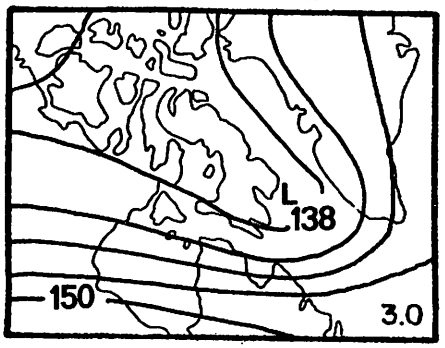

85 CB HEIGHT CONTOURS-DECAMETERS

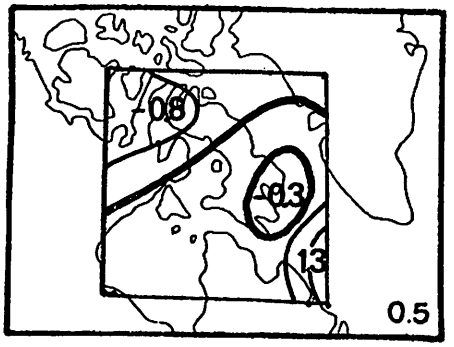

85 CB VERTICAL VELOCITY - CM. SEC.$^{-1}$ TOTAL

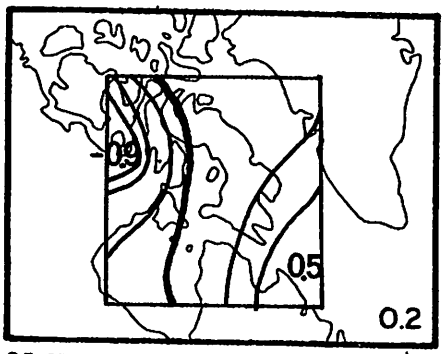

85 CB VERTICAL VELOCITY - CM. SEC.$^{-1}$ VORTICITY ADVECTION

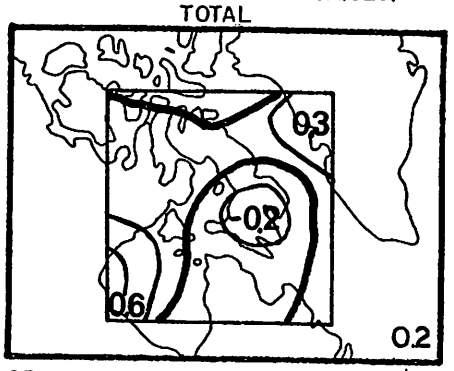

85 CB VERTICAL VELOCITY - CM. SEC.$^{-1}$ THICKNESS ADVECTION

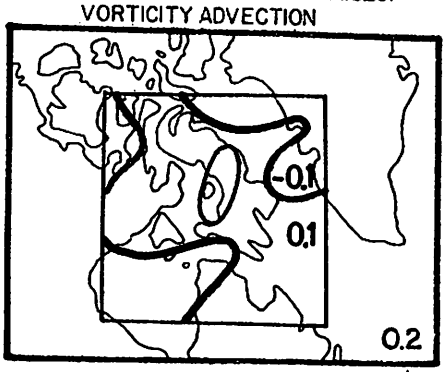

85 CB VERTICAL VELOCITY - CM. SEC.$^{-1}$ SURFACE ENTHALPY FLUX

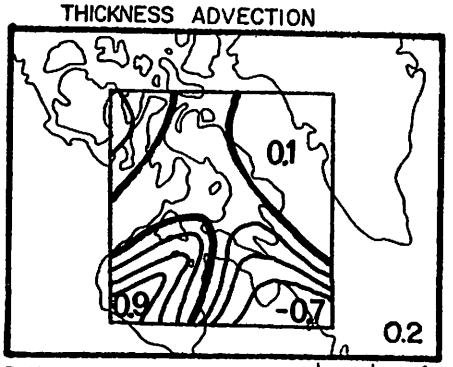

THERMAL ADVECTION - KJ. KG.$^{-1}$ SEC.$^{-1}$ $\times 10^{-4}$

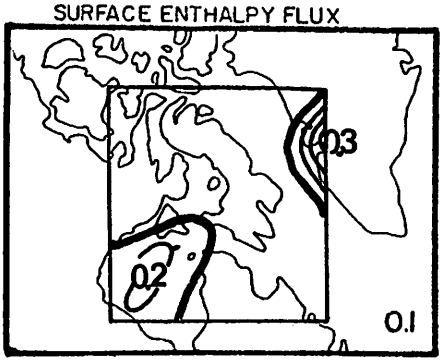

PRECIPITATION - MM HR^{-1}

VAPOUR FLUX DIVERGENCE MM CM^{-2} HR^{-1}

FIGURE II SYNOPTIC ANALYSIS JULY 19 1973

cm s^{-1} along the east side of the trough ahead of the depression promoting vortex development in this direction.

Two features are worthy of note. The influence of the Polar low is now evident in the positive thermal advection (4×10^{-5} kj kg^{-1} s^{-1}) to the northwest as cyclonic flow crosses the isotherms (Figure 15) of the cold tongue. This increases in magnitude and southward extent in the next map. There is also an 'anomolous' precipitation zone on the west limb of the trough where there should be net subsidence (cf. synoptic discussion in Chapter Three) due to negative thickness and vorticity advection. However, there is significant onshore frictional convergence and orographic uplift along the west shore of Baffin Island with a total surface ascent of 0.3 to 0.5 cm s^{-1}. This is responsible for the net uplift and precipitation at 85 cb.

The configuration of the cold dome (Figure 15) with respect to the isobars is such that inflow is from the northwest across a very weak temperature gradient with a small horizontal advective heating of 4×10^{-7} kj kg^{-1} s^{-1}. The advective cooling at the outflow, to the northeast (note the reversal of relative flow from July 17) is -3×10^{-5} kj kg^{-1} s^{-1}. The corresponding figures for the surface enthalpy flux effect are 1×10^{-7} kj kg^{-1} s^{-1} over land at the inflow and -6×10^{-6} kj kg^{-1} s^{-1} over south Baffin Bay. The adiabatic effect is positive (1×10^{-5} kj kg^{-1} s^{-1}) over land due to subsidence in the lee side of Baffin Island, and

negative at the outflow (-6×10^{-6} kj kg^{-1} s^{-1}). The net result at the outflow region is a strong cooling of 3.6 C^{o} dy^{-1}, dominated by advective cooling in this situation. At the inflow adiabatic compression dominates a heating of 1 C^{o} dy^{-1}. The conclusion of Reed and Tank (1956) and Reed (1958) that adiabatic cooling is the dominating factor in the maintenance of the cold low is obviously an oversimplification. The controlling parameter changes with shifts in the isobar-isotherm patterns and in relations between local features and the large scale flow. It is necessary to use more detailed grid resolution to make more confident conclusions.

With the eastward displacement of the cold dome w_{TH} becomes significantly positive to the east-southeast of the depression. This augments an increased w_V as the circulation intensity increases with the combination of the Polar and Baffin Island lows in a trough. There is a definite impetus for development towards the south of Greenland resulting from advective effects. Note the increased thickness advection has its roots in local intensification of the cold dome on the previous map.

On July 21 (Figure 12) the vortex has indeed moved southeast and the height of the 85 cb surface is stabilized. It remains at 136 dm from July 19 through 21 (Figure 6). The Polar low has deepened to 120 dm and the increased influence is evident in the cyclonic curvature over the northern half of the grid. Over the southern section the anticyclonic

CONTOUR INTERVAL LOWER RIGHTHAND CORNER
ZERO CONTOUR: HEAVY LINE

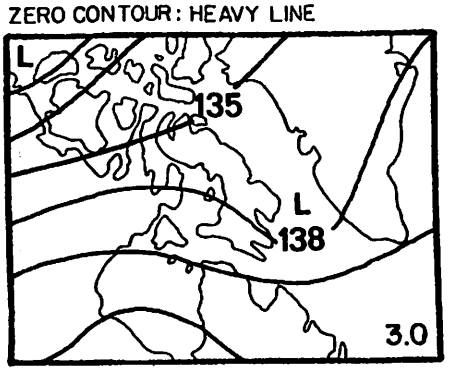

85 CB HEIGHT CONTOURS-DECAMETERS

85 CB VERTICAL VELOCITY - CM. SEC.$^{-1}$
TOTAL

85 CB VERTICAL VELOCITY - CM. SEC.$^{-1}$
VORTICITY ADVECTION

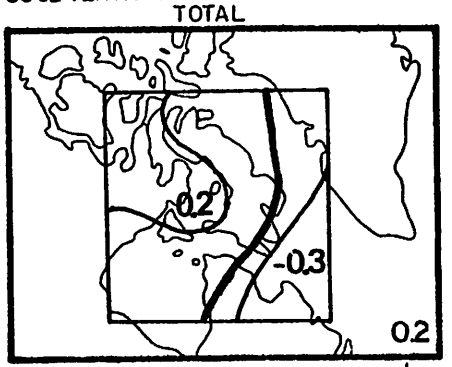

85 CB VERTICAL VELOCITY - CM. SEC.$^{-1}$
THICKNESS ADVECTION

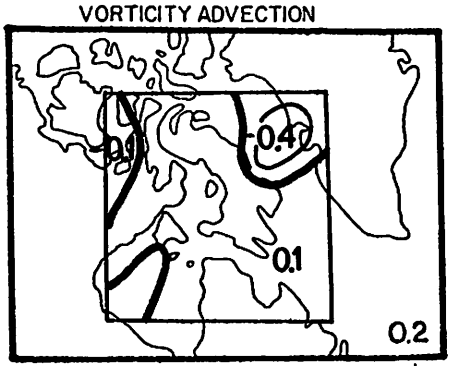

85 CB VERTICAL VELOCITY - CM. SEC.$^{-1}$
SURFACE ENTHALPY FLUX

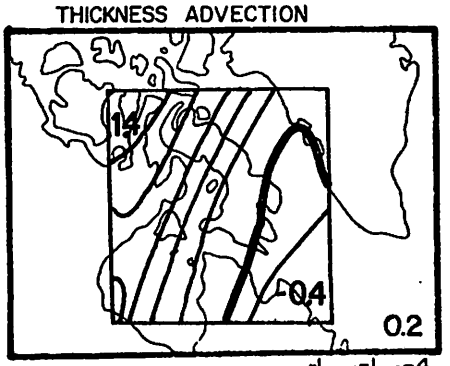

THERMAL ADVECTION - KJ. KG.$^{-1}$ SEC.$^{-1}$ $\times 10^{-4}$

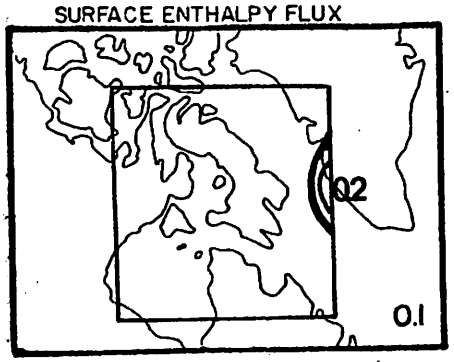

PRECIPITATION - MM HR^{-1}

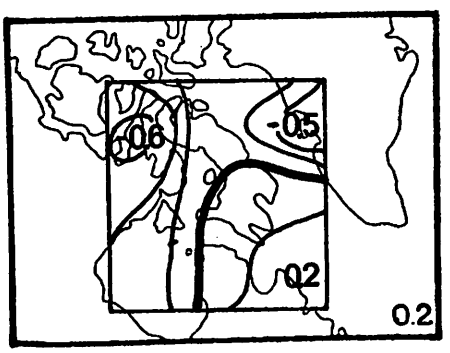

VAPOUR FLUX DIVERGENCE
MM CM^{-2} HR^{-1}

FIGURE 12 SYNOPTIC ANALYSIS JULY 21 1973

curvature is part of a major high over the central Canadian plains. The net result of the two opposing systems is strong upper level diffluence over the Baffin Bay-Davis Strait region. This phase may be considered as a transition between the dominance of a southerly depression system and the Polar low, the development of the latter paradoxically initiating a period of strong positive thermal advection over the Baffin Island region.

The relative warming is a result of west - northwest flow into the cold dome (Figure 15), which is now stationed over Davis Strait. It is behind the southern depression and the cold low configuration no longer exists. The advective warming and adiabatic compression at the inflow of the cold dome (northwest sector) is 4×10^{-6} kj kg^{-1} s^{-1} and 1×10^{-5} kj kg^{-1} s^{-1}, respectively. The corresponding figures at the outflow sector are -6×10^{-6} kj kg^{-1} s^{-1} and -1×10^{-5} kj kg^{-1} s^{-1}. However, cooling at both locations due to downward enthalpy flux toward the water surface is strong (-4×10^{-5} kj kg^{-1} s^{-1}). The dominance of this latter factor over adiabatic and advective effects no doubt accounts for the anchoring of the cold dome over Davis Strait behind the low for the period from July 20 to 23.

The pattern of w_v opposes the ascent to the west and descent to the east due to this thickness advection. The trough containing the low along the west coast of Greenland promotes uplift due to positive differential vorticity advection and

to the west the anticyclonic curvature around the mid-plains high seems to predominate. However, the combined effects of the weak opposing fields of w_V and w_{TH} seems to result in a broad region of quiescent vertical circulation. With this nearly zonal flow topographic controls are again important. Over Greenland the orographic uplift (0.2 to 2.0 cm s^{-1}) and onshore frictional convergence (0.3 to 0.5 cm s^{-1}) combine to produce strong ascent in this sector. This is reinforced by latent heat release with additional uplift of 0.2 cm s^{-1} at 85 cb. Over west Davis Strait-Baffin Bay there is a general subsidence due to combined topographic descent in the lee of Baffin Island (-0.4 cm s^{-1}) and frictional effects (-0.2 cm s^{-1}) as air accelerates eastward from land to sea.

The Polar low has shifted to the east and extended the cyclonic influence in the grid region by July 23 (Figure 13). On July 22 it had reached the maximum depth of 116 dm. The trough extension along the west coast of Greenland on the previous map (Figure 12) is now almost a cutoff low between Greenland and Iceland with a relatively shallow height of 135 dm. The northwest flow along the west side of this trough has shifted the cold dome to the south near the coast of Labrador.

The contribution by differential vorticity and thickness advection is still weak. The maximum w_V of +0.6 cm s^{-1} is located over northern Baffin Island where the cyclonic circulation is analagous to a mid-latitude trough with positive

CONTOUR INTERVAL: LOWER RIGHTHAND CORNER
ZERO CONTOUR: HEAVY LINE

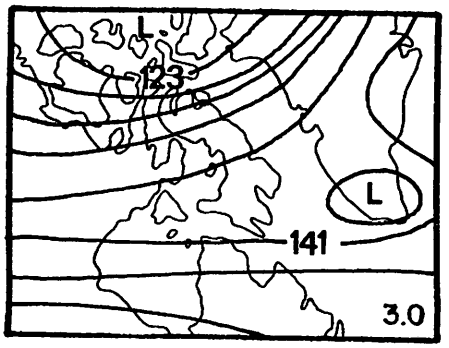

85 CB HEIGHT CONTOURS-DECAMETERS

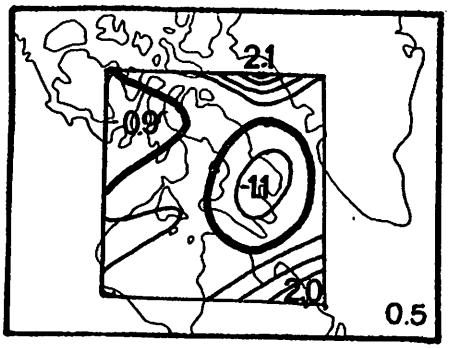

85 CB VERTICAL VELOCITY - CM. SEC.$^{-1}$
TOTAL

85 CB VERTICAL VELOCITY - CM. SEC.$^{-1}$
VORTICITY ADVECTION

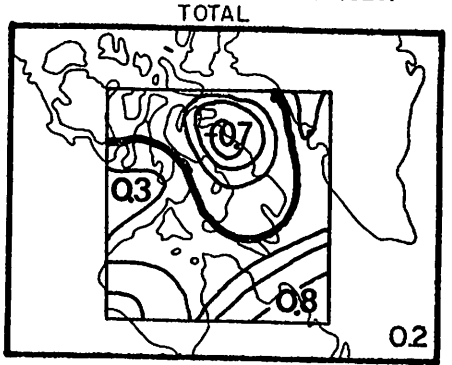

85 CB VERTICAL VELOCITY - CM. SEC.$^{-1}$
THICKNESS ADVECTION

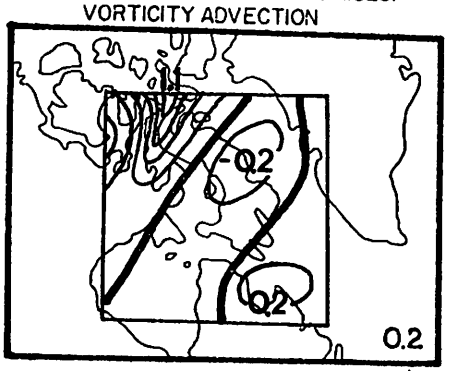

85 CB VERTICAL VELOCITY - CM. SEC.$^{-1}$
SURFACE ENTHALPY FLUX

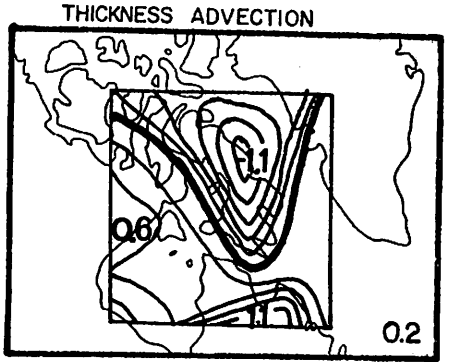

THERMAL ADVECTION - KJ. KG.$^{-1}$ SEC.$^{-1}$ x 10^{-4}

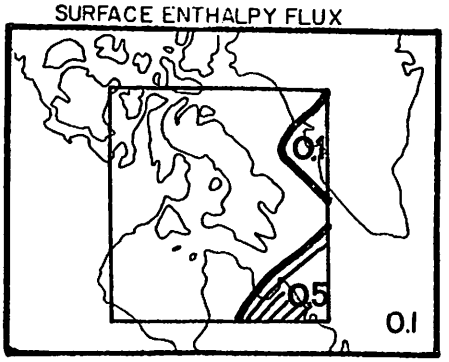

PRECIPITATION - MM HR^{-1}

VAPOUR FLUX DIVERGENCE
MM CM^{-2} HR^{-1}

FIGURE 13 SYNOPTIC ANALYSIS JULY 23 1973

vorticity advection to the east and negative advection and descent along the western limb. To the southeast the anticyclonic curvature represents an export of vorticity from the high towards the low to the east of Greenland with a corresponding descent of -0.7 cm s^{-1}.

The Baffin Bay maximum of w_V is opposed by w_{TH}(-0.7 cm s^{-1}) as cold air is transported from the temperature minimum over the Queen Elizabeth Islands. Over Davis Strait positive thickness advection and warming is associated with the same flow but which is directed into the cold tongue (Figure 15). It is a combination of the Polar low circulation and the position of the cold tongue (previously a part of the southerly depression system) which accounts for the marked warming interval around July 21 (Figure 5). The effect subsided as the cold dome shifted southward.

As on the 21st, extremes of w_V and w_{TH} are nearly self-cancelling and the major vertical motion features are related to the local effects, predominantly the strong orographic ascent of 4 cm s^{-1} at the surface over western Greenland. Net subsidence over Baffin Island is clearly related to topographic descent and frictional divergence of the anticyclonic curvature.

The map of July 25 (Figure 14) illustrates the decay of the Polar low to 133 dm as it drifts southward along the west coast of Greenland, undoubtedly prompted by strong surface orographic ascent and latent heat release in this area on the previous map(Figure 13).

CONTOUR INTERVAL LOWER RIGHTHAND CORNER
ZERO CONTOUR: HEAVY LINE

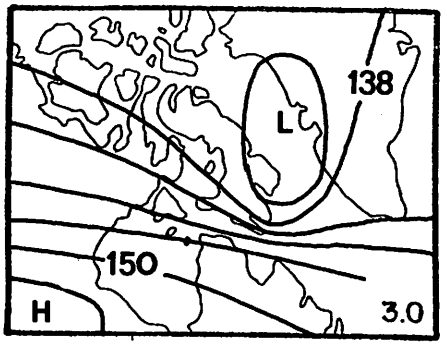

85 CB HEIGHT CONTOURS-DECAMETERS

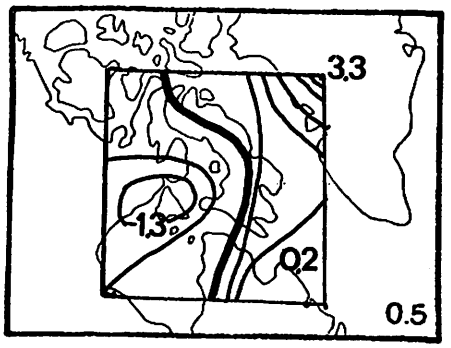

85 CB VERTICAL VELOCITY - CM. SEC.$^{-1}$
TOTAL

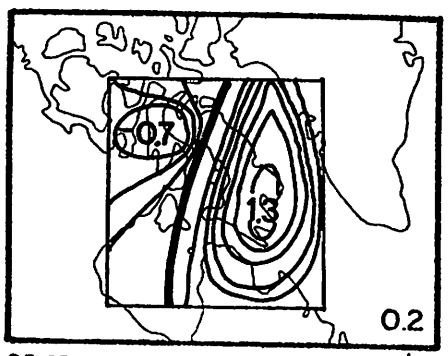

85 CB VERTICAL VELOCITY - CM. SEC.$^{-1}$
VORTICITY ADVECTION

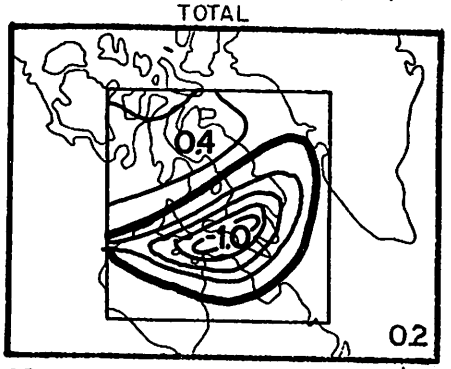

85 CB VERTICAL VELOCITY - CM. SEC.$^{-1}$
THICKNESS ADVECTION

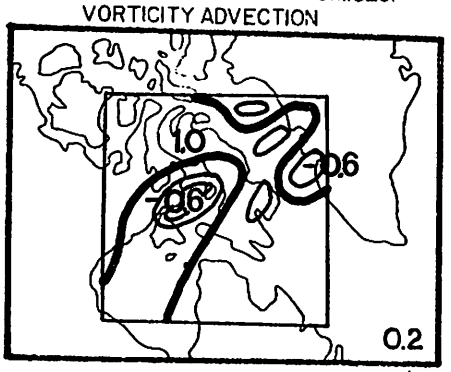

85 CB VERTICAL VELOCITY - CM. SEC.$^{-1}$
SURFACE ENTHALPY FLUX

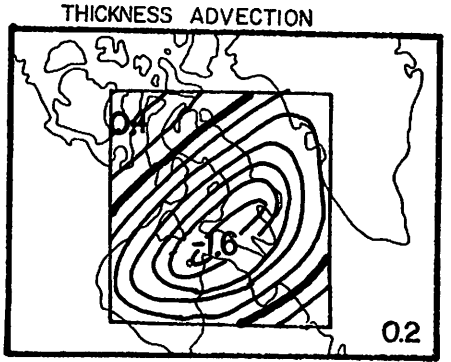

THERMAL ADVECTION - KJ. KG.$^{-1}$ SEC.$^{-1}$ $\times 10^{-4}$

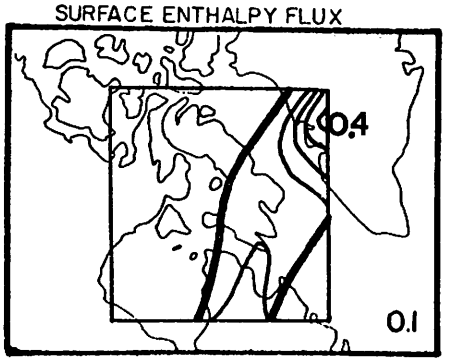

PRECIPITATION - MM HR^{-1}

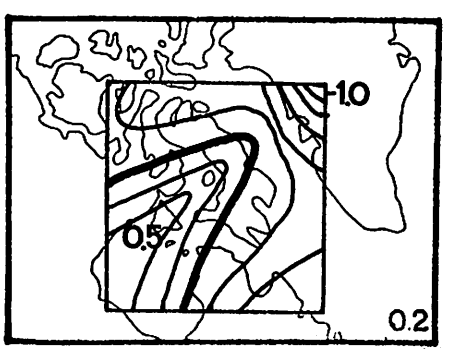

VAPOUR FLUX DIVERGENCE
MM CM^{-2} HR^{-1}

FIGURE 14 SYNOPTIC ANALYSIS JULY 25 1973

With the southward intrusion of the low, coupled with the almost complete disappearance of the cold tongue, there is a general negative thermal advection approaching -2×10^{-4} kj kg^{-1} s^{-1} at Baffin Island. The cold advection accentuates the effects of land-sea temperature contrast on the surface enthalpy flux. Over Baffin Island the positive heating approaches 8×10^{-5} kj kg^{-1} s^{-1} in the north and 2×10^{-5} kj kg^{-1} s^{-1} in the south as compared with a cooling of -4×10^{-5} kj kg^{-1} s^{-1} over central Davis Strait. The abruptness of the change gives rise to intense gradients of w_H : 1.0 cm s^{-1} over Baffin Island and -0.5 cm s^{-1} over Foxe Basin and Davis Strait. Under conditions of warm air advection the fluxes over land are reduced and horizontal gradients are subdued with the result that the resultant vertical motion field of w_H does not have the intense gradients and extremes of this case.

As expected from the classical model of trough circulation there is strong ascent due to positive vorticity advection at the base of the wave (1.3 cm s^{-1}) and descent to the west (-0.7 cm s^{-1}). Both extremes are much stronger than on the previous example. However, they are opposed by the thickness advection to produce a quiescent vertical motion field, the noticeable exceptions may be attributed to local factors.

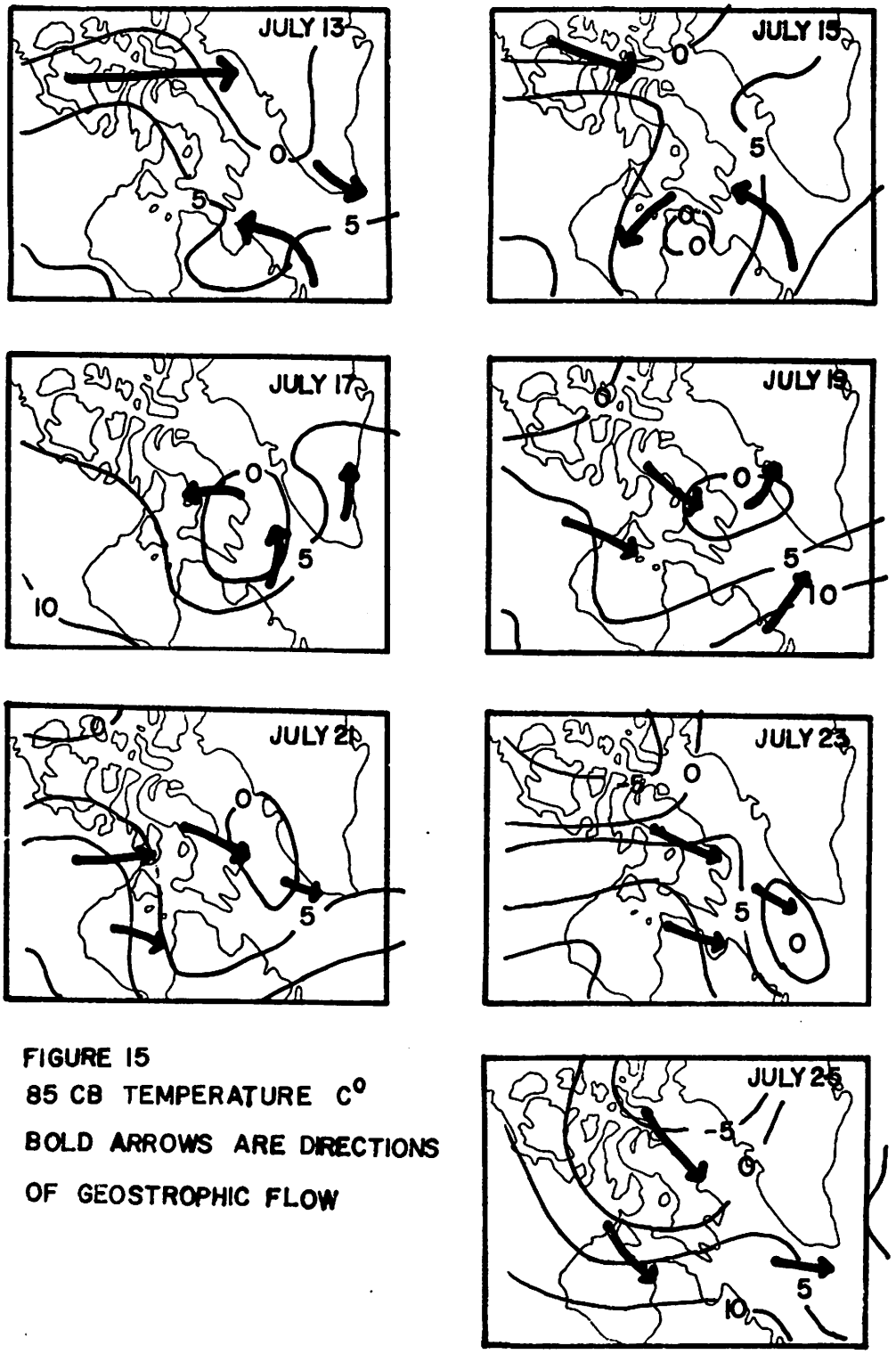

FIGURE 15
85 CB TEMPERATURE C^0
BOLD ARROWS ARE DIRECTIONS
OF GEOSTROPHIC FLOW

85 cb Thermal Regime for East Baffin Island, Davis Strait and Baffin Bay

Since the period studied in the preceding section was selected partly on the basis of the interesting temperature and ice melt episode it is useful to examine some thermal characteristics of the synoptic event at selected locations. The model generated heating rates at 85 cb are presented in Table VI and Figure 16 for east Baffin Island, Baffin Bay and Davis Strait. The data for Baffin Island most closely represent the synoptic data for Broughton Island in Figure 5. In Figure 17 the positions of maxima of horizontal thermal advection within the grid region are plotted. The "trajectories" of these centers are based on subjective interpretation of Figures 7 through 14. There is a boundary problem in that the absolute maximum for a given system may be off the grid. This map should not, therefore, be considered as a complete analysis but serve only to indicate sectors where advective influences are prominent and the probable time-space relationships of these centers.

The two warming periods identified in Figure 5 are evident at 85 cb (Figure 16) for east Baffin Island. There is a small warming of 4 C^{o} centered on July 16 and a major episode around July 22. At Broughton Island the recorded 48 hr ice melt (beginning on July 19) was 25 cm, the highest rate observed during the 1973 season. The interval between observations was too great to associate a definite melt rate

TABLE VI

85 CB THERMAL DATA FOR SELECTED LOCATIONS

Line 1: east Baffin Island
Line 2: Davis Strait
Line 3: Baffin Bay

Date	Heating Rates: kj kg^{-1} s^{-1}				Temperature: ^{o}C
July	Vertical Advection	Horizontal Advection	Surface Enthalpy Flux	Latent Heat Release	
13	2.1E-5	-2.3E-5	-5.4E-7	0	0.5
	4.4E-6	1.5E-5	-5.5E-6	0	2.2
	-5.5E-6	3.4E-5	-6.1E-6	0	2.5
14	-1.2E-5	-3.6E-5	8.1E-6	0	2.4
	-1.1E-5	2.8E-4	-1.9E-5	0	-0.8
	-4.0E-5	-1.7E-5	-3.6E-6	0	3.2
15	-4.0E-5	-5.8E-5	3.7E-5	0	3.0
	-2.6E-5	4.4E-5	-1.1E-5	1.1E-5	3.8
	-1.5E-5	4.1E-6	-6.5E-6	0	-4.0
16	-6.9E-5	3.6E-5	3.9E-5	0	4.2
	-2.1E-5	-4.0E-6	-8.8E-6	0	4.2
	2.9E-6	2.2E-5	-9.5E-6	0	2.7
17	-3.7E-5	-1.1E-5	3.3E-5	1.6E-5	0.2
	-1.7E-5	3.3E-5	-6.8E-6	6.3E-6	-1.4
	-2.3E-5	-7.8E-6	-1.9E-5	1.3E-5	3.1
18	-9.5E-6	3.3E-6	7.0E-6	4.3E-6	-0.3
	-1.9E-5	3.7E-5	-6.3E-6	9.3E-6	1.4
	-1.1E-5	-1.4E-5	-6.5E-6	0	2.8
19	-8.0E-6	4.0E-7	1.2E-7	4.0E-6	0.5
	-1.0E-5	-3.3E-5	-5.7E-6	5.2E-6	2.0
	7.6E-6	4.1E-6	-5.9E-6	0	0.3
20	-1.7E-7	1.0E-5	-1.8E-6	4.5E-7	0.5
	4.9E-6	-6.3E-5	-1.1E-5	0	-0.3
	-2.5E-5	-1.2E-5	-4.5E-6	1.2E-5	2.0
21	1.3E-5	4.5E-6	-4.3E-6	0	2.5
	3.1E-7	1.1E-6	-1.6E-5	5.2E-7	1.4
	-5.6E-6	6.9E-6	-4.4E-6	3.4E-6	0.7
22	3.8E-5	8.5E-5	-2.4E-5	0	7.1
	9.8E-6	2.2E-5	-8.3E-5	0	2.8
	-1.7E-5	4.2E-5	-3.5E-5	0	5.7
23	5.3E-5	-9.2E-5	-4.0E-5	0	3.6
	8.9E-6	-5.0E-7	-1.6E-5	0	7.0
	-1.3E-4	-4.2E-5	-1.6E-5	0	-2.0
24	-4.3E-5	-9.6E-5	7.7E-6	0	2.1
	-2.0E-5	6.0E-5	-1.8E-5	0	11.0
	-5.0E-5	1.1E-6	-4.5E-6	0	-7.1
25	-6.6E-5	-8.2E-5	6.9E-5	2.0E-5	-6.3
	-5.9E-5	-1.2E-4	-7.4E-6	2.5E-5	-0.8
	-1.4E-5	2.6E-5	-5.1E-6	0	-4.3

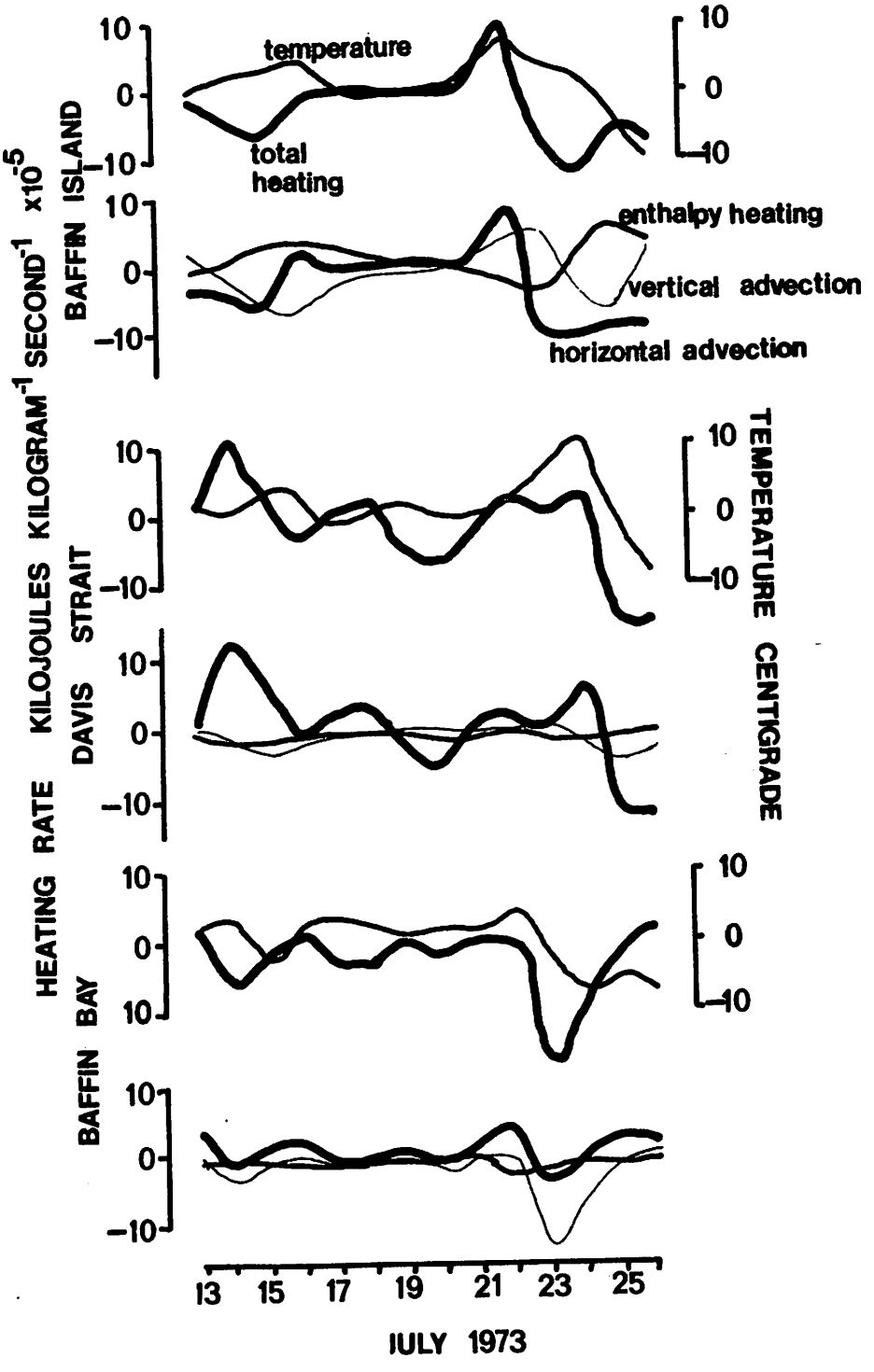

Figure 16 85 CB HEATING RATES

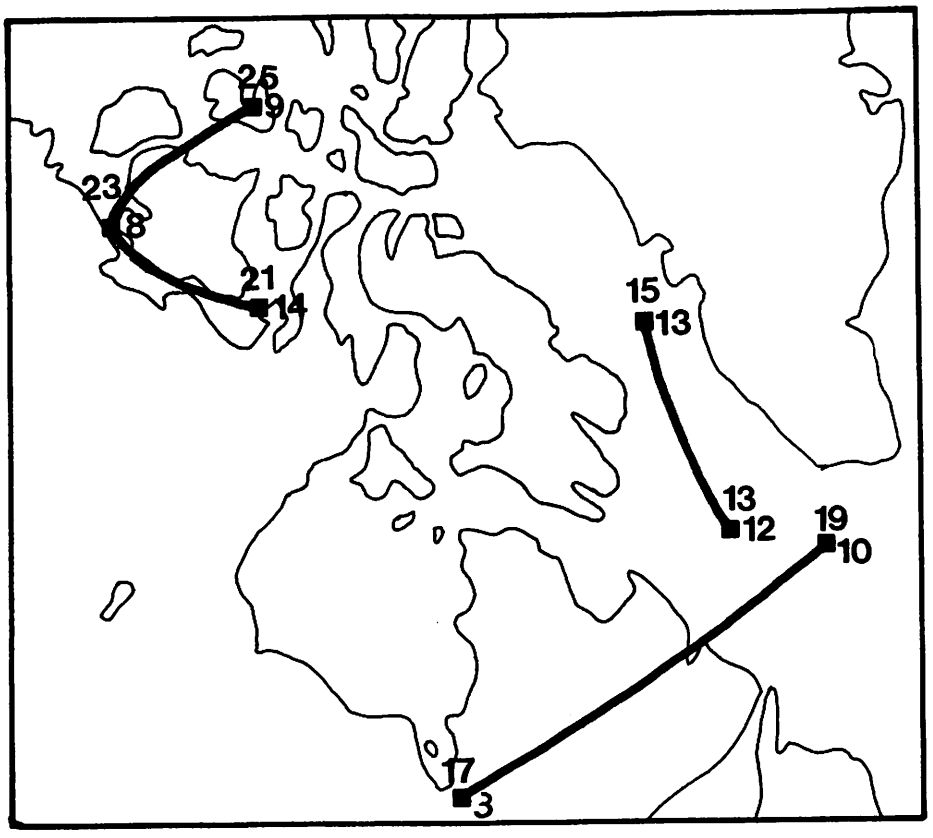

19 DATE JULY 1973
■10 ADVECTIVE HEATING KJ $KG^{-1}S^{-1} * 10^{-5}$

Figure 17 CENTERS OF ADVECTIVE HEATING AT 85 CB

with the first warming episode, but it was noticeably smaller.

The net heating attributed to horizontal advection, vertical (adiabatic) advection, surface enthalpy flux and latent heat release does not correspond very well with the temperature trend (Figure 16). This may be related to the accumulation of errors (most suspect is the surface enthalpy flux), the coarse grid resolution used to calculate the advective components and the fact that the data represent instantaneous rates at a point rather than accumulated energy (indicated by temperature) between observations. Despite these restrictions there is some indication of a net heating increase on July 16 at Baffin Island and the maximum of July 22 is clear.

The development of the cold tongue in the Baffin Island region as a result of shear between the St. Lawrence low and the primary depression southeast of Greenland has been discussed in the previous section. The formation of this feature accounts for the unexpected sharp drop in temperature from the maximum on July 12 (Figure 5) while the regional pressure drops as the southerly depression moves north. The delayed warming episode on July 16 was initiated by strong horizontal advective heating (cf Figure 17) when the depression intensified over north Quebec and the increased circulation brought southerly air into the cold dome over Baffin Island. The regional effect is more obvious in the Davis Strait illustration (Figure 16) where advective heating increased sharply on July 14 to 12 x 10^{-5} kj kg^{-1} s^{-1}

(equivalent to 10 C^{o} dy^{-1}). The warmed air would subsequently be advected northwest under the cyclonic regime. This explains the relative delay of advection maximum and the lower rate over Baffin Island.

Over Baffin Island the horizontal advective heating is of the same scale as the surface heating during this early episode, but both values are opposed by adiabatic expansion resulting from orographic uplift. Over the ice (Broughton Island area) the rate of uplift would be smaller and advective heating would contribute to a net energy increase. The correspondence between net heating and observed temperature change would then be closer than indicated in Figure 16.

After the 19th the advective effects are related to the flow of the Polar low into the same Baffin Island cold center (Figure 17). The maximum rates (14 x 10^{-5} kj kg^{-1} s^{-1}) are comparable to those identified with the southerly system and are found to the northwest over Victoria Island. There is a strong eastward gradient of this heating (cf Figure 12) and values over Baffin Bay reach a maximum of only 8 x 10^{-5} kj kg^{-1} s^{-1}; which is, however, greater than the maximum of the previous episode (July 16). This is augmented by heating due to adiabatic compression in the lee of Baffin Island (4 to 5 x 10^{-5} kj kg^{-1} s^{-1}). Descent is related to the negative vorticity advection aloft and shift of the flow over the east coast so that topographic and frictional effects are reversed as the depression shifts eastward.

There is an abrupt change in the energy regime on July 23 over Baffin Island and Baffin Bay, and on July 24 over Davis Strait, as the decaying Polar depression enters the region bringing cold air with an advection rate of -4 to -10 x 10^{-5} kj kg^{-1} s^{-1} and an end to the ice melt episode.

To summarize, we note that over Baffin Island the energy regime is a balance of a wide range of fluctuations in all the energy sources. At times the surface enthalpy heating may reach the same magnitude as the advective influences. Latent heat release is commonly an order of magnitude smaller. Over the water surfaces, however, the dominant control is the horizontal advection. In this example, there are no large surface to air temperature contrasts, nor the large enthalpy fluxes found over land. Adiabatic effects are controlled by the large scale flow which usually results in weak vertical velocities in the Arctic. Consequently, the rates of vertical advection are much less than over land surfaces where topographic and frictional uplift is important. One exception, which may be related to the grid point resolution and computational design, is the adiabatic cooling on July 23 over Baffin Bay which is related to strong orographic uplift over Greenland with the onshore flow.

In this discussion we have identified only the magnitudes and nature of the synoptic scale thermal interactions for a particular case. In particular we have speculated that the

major coastal ice melt of east Baffin Island was related to warm advection from the west, prompted by the circulation of the Polar depression, coupled with adiabatic compression in the lee of the island. With the present grid resolution (350 km) we cannot determine the perhaps significant effect of subgrid advection on the surface energy balance. This may be large at the land sea boundary. It would also be useful to determine the adiabatic contribution when the local, steep topographic gradients are considered. However, a meso-scale time dependent model (the three dimensional sea breeze model of Pielke, 1974, for example) with a much finer grid mesh is required to investigate such situations in more detail.

Summary and Discussion

In this chapter a detailed analysis of the components of the omega field at 85 cb in the eastern Canadian Arctic has been present at 48 hr intervals from July 13 to 25, 1973. The purpose is to examine the changes in the imbalance of the physical processes contributing to omega at various points in the evolution of a typical summer synoptic system within the region. Of particular interest is the relative importance of the advected versus the local terms in the vertical circulation and their effect on the behavior of the system.

During this period a developing mid-latitude depression moved into the grid area from the St. Lawrence and drifted out, south of Greenland, as a decaying system. Following this a

deep Polar low also passed through the region in its decaying stages, although its regional influence was evident from the beginning of the study period. This particular case was chosen because there were two marked warming episodes, one of which had a significant influence on the surface energy balance in that there was a major ice melt along the east coast of Baffin Island.

In June the hemispheric circulation was predominantly zonal but there was a major transition to meridional flow which characterized most of July (Wagner, 1973). This was prompted by blocking over west Canada and north Europe, and a deepening of the Azores high. A trough over Davis Strait, which extended to Texas, is evident on the mean July map. In Davis Strait the 70 cb height was approximately 25 meters below (low pressure) the normal while over central Canada, north Europe and the central North Atlantic it was 40, 80 and 70 meters, respectively, above normal. In the grid area of this study the pressure surface dropped 70 meters from the June 1973 average.

As the southerly depression entered the region on July 13 it can be identified with the characteristics of a developing system as described by Krishnamurti (1968b). Vorticity and thickness advection patterns are in phase and the upward circulation in advance is augmented by strong diabatic effects. At the maximum depth of the vortex on July 15 these advective patterns are no longer coincident. At 85 cb there is almost

no vertical motion and the depression would quickly fill since there is still strong low level frictional convergence with the cyclonic circulation. This would be identified as the occlusion stage according to the classical model and indeed the NMC surface analysis indicates an occluding front.

This out of phase shift of the thickness advection relative to the vorticity advection is related to the development of a deep cold tongue through Hudson Bay - Davis Strait which was initiated by the sudden transfer to meridional circulation and the formation of a strong deformation of the isotherms between an Icelandic low, a Polar low and the mid-latitude system. The position of this cold tongue is important throughout the entire study period. In addition to prompting the destruction of the southerly system it leads to the development of a cold low.

As the two advective terms become self-cancelling the local effects become important and act to stabilize the vortex. Orographic as well as frictional ascent and a strong surface enthalpy flux produce a region of intense vertical motion over southern Baffin Island. There is also latent heat release and furthur uplift. The maximum 85 cb ascent of 1.5 cm s^{-1} on July 15 in this area is less than the previous maximum (4 cm s^{-1}) to the south when advective terms dominated but nevertheless it is sufficient to force the northward drift of the low.

The cold dome intensifies over Davis Strait with attendant thickness advection to the southeast of the system on July 19.

This coincides with intensified vorticity advection in this area as the low becomes a trough extension of the Polar low as the two circulations combine. This rejuvination of the advective terms initiate development towards the south of Greenland and the low eventually leaves the region by July 23.

Previous studies of the cold low feature have emphasized the role of adiabatic expansion due to uplift within the vortex in the formation of the mid-tropospheric cold center (Reed and Tank, 1956; Scherhag, 1957). In this case study, however, the physical relationships are more complex. The initiation of the isotherm configuration can be traced, prior to the cold low formation, to the horizontal deformation over Hudson Bay - Davis Strait between three depression centers. The cold low forms over the east coast of Baffin Island as the southerly system moves northward and the isobars coincide with the closed isotherms. The movement is not a result of large scale flow but rather of local ascent over Baffin Island. Adiabatic cooling is important at the upstream sector of the cold low, but downstream the feature is degraded by strong surface heating and latent heat release over the island. The net result is a retrograde travel of the cold center with intensification against the direction of flow. 48 hours later the flow characteristics have changed such that intensification is in the direction of flow but horizontal advective cooling dominates. On the following map (48 hours later) the cold

dome is stabilized over Davis Strait by strong cooling related to the downward enthalpy flux. It is evident that local as well as advective effects are influential in the maintenance of the cold low, for this example. As the flow changes and the nature of the underlying surface varies, the mechanisms change. More detailed study is necessary using more examples with a finer mesh grid. It may be that this complex situtation, involving imbalances of land-sea thermal effects, the large scale flow (horizontal advection) and orographic ascent, may be an anomaly, especially in light of the very high frequency of cold lows found spread over all sectors of the Arctic (cf. Flohn, 1952).

When choosing the period for this detailed study it was noted that the rapid cooling at Broughton Island at the onset of an interval of decreasing pressure is unexpected in that the reduced pressure is usually associated with advection of warm southerly air. This cold episode has been traced to the development of the cold tongue over Hudson Bay - Davis Strait. The expected warming is observed on July 16 over Baffin Island. The peak is 24 hr earlier over Davis Strait and is of greater magnitude. This is obviously the effect of warm air advection with the northward moving mid-latitude system. However, the more intense warming centered on July 22, which was coincident with a vigorous melt of the fast ice in the Broughton Island area, is associated with a different system and an additional physical process. The cyclonic flow around the Polar low

has intensified in the central grid sector bringing relatively warm air from the west into the cold tongue. This advection is augmented by adiabatic compression as the air descends the east coast of Baffin Island. The two heating effects are of similar magnitude. The subgrid scale effect of surface heating of air over land and its subsequent advection over nearby ice cannot be evaluated with the present grid resolution.

The grid averages and standard deviations of the model generated data at 24 hr intervals are in Appendix Three. Since they are not restricted to the synoptic system they do not adequately represent the synoptic behavior and therefore are not discussed in the day by day analysis. However some general features are worth of note. The vigor of the 85 cb vertical circulation is not comparable to that furthur south. The grid average for a polar outbreak in middle latitudes (Table I, April 15) is 1.6 cm s^{-1}, with a large standard deviation of 3.2 cm s^{-1}. By contrast the comparable statistics for a mature Arctic system (July 15) are 0.02 cm s^{-1} and 0.7 cm s^{-1}. Krishnamurti (1968b) reports extremes of vertical circulation of +11 to -13 cm s^{-1} for a mid-latitude storm in the United States. The more quiescent Arctic circulation is, in part, related to the lower static stability with the lower temperatures and smaller specific volumes. For the United States a typical value is 3.13 at 50 cb (Stuart, 1970) while for the Arctic it is 2.58. At 30 cb the difference increases (11.08 and 3.54, respectively). In this respect a useful study would be a

comparison of the magnitudes of the contribution to omega by the various processes (advected and local) for Arctic and mid-latitude systems to find additional causes for the different vertical circulations.

Also of interest is the relatively large grid average contribution by diabatic effects at 85 cb. In several cases (e.g. July 15, 18, 20,23) the contribution to the total vertical motion is of the same scale as the advective terms. In one instance (July 19), the latent heat release dominates the total vertical circulation.

For the purposes of this study the grid format is not ideal. The eight by eight by six data grid was chosen to restrict computer storage to within reasonable limits for an exploratory study. At present the storage of the model has exceeded the core limit of a CDC 6400 computer. The size of the grid, however, is not sufficient to identify with confidence origins and maximum magnitudes of advective processes through the history of the disturbance. In the discussion of the daily features it has been noted that significant sectors are often at the edge or entirely off the grid. Sutcliffe and Forsdyke (1950) recommend a hemispheric scale to analyze adequately synoptic evolution. An alternate scheme would be to use a movable grid referenced with respect to the depression center, such as that employed by Petterssen et al (1962). However, this would entail re-analysis of the input fields at each calculation to fit the data with the new grid position.

The results of this chapter have illustrated the suitability of the steady state omega equation for discussion of synoptic systems in the Arctic. The influences of advective and local energy sources and sinks can be clearly differentiated and studied. The observed synoptic behavior closely follows that expected from an examination of the model generated data and characteristics of the local climate can be interpreted adequately from these data. A more comprehensive examination of the energetics of the local climate would require a time dependent model of greater resolution to couple local surface effects with the large scale flow.

CHAPTER FIVE

EMPIRICAL ANALYSIS OF WINTER AND SUMMER VERTICAL VELOCITIES

Introduction

In Chapter Four a single synoptic event is analyzed in detail throughout its history in the eastern Canadian Arctic. The purpose is to identify magnitudes of the vertical motion at various stages of development and decay and to determine the intensities and types of the physical processes affecting the vertical circulation. By this type of subjective examination it would be difficult to consider a large sample of cases in order to reach general conclusions regarding synoptic processes.

In this chapter attention is focused on seasonal and inter-seasonal synoptic characteristics. With the large amount of data it is necessary to investigate empirical techniques which reduce the products of the omega computations to statistics which may be interpreted according to synoptic principles. From these statistics major temporal trends and physical relationships for the total vertical velocity may be identified and discussed.

In many climatological studies a spatial field is decomposed into characteristic patterns and a large sample is thus reduced into fewer categories and attendant frequencies. If system evolution and history is of interest the data may be air parcel trajectories or depression tracks (kinematic

classification). A spatial data set representing an instant in time falls into a static classification. The emphasis is on morphology and a pattern illustrates the mean location and configuration of a synoptic feature. The data and objectives of this study in the eastern Canadian Arctic dictate a static view.

The majority of the studies reported in the literature have concentrated on the pressure field and the patterns may be interpreted in terms of depression systems and flow characteristics. Numerous examples have been reviewed by Barry and Perry (1973). These classified patterns may be related to local climatic elements (Barry, 1974; Fogarasi, 1972), hemispheric scale atmospheric dynamics (Craddock and Flintoff, 1970, Dzerdzeevski, 1968), patterns of other climatic or biological data (Fritts et al, 1971; LaMarche and Fritts, 1971) or the classification itself may be of interest (Kirchhofer, 1974). To date the emphasis has been on averaged conditions, and the seasonal characteristics of the patterns and the variable intensity within patterns have not received much attention (Barry and Perry, 1973).

In a static classification the major patterns reveal mean or preferred locations of the most common synoptic features. Unless pattern sequences are examined this technique is not amenable to historical studies (Chapter Four, for example), however static analysis is most suitable for comparison of

patterns with those of other fields recorded at the same time for the same region. In this chapter the total vertical velocity at 85 cb is broken into characteristic patterns or eigenvectors for the eastern Canadian Arctic which are compared with patterns of the component fields to determine the probable physical mechanisms responsible for the major synoptic features of the region. The sample interval is from January 2 through August 24, 1973 and includes the winter, transition and summer periods. This chapter is organized as follows:

Pattern identification for 85 cb total vertical velocity. The technique of empirical pattern classification is discussed and applied to the 85 cb total vertical velocity (w_T), the 85 cb geopotential height (Φ) and the six component fields of the total vertical velocity - w_V, 85 cb vertical velocity due to vorticity advection; w_{TH}, 85 cb vertical velocity due to thickness advection; w_{LP}, 85 cb vertical velocity due to latent heat release; w_H, 85 cb vertical velocity due to surface thermal effects; w_F, surface vertical velocity due to friction and w_O, the surface orographic vertical velocity. The patterns of the total vertical velocity and their seasonal trends are described.

Canonical analysis of the eigenvector weights. The patterns of the fields mentioned above are compared throughout the entire sample to find those patterns and fields which are highly correlated throughout time for specific synoptic features. The objective is to define the physical processes (w_V, w_{TH} etc.) which are responsible, on the average, for each feature in w_T.

Seasonal interpretation of the first five eigenvectors of w_T. The seasonal variations in intensities of the major synoptic systems of the region and changes in the physical mechanisms responsible for those systems are discussed.

Case studies of eigenvector relationships. Cases from the detailed study interval of Chapter Four which illustrate two major patterns or eigenvectors of total vertical velocity are examined. The probable physical relationships for the synoptic features in each pattern which have been identified empirically from canonical analysis are compared with the relationships found by the subjective analysis of Chapter Four.

Summary and discussion. The major synoptic features in w_T and their probable physical mechanisms are summarized. The validity of the empirical techniques used in this chapter is discussed and modifications and improvements are proposed.

Pattern Identification for 85 CB Total Vertical Velocity

The classification schemes of Barry (1974) and Kirchhofer (1974) are based on the recognition of dominant or 'key' patterns in the spatial field of pressure and the grouping of other days with similar configurations into the respective categories. The advantage is that each day or case is associated with only one 'key' pattern but there is also a tendency to define a large number of categories so that as much of the sample as possible may be classified. The Barry catalogue includes forty 'types' of sea level pressure for the eastern Canadian Arctic. The derivation of a catalogue may be

based on a laborious subjective examination of maps (Barry, 1974) - a procedure which invokes circularity arguments when the results are analyzed since selection of classes is usually based on an a priori understanding of the major circulations involved (Barry and Perry, 1973). The Kirchhofer method uses a time consuming computer programme but large amounts of data may be handled easily and operator bias is relatively insignificant.

An alternate method, which is more economical in terms of computer requirements, is to decompose a spatial field into eigenvectors. These are non-correlated mathematical surfaces in the spatial field. Each surface or eigenvector has an associated weight for each case which is an indication of the importance of that vector in the original data for that day. A disadvantage is that each case may be represented by a multiplicity of surfaces or patterns, but the number of significant patterns is usually less than for 'key' day techniques.

The use of eigenvectors to represent two dimensional meteorological fields was first described by Lorenz (1956) but, presumably on account of limited computer storage, reports of extensive applications have been made only recently (Sellers, 1968; Craddock and Flood, 1969; Peterson, 1970; for example).

In this study eigenvector analysis is applied to products of the omega computations in the eastern Canadian Arctic for a 234 day sample to decompose the data fields into characteristic anomaly patterns which may form the basis for classification

and furthur analysis. Since eight data sets are to be examined (w_T, w_V, w_{TH}, w_{LP}, w_H, w_F, w_0, Φ) computer expense is of primary concern and for this reason the Kirchhofer method is not used. In the next section we investigate the hypothesis that characteristic patterns of w_T may be related to patterns of particular physical processes. If each case has several component patterns of different relative importance (i.e. eigenvectors) it is more probable that one of these patterns may be related to a particular assemblage of physical processes which may always be present, but at different intensities for different days, than if each case has only one pattern. This is the second reason for the adoption of the eigenvector technique.

The utility programme for eigenvector analysis restricts the number of variables (grid points) to 25. The western column and southern row of the original matrix are deleted and the 5 x 5 grid encompassing Baffin Island and Baffin Bay - Davis Strait is retained. The data for each case are standardized with a spatial mean of zero and standard deviation of one. This has the effect of preserving patterns in the data while enabling comparison of fields with different units (for example vertical velocity and geopotential height). This procedure has the adverse property of subduing intensities so that two cases with similar spatial relationships but very different ranges of values would be depicted as being identical.

The methodology of eigenvector analysis in meteorological applications is well established (e.g. Sellers, 1968). The standardized observational data are represented by the matrix mFn (m=25, n=234) which is transformed into a correlation matrix mCm. The eigenvector matrix mEm is determined from:

$$mCmEm = mEmLm$$

where mLm is the diagonal matrix of the latent roots (or eigenvalues) of the correlation matrix. The weights (mXn) of each eigenvector are determined for each case.

$$mFn = mEmXn$$

The eigenvalue may be interpreted as a single number representing a topographic surface found in the original data field (Gould, 1967). A high value may indicate a nearly planar surface while successively lower values are considered to be convoluted surfaces of greater complexity with wider ranges of heights.

The eigenvectors are realizations of these eigenvalues in the variables (grid points). Each eigenvector may be plotted and contoured. The plot then displays the spatial topography which the eigenvalue represents, and, since each eigenvector is orthogonal to those preceding it, each map is uncorrelated with the others. These maps are termed 'characteristic anomaly pattern(s)' (Grimmer, 1963) and form the basis for classification of the data. A summation of all eigenvector patterns results in a pattern of the original data averaged through all the cases (n). The first few eigenvectors may be interpreted in physical terms

but higher order maps represent high frequency variability which is usually considered noise. According to the Kaiser criterion (Kaiser, 1960) only those vectors with eigenvalues greater than unity have physical significance.

The weight of an eigenvector is an indication of the relative importance of that pattern in the data for each case. If the value is large (on a relative scale), the vector closely resembles the original field. If the value is large but negative the patterns are similar but the data are opposite in sign to the terms of the eigenvector.

The 85 cb geopotential and seven vertical velocity fields are decomposed into their respective patterns. The major eigenvalues and cumulative variance of each are in Table VII.

Since the total vertical velocity is the final objective of the omega computations and is an indicator or synoptic activity, the patterns of this field are discussed in detail. The contours of the eight eigenvectors for the 234 day sample are plotted in Figure 18. The ten day means of the weights are in Figure 19 with plus and minus one standard deviation. The weights are tested for linear trend of the relative importance of each eigenvector through time. The F - statistics, indicating the significance of such trend, are in Table VIII.

Eigenvector one: has an eigenvalue of 4.5 and accounts for 18 per cent of the variance in the original data. Two synoptic features are evident in this anomaly pattern. There is a circular region of ascent (we interpret the patterns for cases of positive

TABLE VII

EIGENVALUE SUMMARY FOR THE EASTERN CANADIAN ARCTIC

Format: Eigenvalue
Cumulative Proportion of Total Variance (per cent)

See introduction of this chapter for a definition of the data field symbols.

Data Field	Eigenvalue Number									
	1	2	3	4	5	6	7	8	9	10
w_T	4.5	4.1	3.2	2.5	2.2	1.7	1.3	1.1		
	18	34	47	58	66	73	79	83		
w_V	4.3	3.9	2.7	2.6	2.4	1.7	1.3	1.1		
	17	33	44	55	64	71	76	80		
w_{TH}	3.7	3.3	2.7	2.3	2.0	1.8	1.6	1.2	1.1	
	15	28	40	49	57	64	70	75	80	
w_{LP}	2.5	2.2	1.7	1.6	1.5	1.4	1.3	1.2	1.1	1.0
	10	19	26	32	38	44	50	54	59	63
w_H	6.0	2.1	1.8	1.6	1.4	1.1	1.0			
	24	33	40	46	52	56	60			
w_F	4.7	4.2	3.6	2.5	2.1	1.8	1.2			
	19	36	50	60	68	76	80			
w_O	9.7	4.9	2.8	1.8	1.6	1.3				
	39	59	70	77	83	89				
Φ	8.8	6.5	3.7	2.2	1.7					
	35	61	76	85	92					

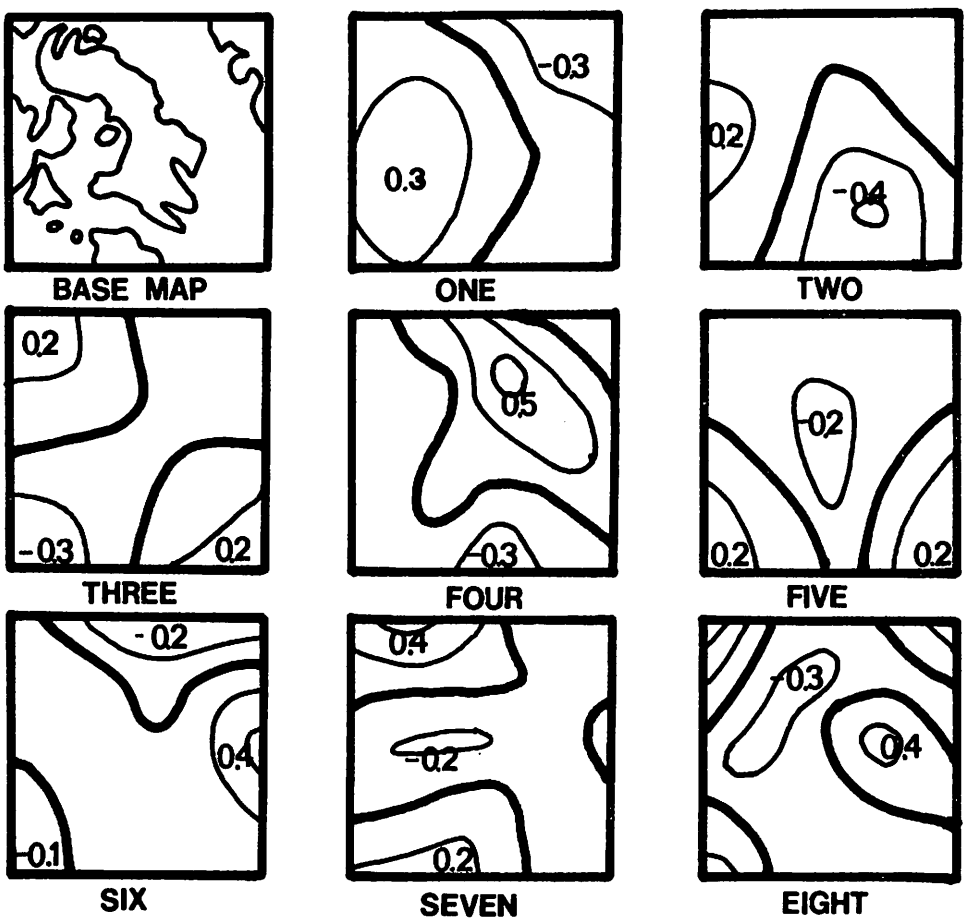

Legend: zero contour : heavy line
contour interval : 0.2

FIGURE 18 EIGENVECTORS OF 85 CB TOTAL VERTICAL VELOCITY

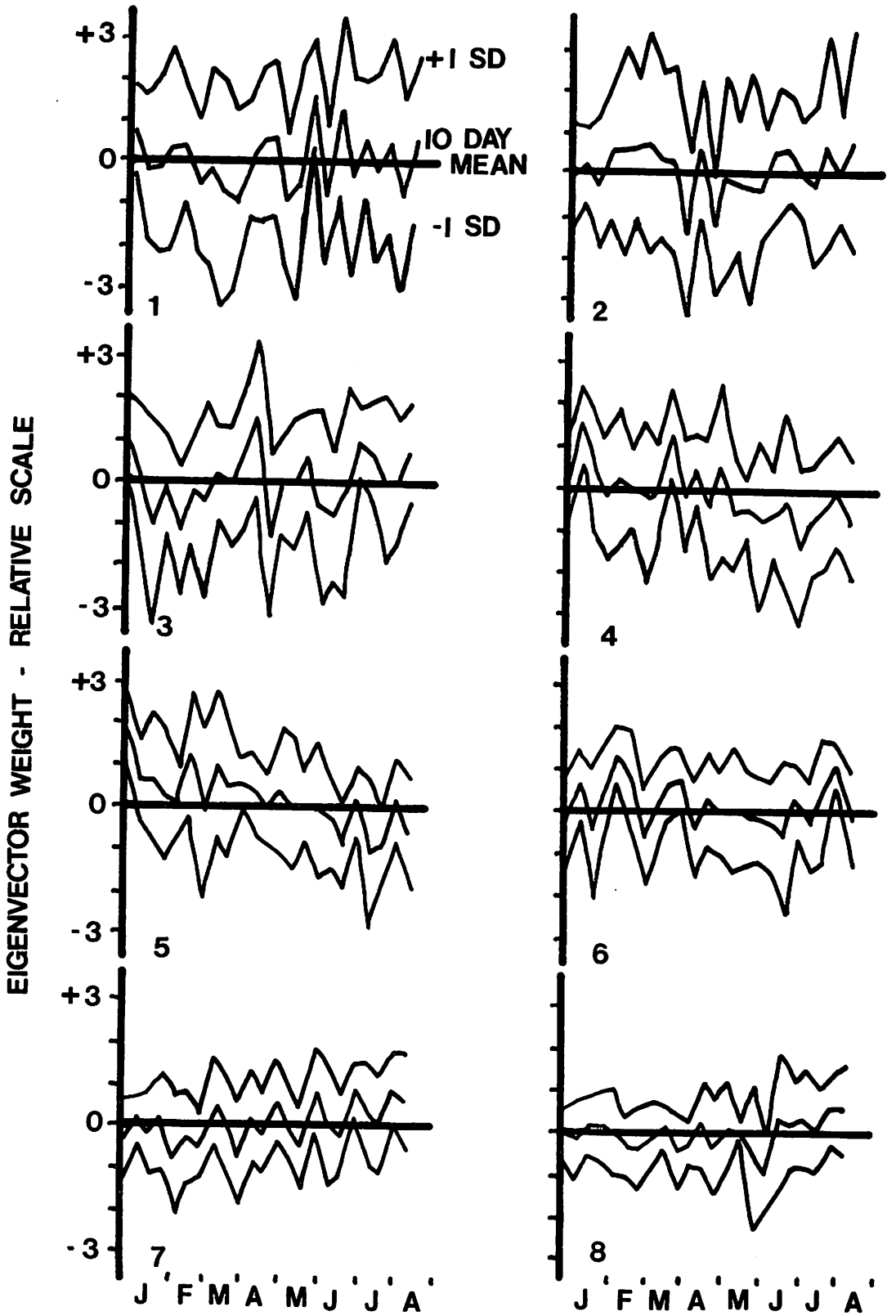

FIGURE 19 EIGENVECTOR WEIGHTS - TOTAL VERTICAL VELOCITY

TABLE VIII

TEMPORAL TRENDS OF EIGENVECTOR WEIGHTS FOR W_T

The weights are tested for linear trend with time.
If the trend is significant at the 0.05 level the equation is presented. y is the weight and x is the day according to the Julian calender.

Eigenvector	F-statistic	Equation of Trend
1	0.481	
2	0.057	
3	1.478	
4	16.310	$y = 0.71 - 0.01x$
5	26.225	$y = 0.82 - 0.01x$
6	3.890	$y = 0.29 - 0.02x$
7	5.595	$y = -0.31 + 0.02x$
8	2.632	

weights) centered over Foxe Basin. From this location there is a broad even drop in the topography to a feature of opposite sign over the Baffin Bay - west Greenland sector. This may represent an extensive system not represented completely within the grid space.

There is not any significant linear trend of the weights between the winter and summer seasons, although there is a marked increase in magnitude of both positive and negative ten day means beginning in mid-May. This may be interpreted as an increase in the significance of this pattern in the data for average conditions. The one standard deviation envelope may exceed plus or minus three on a relative weight scale in both seasons. These large standard deviations (relative to higher order eigenvectors) are indicative of cases with very large weights when the configuration of the data may be very similar to this idealized pattern.

Eigenvector two: accounts for an additional sixteen per cent of the variance in the data. There is a steep anomaly over central Davis Strait with a vector value of -0.4 at the center. A smaller secondary feature of limited extent and reverse circulation (vector value of +0.2) is found to the west over Melville Peninsula.

No temporal trend is associated with the weights of this pattern. Except for a brief period in April the ten day averages vary about zero but the one standard deviation envelope has a range similar to that of the first eigenvector.

Eigenvector three: (thirteen per cent of the variance) represents dual centers of positive anomaly, each of equal significance, over south Davis Strait and northwest Baffin Island. They are separated by a quiescent zone of near zero circulation over Baffin Island. A more intense anomaly of opposite sign is situated to be southwest but this is very restricted in area on this grid. It may be the edge of a more extensive system over Hudson Bay.

The weights do not illustrate any significant seasonal trends for this vector.

Eigenvector four: has an eigenvalue of 2.5 and accounts for eleven per cent of the variance. With the smaller eigenvalue the topography of the pattern becomes more complex with greater extremes of vector values, indicating more intense vertical circulations. Maximum vector values for patterns one and two are 0.3 and 0.4, respectively. These should be compared with a maximum value of 0.5 for this pattern which is situated over the northeast coast of Baffin Island. The major axis of this elliptically shaped feature runs parallel to the coast. The edge of another system of opposite vertical circulation is found over north Quebec.

This is the first eigenvector which has a distinct seasonal trend. The F - statistic for a linear trend (Table VIII) is 16.3. In Figure 19 we see that there is a bias towards positive weights during the winter months (ascent with a positive vector anomaly over east Baffin Island) and negative weights during

the summer (an opposite circulation for the anomaly feature). Note that the variance of the weights is reduced considerably when compared to that for the three previous patterns. This means that this eigenvector is rarely as predominante in the original data as patterns one, two or three. Probably it is more often found in combination with other patterns.

Eigenvector five: includes eight per cent of the variance of the data. There is an anomaly over central Baffin Island (maximum vector value of -0.2) with systems of opposite sign but equal intensity over south Davis Strait and Hudson Bay (vector values of +0.2 for each). These two features may be sectors of vortices which have their major areas outside of the grid.

For this pattern there is also a distinct seasonal trend, slightly more extreme than for the previous vector (cf. the slopes of the regression equations in Table VIII). Weights are positive during the winter. At the start of the sample the ten day average is +2. During May they become negative and remain so for the rest of the sample.

Eigenvector six: (seven per cent of the variance) includes a negative anomaly over Baffin Bay and a major feature (vector value of +0.4) over the west Greenland coast. This is very restricted in area. There is a small but significant linear seasonal trend of the weights. Ten day averages oscillate about zero from April through June, however, there is pronounced increase in mean activity of this pattern (for both positive and negative weights) during the winter months of January, February and March, and the

summer months of July and August.

Eigenvector seven: (six per cent of the variance) represents a major anomaly over north Baffin Island (maximum vector value of +0.6). Less intense features are found over north Quebec (+0.2) and central Foxe Basin (-0.2). There is a small seasonal trend of the weights with a summer bias towards positive values; however, the ten day means are very close to zero and the standard deviations are small when compared to those of the previous patterns.

Eigenvector eight: contains only four per cent of the variance. It is difficult to physically interpret some of the features of these higher order patterns which explain very little variance in the data. In eigenvector eight, the most intense gradients, which are all of the same sign, are at the three corners of the grid. They may represent systems moving into or out of the region, but there is also a suspicion of model edge effects. Two distinct modes of anomaly are found within the grid - one over the east coast of Baffin Island (vector value of +0.4) and another, of opposite sign, over the west coast. There is not any distinct linear seasonal trend of the weights of this pattern, although there is a noticeable but relatively minor increase in activity towards the summer months (Figure 19).

These eight vectors account for 83 per cent of the total variance in w_T. Using another routine for the total vertical motion field only, the grid number may be increased to the total 36 and the number of major vectors is increased to twelve as more information is included. However, this programme is too

expensive to use on all of the fields considered in this chapter.

There is ample evidence in the literature for periodicities and repetition of sequences in synoptic data. Much of the subjective synoptic forecasting is based on these features. For example, Lamb (1964) found evidence of a 30 day wave in the strength of anticyclones over central Europe and Craddock (1956) found that the first two Fourier components of the annual temperature series in central and northern Europe accounted for 99 per cent of the variance. He also showed evidence of autocorrelation at a five day lag. Numerous examples are cited in Barry and Perry (1973). To examine the possibility of recurring sequences of patterns for total vertical velocity which could be interpreted in terms of synoptic histories the eigenvector weights for each day are examined and the vector or pattern with the largest (positive or negative) weight is recorded. For the majority of the cases there is a clear dominance of one vector or pattern over the others. A series of pattern types is so constructed, with one (dominant) pattern identification for each day. This series (Figure 20) is tested for periodicity using Fourier analysis and autocorrelation is examined at various lag intervals using a routine designed for integer data (Davis, 1973). The variance explained by a harmonic component is always less than four per cent. At most lag intervals the autocorrelation is significant; however, the number of autocorrelated cases at a specific lag is always less than

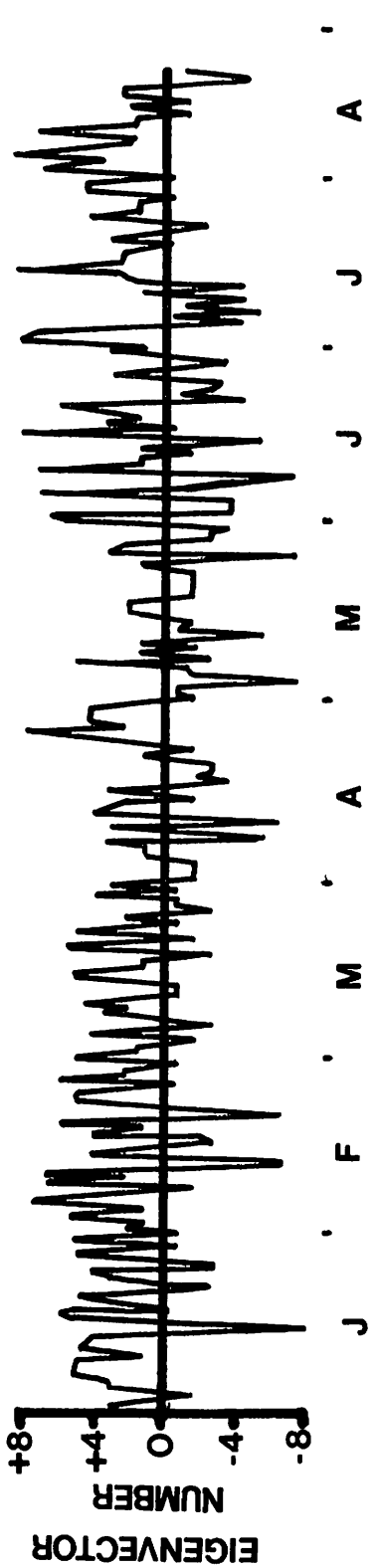

FIGURE 20 SEQUENCE OF DOMINANT EIGENVECTORS OF TOTAL VERTICAL VELOCITY

fifteen per cent of the sample. Visual inspection of the series does not reveal persistence of any one pattern for more than two days. We may conclude that there are no significant sequences of eigenvectors which recur at regular intervals.

Since previous synoptic studies for this region (Barry, 1974; Barry et al, 1975) have emphasized pressure classification, the eigenvectors of the 85 cb geopotential field are illustrated in Figure 21. These data are standardized with a mean of zero so negative components of the vector indicate a negative anomaly or low pressure (relative to the mean field) when the weight is positive or high pressure when the weight is negative. A direct comparison with the subjective classification of Barry et al (1975) is not strictly valid since this was based on sea level pressures. However, some general correspondences are apparent and the numeric identification of the similar type from the Barry catalogue is presented in Table IX. The five eigenvectors account for 92 per cent of the variance in the original data. These patterns are discussed in detail in the next section.

Canonical Analysis of the Eigenvector Weights

In this section an attempt is made to interpret the synoptic features of the eight eigenvectos of w_T in terms of the regional 85 cb height field and the six component vertical velocity fields representing the physical processes affecting w_T (w_V, w_{TH}, w_{LP}, w_H, w_F and w_0). There are two independent types of empirical analysis. In the first (canonical analysis of the

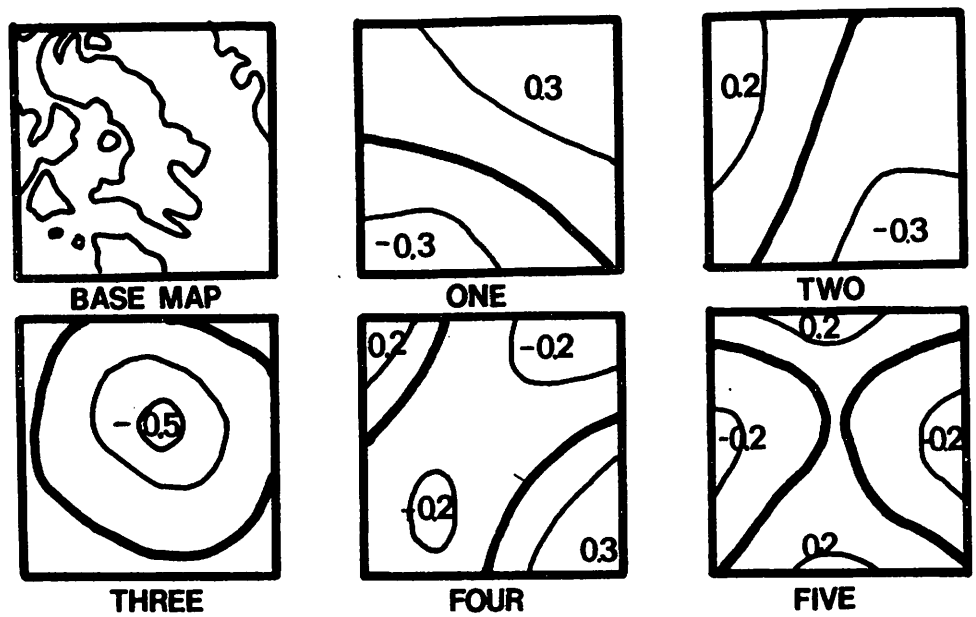

Legend : fig 18

FIGURE 21 EIGENVECTORS OF 85 CB HEIGHT

TABLE IX

RELATIONSHIP BETWEEN THE 85 CB HEIGHT EIGENVECTORS

AND THE BARRY PRESSURE CLASSIFICATION

I indicates that the correspondence with the Barry catalogue is with the inverse of the pattern of Figure 21 (a negative weight). Note that the areas of the eigenvectors of Figure 21 are not identical to those illustrated in the Barry catalogue (Barry et al, 1975).

85 cb Height Eigenvector Number from Figure 21	Surface Pressure Pattern Identification from the Barry Catalogue (Barry et al, 1975)
1	C3 (I), C4
2	C2 , A4 (I), A5
3	C1
4	A2 (I)
5	

eigenvector weights) we are dealing with standardized data and are therefore only investigating relationships between spatial configurations. The results are verified in the second analysis (multiple regression of magnitudes at a grid point). The relative contribution by each process to the total intensity of the vertical circulation is determined using raw data.

The premise for the first empirical analysis of this section is stated as follows. An eigenvector of w_T illustrates the mean morphology of a particular synoptic feature. There is a specific assemblage of physical processes, each with an average pattern, which interact to develop this feature. This characteristic pattern of each process is revealed by an eigenvector of the respective field. Weights of the pertinent eigenvectors for w_T and the component fields will be highly correlated through time if these physical relationships hold throughout the entire sample interval.

Multivariate regression techniques are used to identify the eigenvectors of w_T and of the seven other fields which are highly correlated throughout the sample (234 days). It is possible that the correlations may be fortuitous and not represent a physical relationship at all or they may be biased by match or mismatch of the patterns in areas of the grid external to the synoptic feature of interest. Consequently a subjective examination of the pattern assemblages identified by correlation analysis is necessary and independent tests are helpful.

The correlation of eigenvector weights (each weight

indicating the degree of dominance of the respective pattern) with meteorological variables is the basis of the work of Peterson (1970) and LaMarche and Fritts (1971). These authors used multiple step-wise regression to determine a series of weights most highly correlated with a variable. When the dependent variable is decomposed into eigenvectors and weights one has several dependent as well as independent variables and, rather than test all possible combinations using linear regression, canonical analysis is used to identify correlated patterns.

Canonical analysis was first described in a meteorological context by Glahn (1968) and used by Fritts et al (1971) to related eigenvectors of tree ring width and atmospheric pressure. A summary of the theory is given by Clark (1975) and Cooley and Lohnes (1971). It is similar to factor analysis except that for canonical analysis vectors are selected which maximize the covariance between two variable sets or domaines rather than maximize the variance within one domain. A vector is selected for each domain such that the correlation between the vectors is a maximum. We are thus identifying the most similar patterns in each data domain. A measure of this similarity is the canonical correlation coefficient ($0 \leq r_c \leq 1$) and the significance may be determined by Chi-square tests. Once the variance explained by these similar patterns is removed, the procedure is repeated to identify the next most important pair of canonical vectors. Therefore each set is orthogonal and uncorrelated to those prededing.

For each canonical vector there is a weight or loading for

each variable in the associated data set which is the correlation coefficient between the data of that variable and the canonical vector. Variables in both domaines with similar and large weights on a certain vector pair are highly correlated with each other. The interpretation of 'similar' and 'large' is subjective and may vary with the investigator. Extraction of significant canonical correlations is usually made with some knowledge of the probable relationships and this is a serious handicap. The advantage is that several complex interactions of many variables may be summarized quickly and efficiently.

Canonical analysis is performed between the eigenvector weights of w_T and each of the seven other fields. Those canonical vectors significant at the 0.05 level (determined by Chi-square tests) are in Table X with the highly correlated variables and their canonical weights. A furthur restriction is that canonical correlations of less than 0.3 represent 'trivial' vectors (Cooley and Lohnes, 1971) and are excluded.

Problem one is a correlation of w_T with 85 cb height eigenvectors. On the first pair of canonical vectors (canonical correlation of 0.78) there is a high association between height pattern one and the inverse of w_T pattern two. Since the canonical weights are of opposite sign (-0.75 and 0.87) the similarity in temporal patterns is between eigenvector weights of opposite sign, and therefore the inverse of one pattern is considered. From inspection of the eigenvector contours (Figures 18 and 21) we see that this is an intuitively reasonable

TABLE X

SUMMARY OF CANONICAL ANALYSIS OF EIGENVECTOR WEIGHTS

Variable subscript refers to eigenvector identification in Table VII.

Canonical Vector Pair	Canonical Correlation	Chi-Square	D.F.	Highly Weighted Variables Canonical Weights in Parentheses
Problem one: relate $w_T(A)$ and 85 cb height (B)				
1	78	603	40	$A_2(0.87)$, $B_1(-0.75)$
2	74	382	28	$A_4(-0.67)$, $B_3(-0.73)$
3	61	192	18	$A_3(-0.73)$, $A_1(0.46)$, $B_4(0.83)$
4	53	92	10	$A_4(0.69)$, $B_2(0.68)$
Problem two: relate $w_T(A)$ and $w_V(B)$				
1	76	724	64	$A_2(-0.64)$, $B_2(0.91)$
2	72	528	49	$A_3(-0.68)$, $B_4(-0.85)$
3	67	362	36	$A_5(-0.60)$, $B_3(-0.73)$
4	59	228	25	$A_1(-0.38)$, $A_4(0.74)$, $B_1(-0.80)$
5	40	129	16	$A_6(0.49)$, $B_6(0.78)$
Problem three: relate $w_T(A)$ and $w_{TH}(B)$				
1	71	718	72	$A_2(0.71)$, $B_2(-0.81)$
2	69	555	56	$A_2(0.66)$, $B_1(0.81)$
3	66	411	42	$A_4(0.43)$, $B_7(0.56)$
				$A_7(-0.51)$, $B_6(-0.49)$
				$A_8(-0.53)$, $B_4(-0.51)$
4	63	282	30	$A_4(-0.60)$, $A_5(0.61)$, $B_4(0.74)$
5	56	164	20	$A_3(0.53)$, $B_3(0.85)$
6	45	80	12	$A_6(0.55)$, $B_5(0.62)$
				$A_7(-0.52)$, $B_6(-0.52)$

TABLE X (continued)

Canonical Vector Pair	Canonical Correlation	Chi-Square	D.F.	Highly Weighted Variables Canonical Weights in Parentheses
Problem four: relate $w_T(A)$ and $w_{LP}(B)$				
1	75	877	80	$A_2(-0.80)$, $B_2(\ 0.71)$
2	71	692	63	$A_1(-0.82)$, $B_1(-0.63)$
3	71	533	48	$A_3(-0.97)$, $B_3(-0.71)$
4	68	376	35	$A_4(-0.70)$, $B_4(\ 0.77)$
5	65	235	24	$A_4(\ 0.44)$, $A_5(\ 0.47)$, $B_5(\ 0.68)$
6	48	109	15	$A_8(-0.99)$, $B_8(-0.74)$
Problem five: relate $w_T(A)$ and $w_H(B)$				
1	52	209	56	$A_5(\ 0.66)$, $B_1(\ 0.88)$
2	46	135	42	$A_3(-0.62)$, $B_2(\ 0.62)$
3	39	80	30	$A_4(\ 0.57)$, $B_3(\ 0.65)$
Problem six: relate $w_T(A)$ and $w_F(B)$				
1	82	990	56	$A_4(-0.56)$, $B_4(-0.51)$
2	81	736	42	$A_4(\ 0.62)$, $B_3(\ 0.68)$
3	75	490	30	$A_1(\ 0.51)$, $B_1(\ 0.59)$
				$A_7(-0.54)$, $B_7(-0.56)$
4	67	303	20	$A_5(\ 0.55)$, $B_7(\ 0.49)$
5	58	166	12	$A_2(\ 0.50)$, $B_5(\ 0.71)$
Problem seven: relate $w_T(A)$ and $w_0(B)$				
1	89	1199	48	$A_1(-0.51)$, $B_1(-0.56)$
				$A_6(\ 0.49)$, $B_6(\ 0.44)$, $B_3(\ 0.44)$
2	85	827	35	$A_2(-0.67)$, $B_5(-0.67)$
3	78	525	24	$A_1(-0.63)$, $B_1(-0.52)$
4	69	303	15	$A_4(\ 0.67)$, $B_3(\ 0.63)$

relationship. For positive eigenvector weights of the 85 cb height pattern one there is a low pressure cell over the southwest of the grid. The inverse of w_T pattern two includes a major region of ascent in the northeast sector of this low pressure vortex. This displacement of the pressure and ascent centers is consistent with the observations of a developing depression in Chapter Four (case studies of these relationships are discussed below).

On the second set of canonical vectors there is a significant relationship between w_T pattern four with a positive anomaly (ascent for instances of positive eigenvector weights) over the east coast of Baffin Island and 85 cb height eigenvector three with a widespread central low. Again, this is a plausible association.

The same is true for the correlation on the third canonical vector pair between w_T pattern three and the inverse of the 85 cb height pattern four. For negative anomalies (low pressure) in the northwest and southeast quadrants there is ascent (positive anomalies) of almost identical spatial configuration. There is a less obvious relationship between this pressure pattern and w_T pattern one. The canonical weight is low and the association seems to be restricted to south Davis Strait (a high pressure cell with moderate widespread descent).

For the last significant pair of canonical vectors there is a relationship between w_T pattern four and height pattern two. Both the canonical correlation and the canonical weights are

lower than for the previous groupings and the visual correspondence of contours is poor. A physical linkage between the two data fields is not as obvious.

In this problem the associations revealed by canonical analysis of the eigenvector weights are realistic in a physical sense with areas of ascent related to depression systems. When the canonical weights are high the contour maps for each field are very similar. If the canonical correlations are low or the canonical weights are low and very different for the two variables, certain sectors of the maps seem to correspond while others do not.

If the canonical weights are very low or obviously very different for two variables, the respective patterns may not have been included in Table X since selection of groupings is based on a highly subjective consideration of the largest canonical weights for the canonical vector pairs. The low weight may be related to low association throughout the entire sample when in fact there may be higher correlation for one segment of the sample, perhaps for one season. In future analysis it may be desirable to subdivide the sample and analyse each season separately to isolate possible differences in the mechanisms responsible for a given pattern of total vertical velocity.

The assemblages of similar eigenvectors in all the vertical velocity and height fields revealed by the canonical analysis are summarized in Table XI. Only those eigenvectors of the component velocity fields found to be related to patterns of w_T are presented

TABLE XI

SUMMARY OF CANONICAL RELATIONSHIPS

These eigenvector assemblages are based on subjective interpretations of the canonical relationships of Table X.
Number in parentheses indicate a relatively low correlation over the grid, an evaluation based on the canonical correlation and subjective comparison of the points of correspondence in the patterns.
A negative number indicates an association of the inverse of the pattern with w_T.
See the introduction of this chapter for the definition of the data field identifications.

Data Field Identification	Eigenvector Number							
w_T	1	2	3	4	5	6	7	8
85 cb height		-1	-4	3				
w_V		-2	4	-1	3	6		
w_{TH}		-2,1	3	-4	4	5	6	(4)
w_{LP}	1	-2	3	-4	(5)			8
w_H					1			
w_F	1	(5)		4,3	7			
w_O	1	5		(3)		6		

in Figures 22, 23 and 24.

W_T eigenvector one: is clearly related to local effects in this analysis. The high canonical correlations are with the first patterns of latent heat release, friction and orography. The visual correspondence between the maps is striking. The broad region of total ascent centered over Foxe Basin (Figure 18) has contours similar to those depicting ascent due to latent heat release and frictional convergence (Figure 23). The feature over Baffin Bay - west Greenland is obviously associated with orographic and frictional processes. The pattern in this sector is also similar to that for latent heat release (w_{LP} pattern one) and this mechanism may be a contributing factor for cases of ascent (negative eigenvector weights).

W_T eigenvector two: includes the well defined circulation feature over central Davis Strait. This is related to advective effects (w_V and w_{TH} patterns two, note that the canonical correlation is with the inverse of these patterns) with a contribution by latent heat release (for negative eigenvector weights with ascent only) and friction. For the circulation feature of opposite sign to the west (centered over Melville Peninsula) these same patterns of vorticity and thickness advection, and latent heat release (for positive weights with ascent only) have similar contours. There is an additional orographic effect (w_0 pattern five) over the west coast of Baffin Island.

For negative weights of w_T pattern two there is a low pressure system over north Quebec. Positive vorticity and thickness advection produce ascent in the northeast sector of the depression

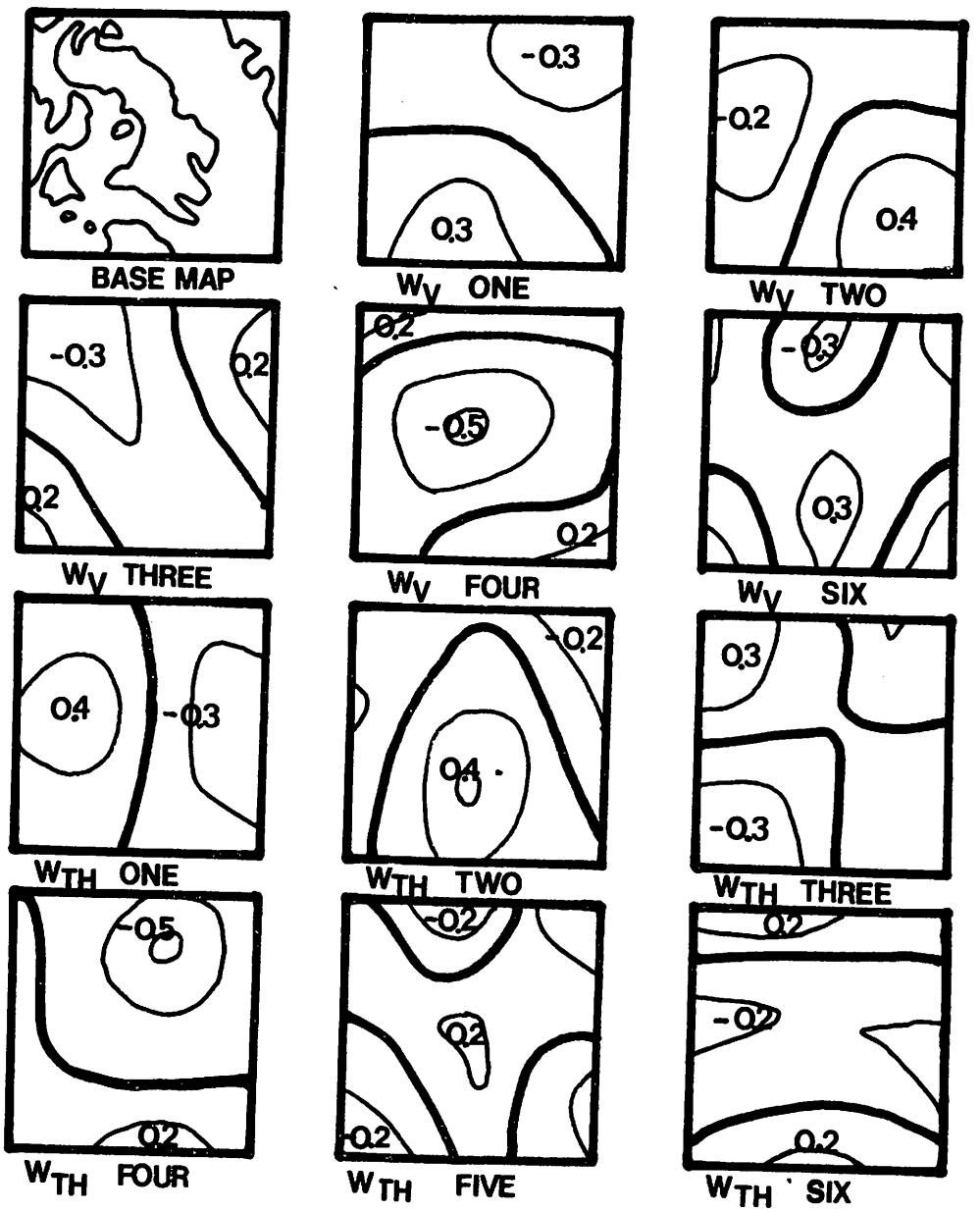

Legend: Figure 18

FIGURE 22 EIGENVECTORS OF VERTICAL VELOCITY COMPONENTS

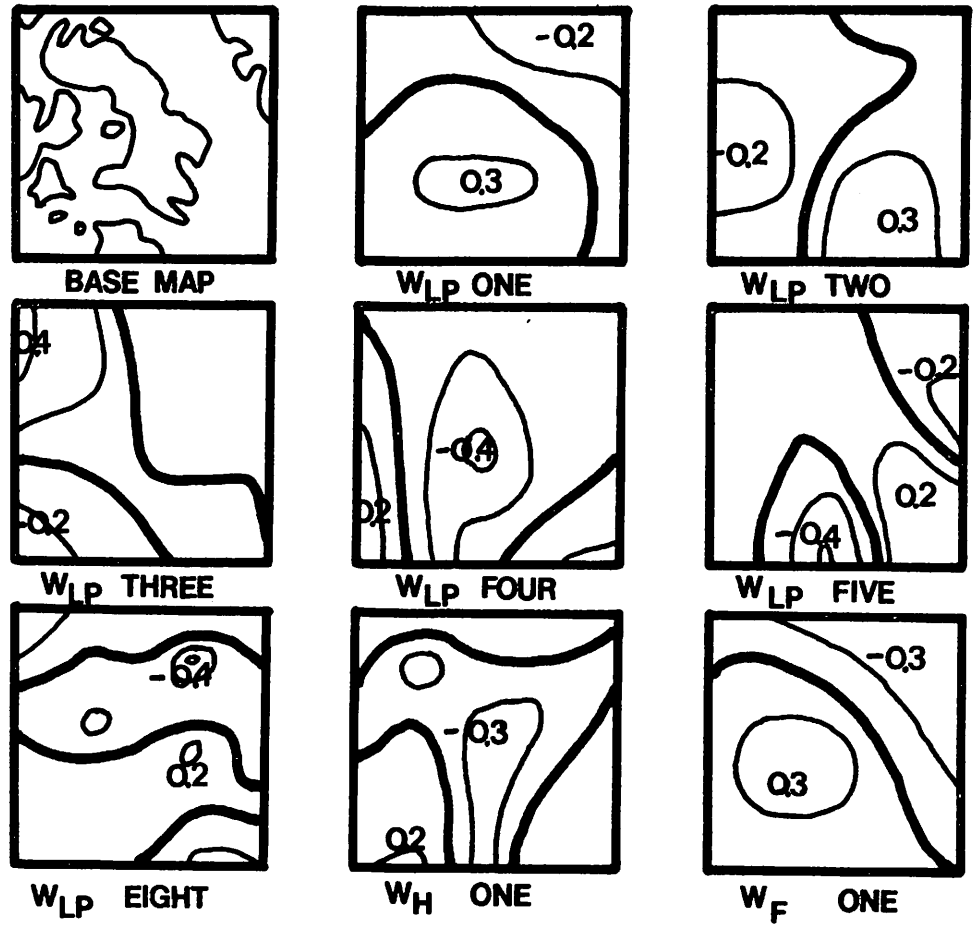

Legend : Figure 18

FIGURE 23 EIGENVECTORS OF VERTICAL VELOCITY COMPONENTS

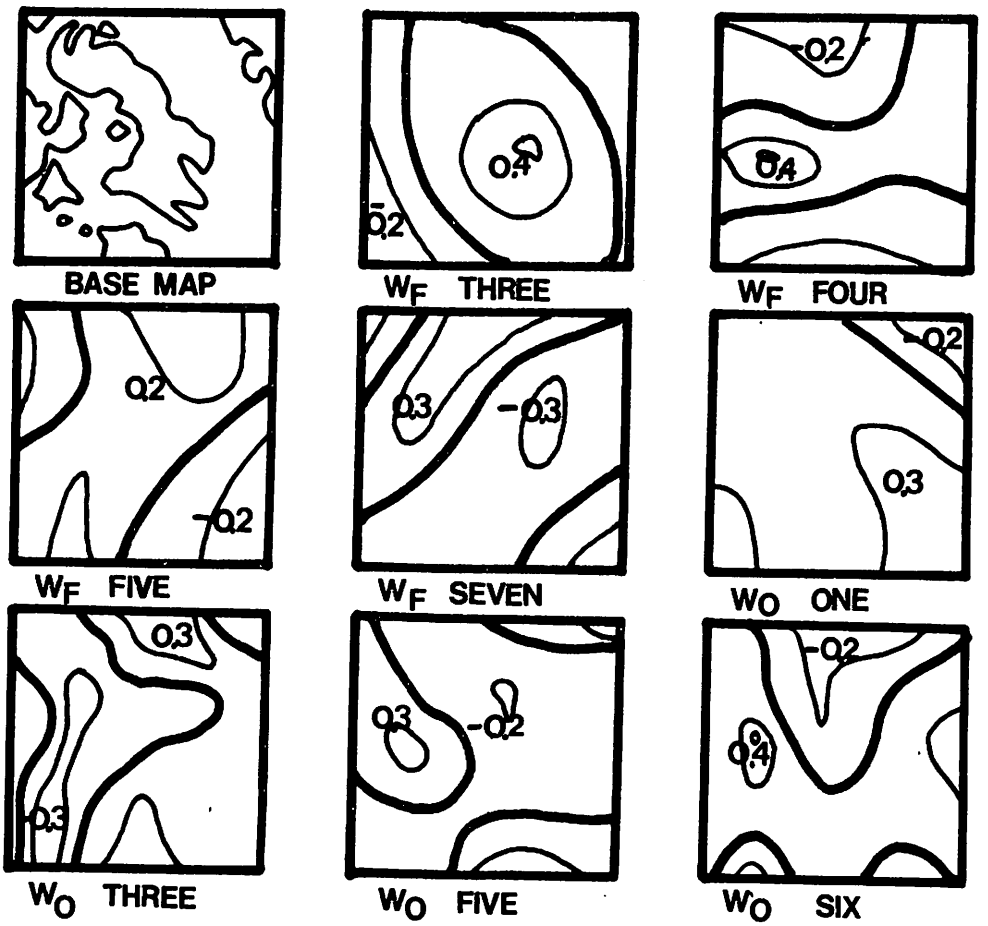

Legend : Figure 18

FIGURE 24 EIGENVECTORS OF VERTICAL VELOCITY COMPONENTS

which is augmented by latent heat release and frictional convergence. At the same time the advection terms produce subsidence to the north of the low over Foxe Basin and Melville Peninsula. As the easterly flow crosses Baffin Island orographic descent adds to this feature. For positive weights all signs are reversed and latent heat release is effective over Foxe Basin and not Davis Strait.

For the assemblage related to this eigenvector the correspondence of canonical weights is not always ideal and subjective interpretation is necessary. The relationship between w_T pattern two and w_F pattern five (canonical weights of -0.50 and -0.71 respectively with a canonical correlation of 0.58) is an example. There is an obvious relation over southern Davis Strait and part of Foxe Basin but elsewhere there is complete mismatch. In the north and northeast sectors the sign of the contours of the two fields is reversed. Here w_F pattern five is correlated on this canonical vector pair with the inverse of w_T pattern three (canonical weight of -0.38). It is difficult to interpret a large eigenvector weight (the basis of the canonical correlations) when in one case it may be biased by good representation in the original data at one sector and in another case the dominance of features in another sector may be responsible. This makes empirical analysis less than perfect and opens the possibility for one pattern to be related realistically to two different patterns of a different data field.

W_T eigenvector three: has two major features of ascent (with positive weights) in the southeast and northwest of the grid space and a region of descent to the southwest over Hudson Bay. W_V pattern four has ascent in these southeast and northwest quadrants separated by a steep dome of descent. W_{TH} pattern three acts to augment the two sectors of ascent, counteract the sector of descent in the center over Baffin Island, and adds to the descent to the southwest. W_{LP} pattern three has very similar contours. It is apparent that the advective terms dominate and the resulting ascent prompts latent heat release. With this vertical velocity pattern and positive weights the pressure field is the inverse of 85 cb height eigenvector four (A2 from Barry's catalogue) with a central ridge from southwest to northeast and low pressure cells in regions of positive vorticity and thickness advection over northwest Baffin Island and south Davis Strait.

W_T eigenvector four: is dominated by an elliptical zone of ascent orientated along the east coast of Baffin Island associated with a widespread low pressure cell (85 cb height pattern three). Vorticity (inverse of w_V one) and thickness (inverse of w_{TH} four) advection have maxima of their respective eigenvectors in this region. There is also a similarity over central Baffin Island with the inverse of w_{LP} pattern four. Frictional convergence (w_F patterns three and four) and orographic ascent (the match with w_O pattern three is evident only along the northeast coast of Baffin Island) also seem to be significant factors in this uplift.

W_T eigenvector five: is the only eigenvector of w_T that is significantly related to a pattern of surface thermal effects (w_H pattern one) in the canonical analysis. The correspondence between the two patterns with a negative anomaly over central Baffin Island and positive anomalies over Davis Strait and Hudson Bay is very clear. In this connection the seasonal trend of w_T eigenvector five (cf. previous section) should be emphasized. In winter the weights are positive with descent over land and ascent over water in the south (to the north there is not any significant distinction between ice covered sea and land) and they are negative in summer with uplift over land and subsidence over the water. This is consistent with the expected effects of the temporal changes in the land-sea constrast of thermal properties on w_H.

The correspondence of this w_T eigenvector with advected mechanisms is restricted to parts of the respective maps with mismatch of contours elsewhere. Vorticity advection pattern three matches to the southwest and central sectors only and thickness advection pattern four matches to the southeast and, to a lesser extent, to the southwest. Over Davis Strait and Baffin Island there is also a relationship with w_F pattern seven.

W_T eigenvector six: is correlated with w_V pattern six and w_{TH} pattern five. Note that these patterns of these two different component fields are nearly identical. Both processes give rise to features of descent (with positive weights) in the north central sector of the grid and over Hudson Bay. Orographic

effects (w_0 pattern six) strengthen the feature of descent to the north, and are responsible for an intense feature of ascent over the west Greenland coast.

W_T eigenvector seven: is related only to w_{TH} pattern six with ascent due to positive thickness advection (with positive weights) to the north and south with a broad band of descent across the central portion of the grid.

W_T eigenvector eight: has correspondence of features on the west and east coasts of Baffin Island with those in pattern eight of w_{LP} - latent heat release. This is also true in the northeast, northwest, and southwest corners of the grid. The relationship with thickness advection (w_{TH} pattern four) is very poor except for the feature at the west coast of Baffin Island.

Note that not all possible relationships indicated in Table X are included in the summary Table XI. Many with low canonical weights, or with widely different weights, or represented on a vector with a low canonical correlation with the data, were rejected after inspection of the eigenvector patterns. In some cases a relationship is indicated between a synoptic feature in w_T and one in a component field in another sector of the grid. This is most probably related to the large scale circulation associated with the w_T feature but not necessarily a component of that feature. This illustrates the ambiguous nature of canonical analysis and the need for independent empirical or subjective verification. It is worth re-emphasizing that the comparison is only of patterns,

not the relative contribution to the total intensity of the vertical circulation since standardized data are used. We are relating features of the circulation which have similar spatial distributions for average conditions.

To test these proposed assemblages independently, we select thirteen grid points which represent seemingly important loci of synoptic activity in the w_T eigenvector patterns. Using a step-wise linear regression of w_T (dependent variable) against the six component fields of the vertical velocity (independent variables) we may determine which physical processes are most highly correlated with the total vertical velocity (non-normalized data are used so we are comparing magnitudes) by an examination of the variance explained by the regression.

If a 'key' day classification were used (e.g. Barry, 1974) we could associate a pattern with a unique sample of data but this is not possible when several patterns may be represented in a given day's data. As a compromise the sample for each grid point regression is taken from those cases when the weight of the eigenvector of interest is very large, which means that the pattern is well represented in the original data. The arbitrary criterion of large is a weight in excess of plus or minus 1.5 standard deviations from the 234 day mean. A level of two standard deviations resulted in a very small sample and one standard deviation included up to one-half of the total period. The final sample size varies from 23 to 33. With high order eigenvectors (i.e. six) the standard deviations of the weights

is relatively small (cf. Figure 19) and the representation of the pattern in the data is not as good in this abbreviated sample as for the first eigenvectors and we expect the verification to be less reliable. The results of the step-wise multiple regression are summarized in Table XII for the synoptic systems selected.

The confirmation of the canonical analysis is very good in many instances. For example, the dominance of orography on the vertical circulation over Baffin Bay - west Greenland for eigenvector one is evident both in a comparison of patterns and a comparison of magnitudes at one point. The related vertical motion field accounts for 58 per cent of the variance in the magnitudes of the total vertical velocity. The linear regression indicates that the two advective terms account for 98 per cent of the variance in the vertical circulation of the central Davis Strait synoptic system (eigenvector two). These terms account for 96 per cent of the variance for the feature over southeast Davis Strait (eigenvector three), 81 per cent of the variance over Hudson Bay (eigenvector three) and 92 per cent over the northeast coast of Baffin Island for eigenvector four. Over west Greenland for eigenvector six orographic influences account for 81 per cent of the variance. These physical linkages are in substantial agreement with those proposed from the pattern analysis.

For eigenvector five, the best visual correspondence is with a pattern of surface thermal effects, yet this factor accounts for only one per cent of the variance in the

TABLE XII

SUMMARY OF STEP-WISE MULTIPLE REGRESSION OF W_T (DEPENDENT VARIABLE) VERSUS THE COMPONENT VERTICAL VELOCITIES (INDEPENDENT VARIABLES)

Samples are bases on cases when eigenvector weights exceed $\pm$ 1.5 standard deviations from the 234 day mean. Figures in parenthesis are increases in per cent variance explained by the linear regression.

Location	Eigenvector	Sample Size	Order of Component Variables
Baffin Bay	one	32	$w_O(58)$, $w_V(22)$, $w_{TH}(19)$, $w_F(1)$ $w_H(0)$, $w_{LP}(0)$
Foxe Basin	one	32	$w_V(47)$, $w_{TH}(44)$, $w_O(5)$, $w_F(4)$, $w_H(0)$, $w_{LP}(0)$
Central Davis Strait	two	32	$w_V(73)$, $w_{TH}(25)$, $w_H(1)$, $w_F(1)$, $w_O(0)$, $w_{LP}(0)$
Melville Peninsula	two	32	$w_F(70)$, $w_{TH}(17)$, $w_V(11)$, $w_O(1)$, $w_H(1)$, $w_{LP}(0)$
Southeast Davis Strait	three	31	$w_V(47)$, $w_{TH}(49)$, $w_O(2)$, $w_F(1)$, $w_H(1)$, $w_{LP}(0)$
Northwest Baffin Island	three	31	$w_F(60)$, $w_V(15)$, $w_{TH}(19)$, $w_O(3)$, $w_H(2)$, $w_{LP}(1)$
Hudson Bay	three	31	$w_V(55)$, $w_{TH}(26)$, $w_O(14)$, $w_F(4)$, $w_H(1)$, $w_{LP}(0)$
Northeast Coast of Baffin Island	four	33	$w_V(73)$, $w_{TH}(19)$, $w_O(6)$, $w_H(1)$, $w_F(1)$, $w_{LP}(0)$

TABLE XII (continued)

Location	Eigenvector	Sample Size	Order of Component Variables
Central Baffin Island	five	29	$w_F(76)$, $w_O(10)$, $w_{TH}(5)$, $w_V(8)$, $w_H(1)$, $w_{LP}(0)$
Hudson Bay	five	29	$w_V(53)$, $w_{TH}(40)$, $w_F(6)$, $w_H(1)$, $w_{LP}(0)$, $w_O(0)$
West Greenland	six	28	$w_O(81)$, $w_V(15)$, $w_{TH}(3)$, $w_H(1)$, $w_{LP}(0)$, $w_F(0)$
North Baffin Island	seven	29	$w_F(59)$, $w_V(12)$, $w_{TH}(27)$, $w_{LP}(2)$, $w_O(0)$, $w_H(0)$
East Baffin Island	eight	23	$w_V(51)$, $w_{TH}(38)$, $w_O(8)$, $w_H(4)$, $w_F(1)$, $w_{LP}(0)$

magnitudes for the entire sample. The highest explanation is for the advective mechanisms over Hudson Bay (93 per cent) and frictional effects over central Baffin Island (76 per cent). In the canonical analysis the significance of these linkages is less certain. Over Baffin Island the visual match of contours is not very good and the Hudson Bay feature is at the corner of the grid and the match of the patterns is restricted to one or two grid points - elsewhere there is complete mismatch. A larger grid space is necessary for this type of analysis.

The poor confirmation of some assemblages may be related to the differences in the two types of analysis. For the system located over Melville Peninsula in eigenvector two the advective terms (which include a total of 28 per cent of the variance) are seemingly insignificant when compared to frictional processes (70 per cent of the variance). A similar situation exists for the northwest Baffin Island feature in eigenvector three. The dominance of friction was not so evident in the visual match of eigenvector contours while those of the advective components compared most favourably with the synoptic systems. Friction may be a local factor influencing only the one grid point chosen for comparison of magnitudes (a point close to a land-sea boundary on Melville Peninsula and northwest Baffin Island) whereas the canonical analysis was based on patterns defined by several grid points. This aspect is an important limitation to the confirmation of the proposed process assemblages.

By comparing magnitudes, we find that the advective terms are important (91 per cent of the variance) in the Foxe Basin center of eigenvector one. From pattern analysis we proposed that the local effects should predominate. From inspection of Table X we see that the first eigenvector of w_T is not correlated at all with any patterns of either thickness or vorticity advection. The reason for this apparent contradiction is not clear.

For high order eigenvectors, the disparity between the two types of analysis may be traced in part to the method of data selection. These eigenvectors have weights with relatively low standard deviations and so have a lower representation in the original data field. Each case of the sample may include another pattern of equal importance which may be related to a different set of mechanistic linkages. Perhaps the cut-off point for case selection could be raised for these patterns but the original sample would have to be increased considerably to get a large enough sub-sample for regresssion analysis.

For the first six patterns of total vertical velocity which represent 73 per cent of the variance in the data these independent tests confirm the interpretation of the canonical analysis of patterns for many synoptic features despite the different approaches. Analysis of similar patterns is most reliable when the patterns match visually over several grid points. When the process is restricted to one or two grid points (localized land-sea frictional contrasts, for example) or when the synoptic system is at the edge of the grid and represented in the grid

space by only one grid point, the results of the canonical analysis will be biased by match or mismatch over the rest of the grid. It is also possible that the patterns may match closely over much of the grid, yet the actual significance in terms of the total magnitude may be minor. Other independent processes may affect both data fields. One mode of analysis cannot be considered sufficient. From a comparison of magnitudes we do not know the regional relationships of the features of circulation and from a comparison of patterns we do not know the relative significance of each process linkage.

Seasonal Interpretation of the First Five Eigenvectors of W_T

From inspection of ten day averages of the w_T eigenvector weights (Figure 19) it was noted that there are distinct seasonal trends for the importance of several of the patterns. It is also possible that there may be seasonal changes in the process linkages proposed in the previous section. In this section this seasonality is discussed with reference to the magnitude and sign of the vertical circulation and the relative contribution by 85 cb processes.

The data for each of the first five eigenvectors are selected only for those cases when the corresponding weights indicate high representation of the pattern in the data. We use the criterion adopted in the previous section to determine cases of high representation. Because of the low standard deviation of weights of the high order patterns the sample so selected does not

necessarily contain a large percentage of cases when the pattern under consideration is highly represented (see the discussion of this point in the previous section) and for this section these eigenvectors are omitted.

For the cases considered the vertical velocity data at 85 cb (non-normalized) are extracted for grid points representing loci of activity in each pattern. The 85 cb vertical velocities attributed to each process at that level (vorticity and thickness advection, latent heat release and surface thermal effects) are calculated by solving each term on the right hand side of the omega equation for ω. By comparison of each with the total of all four terms the per cent contribution by each process may be determined. For 60 day periods the mean total vertical velocity, the contribution by each process and frequency of occurrence are presented in Table XIII. The data are separated for cases of positive and negative weights. Unfortunately orographic and frictional effects cannot be included in this discussion as they are not internal terms of the omega equation at 85 cb but are boundary conditions. Therefore we do not include synoptic centers which, in the previous section, have been shown to be dominated by orographic or frictional controls.

For w_T eigenvector one the Foxe Basin data illustrate the importance of the advective terms, for both positive and negative weights, throughout the year. The contribution by vorticity advection varies from 15 per cent to 67 per cent of the total while the range for thickness advection is 31 to 127 per cent.

TABLE XIII

VERTICAL VELOCITY DATA FOR CASES WHEN THE FIRST FIVE EIGENVECTORS ARE PREDOMINANT

Format: Positive Weights / Negative Weights
Freq. : Number of occurrences in the 60 day period.
W_T : Period mean of total vertical velocity at 85 cb, cm s^{-1}.
W_V, W_{TH}, etc. : Period average of per cent contribution to the total vertical velocity by each 85 cb source

		J-F	M-A	M-J	J-A
Eigenvector One					
Foxe Basin	Freq.	0	2	3	3
		4	7	9	4
	W_T		1.4	0.6	0.3
		-1.2	-0.8	-0.8	-0.6
	W_V		39	15	27
		67	-30	46	-23
	W_{TH}		55	84	64
		31	127	53	71
	W_{LP}		2	2	33
	W_H		4	3	-24
		2	3	1	51
Eigenvector Two					
Central Davis Strait	Freq.	3	6	3	5
		1	8	2	4
	W_T	-0.9	-0.8	-0.9	-0.7
		1.6	0.9	1.1	0.8
	W_V	70	64	81	43
		48	62	12	88

TABLE XIII (continued)

		J-F	M-A	M-J	J-A
Eigenvector Two (continued)	W_{TH}	25	32	21	50
		48	35	83	3
	W_{LP}		4	5	11
	W_H	4	4	-1	8
		4	-1	1	2
Eigenvector Two Melville Peninsula	Freq.	3	6	3	5
		1	8	2	4
	W_T	0.7	0.6	1.4	1.4
		-0.6	-0.5	-0.9	-0.6
	W_V	-45	53	30	53
		63	131	-10	86
	W_{TH}	150	47	60	7
		35	-38	110	31
	W_{LP}	1	1	9	22
		0	0	0	0
	W_H	-6	-1	1	18
		3	7	0	-17
Eigenvector Three Southeast Davis Strait	Freq.	2	6	2	2
		7	5	5	2
	W_T	1.7	0.5	0.4	-0.2
		-0.3	-0.4	-0.3	-0.3
	W_V	45	63	42	-74
		56	-165	-254	88
	W_{TH}	55	34	50	110
		54	249	545	35

TABLE XIII (continued)

		J-F	M-A	M-J	J-A
Eigenvector Three (continued)	W_{LP}	1	1	10	0
		0	0	0	0
	W_H	-1	2	-2	64
		-10	-16	-191	-23
Eigenvector Four Northeast Coast of Baffin Island	Freq.	7	5	3	1
		0	2	6	9
	W_T	0.5	0.8	0.3	0.2
			-0.7	-0.4	-0.9
	W_V	-310	73	231	80
			154	100	79
	W_{TH}	442	22	-77	50
			-57	1	8
	W_{LP}	0	2	0	0
			0	0	0
	W_H	-32	3	-54	-30
			3	-1	12
Eigenvector Five Central Baffin Island	Freq.	5	5	1	0
		1	4	8	5
	W_T	-1.01	-1.23	-0.3	
		-1.6	0.7	0.3	0.1
	W_V	-7	73	36	
		38	53	223	-39
	W_{TH}	102	24	-31	
		59	46	-147	100
	W_{LP}	0	0	0	
		0	1	0	0
	W_H	5	3	4	
		3	0	24	38

There are eight cases with positive weights with a slight bias of occurrence towards the summer and the total ascent has a wide range of values (+0.3 to 1.4 cm s^{-1}). There are more cases with negative weights (24) with a slight increase in occurrence during the March-June interval but the vertical motion is more moderate (-0.6 to -1.2 cm s^{-1}). The local processes are insignificant through all months except July-August when latent heat release contributes 33 per cent towards ascent and descent due to cooling by the water surface (W_H) counteracts 24 per cent of the total for cases of ascent and contributes 51 per cent to the total for cases of descent. For the entire sample, these data tend to confirm the results of the regression analysis of magnitudes in the previous section which characterized this feature as a function of advective processes, but for the summer interval there is evidence for a strong contribution by local effects which supports the interpretation of the canonical analysis of patterns. For this problem a similar seasonal analysis of the functional and orographic terms is needed.

The significance of the advective terms in the central Davis Strait feature of eigenvector two is clearly evident in Table XIII. For positive weights (17 cases) there is moderate descent of -0.7 to -0.9 cm s^{-1} with a slight increase in frequency during the March-April and July-August periods. The two advective terms act in nearly equal strength during these intervals. For negative weights (15 cases) ascent has a wider

range of intensities (0.8 to 1.6 cm s^{-1}) with a minimum frequency (1) during January-February and a maximum (8) during the March-April period. In this period vorticity advection contributes 62 per cent while thickness advection contributes 35 per cent. For these cases of ascent the effect of latent heat release varies from zero during the winter to 11 per cent during the summer.

Over Melville Peninsula, with the same eigenvector, the synoptic system is also dominated by the advective processes, but during the summer (July-August) both latent heat release and surface thermal effects produce significant ascent. Note that the frictional effects considered in the previous section cannot be included here.

The synoptic feature over southeast Davis Strait (W_T eigenvector three) is found most often with negative weights (19 out of a total of 31 cases) and mild descent of -0.3 to -0.4 cm s^{-1}. Negative thickness advection is always a major factor in this descent. It is opposed by less intense positive vorticity advection during March-June but in the other months negative vorticity advection acts to increase the subsidence. Surface heating effects oppose the vertical circulation at all times when there is negative thickness advection (advection of cold air over a warmer water surface). The contribution varies from -10 to -191 (during May-June) per cent.

There are nearly equal numbers of cases with positive weights (16) and negative weights (17) for eigenvector four which includes the synoptic system at the northeast coast of Baffin

Island. Cases with positive weights are biased towards the winter with ascent of 0.5 (January - February) and 0.8 cm s^{-1} (March - April). Both advective terms are significant. They are large but act in opposition during January - February. In the March - April interval they are smaller in magnitude but are additive. Cases with negative weights are biased towards the summer with descent of -0.4 (May - June) and -0.9 cm s^{-1} (July - August). The contribution by negative vorticity advection is 100 and 79 per cent, respectively. The other processes have a small effect. The seasonal trend identified in Figure 19 is clearly evident, as is the significance of the advective terms which was proposed through considerations of the canonical analysis.

The seasonal trend of eigenvector five is apparent in the frequency tabulation of Table XIII. There is a prevalence of positive weights in winter and negative weights in summer. Vertical velocity data are for the synoptic feature over central Baffin Island. From the canonical analysis we found that this eigenvector has a good correlation of weights and visual correspondence with a pattern of w_H (surface thermal effects). During the summer months the surface heating contributes a substantial amount (24 per cent during May - June and 38 per cent during July - August) to the mild ascent (0.3 and 0.1 cm s^{-1}). In the winter the thermal effects are relatively minor and the advective terms tend to dominate the vertical circulation for this feature. Note again that the important frictional term is

not included in this discussion.

From examination of these examples it is apparent that there are seasonal variations in the process linkages for many of the synoptic features. The assemblages derived from canonical analysis of patterns may be valid in one season while those derived from independent regression analysis of magnitudes may be valid in another period. It would be advisable to base the analysis on samples subdivided according to season in future studies in order that more confident interpretations may be made.

Case Studies of Eigenvector Relationships

An eigenvector is an abstract concept. It is one of several mathematical surfaces found in the data for a given case. It is instructive, therefore, to study specific cases in order to identify visual similarities between the raw data and the highly weighted eigenvectors, and to verify the mechanistic linkages that have been suggested by analysis of the canonical relationships. According to the criterion adopted for the dominance of an eigenvector in the previous sections, there are two days in the detail study period considered in Chapter Four which illustrate the first two eigenvectors of w_T - eigenvector one is dominant on July 25, 1973, and eigenvector two is found on July 15. In this section these two cases are studied. For the other days eigenvector one is represented, but less strongly than on July 25, or high order vectors are weighted only slightly more than the others and thus the data pattern is a

composite of several eigenvectors. For each day considered the eigenvector weights of w_T, w_V, w_{TH}, w_H and 85 cb height are in Table XIV. The other fields are not included since the raw data for each are not mapped in Figures 8 and 14 and are therefore unavailable for visual comparison with the respective eigenvectors. Reference is also made to the results of the canonical analysis summarized in Table XI and the contour plots of Figures 18, 20, 22, 23, and 24.

The weights for July 15 emphasize w_T vector two, and, to a lesser extent, vector four. Vector two with a negative weight (all signs are reversed) is evident in the raw data (Figure 8) in a depression system to the southeast of Baffin Island over Davis Strait with a feature of descent over Foxe Basin. Ascent over Davis Strait is 1.5 cm s^{-1} and the mild subsidence over Foxe Basin is -0.2 cm s^{-1}. 85 cb height pattern one is highly represented, which is in accord with the assemblage suggested in Table XI. There is a deep low over north Quebec and a high pressure cell to the northeast. Vorticity advection pattern two with a zone of ascent over east Baffin Island is also highly weighted. Again, this is in agreement with the interpretation of the canonical analysis. The exception is the dominance of the highly convoluted w_{TH} pattern eight. This pattern effectively opposes the w_V pattern so that local effects control the vertical circulation (cf. the discussion of the case in Chapter Four). Since, for average conditions, we see from Table XI that the two advective processes reinforce each other to produce this w_T

TABLE XIV

EIGENVECTOR WEIGHTS FOR SELECTED DAYS OF THE DETAILED STUDY

PERIOD - JULY 13 - 25, 1973

See the introduction of this chapter for definitions of the data field symbols.

Data Field	Eigenvector Number								
	1	2	3	4	5	6	7	8	9
July 15									
W_T	0.3	-3.2	0.3	-1.6	-0.5	-0.8	0.3	0.1	
W_V	-0.7	2.2	-1.9	-1.6	0.7	1.2	1.7	-0.3	
W_{TH}	-1.1	0.5	-1.5	1.0	-1.2	0.3	-2.4	2.8	1.3
W_H	-3.6	-1.8	0.5	-0.7	-0.9	-0.1	-0.1		
85 cb height	4.5	3.2	-0.8	-1.1	-1.0				
July 25									
W_T	-3.9	1.1	2.0	0.5	-2.3	1.3	1.4	-0.5	
W_V	2.4	1.9	0.4	-0.2	-1.6	1.4	-1.6	0.2	
W_{TH}	-0.1	-3.0	3.2	0.2	0.4	0.7	0.5	-0.1	0.3
W_H	-4.0	-0.3	1.1	1.6	0.7	0.6	0.7		
85 cb height	-3.1	1.7	1.1	1.-	-1.3				

pattern, we must conclude that the dominance of local terms at this stage of the depression evolution in the southeast Baffin Island area for this particular case cannot be considered typical.

From subjective analysis in Chapter Four the Foxe Basin descent was attributed to the orographic effects to the lee of Baffin Island. This is one of the mechanisms proposed in Table XI for average conditions.

W_T pattern one has a very large weight of -3.9 on July 25. The correspondence in the data is with the center of ascent over Baffin Bay - west Greenland (with a negative weight the signs are reversed) and a zone of descent over Foxe Basin. The Baffin Bay sector of the pattern was identified in the canonical analysis with an orographic mechanism. This is the case on July 25. Trough flow around a southward moving polar low is forced up over Greenland with a vertical velocity approaching 3.5 cm s^{-1}. This promotes a pattern of latent heat release very similar to w_{LP} pattern two, which, for average conditions, is highly correlated with w_T eigenvector one (Table XI).

In the regression analysis the Foxe Basin system is related to a dominance of the advective terms. For the July 25 example both the thickness and vorticity advection are strong, but are effectively self-cancelling. Vorticity advection is negative, but thickness advection is positive since the flow is directed into a cold low over Davis Strait. For an ideal wave structure (cf. Fibure 1) this would be negative to the west of the trough and both mechanisms would reinfore each other to produce a zone

of descent. From the regression analysis we may conclude that this is normal for this sector of pattern one. In this case, the two effects counteract each other and the cooling over Foxe Basin by the downward enthalpy flux is responsible for the subsidence.

Summary and Discussion

In this chapter empirical techniques are used to identify average locations, types and intensities of major synoptic features for a 234 day sample in the eastern Canadian Arctic. The probable physical mechanisms for those features are also determined.

For the total vertical velocity at 85 cb eight characteristic patterns or eigenvectors are found for a five by five NMC grid which, in total, explain 83 per cent of the variance in the original data. The physical processes responsible for several well defined synoptic features found in the major patterns are found and verified in two independent statistical tests and subjective analysis of individual cases.

In the first test multiple regression (canonical analysis) is used to find patterns in the total vertical velocity and each of the six component fields - each resulting from one physical process - which are highly correlated through time. If similar patterns are related throughout the sample we may assume that there are realistic physical linkages. In the second test the magnitudes of the vertical circulations for each field are compared

for the grid point central to each synoptic feature using step-wise linear regression. In this manner the variance in the total vertical velocity explained by each of the component fields for the entire sample is found. The results of these two independent tests - one comparing spatial features and the other comparing intensities at one point - are in substantial agreement. Two days are found in the detailed study period discussed in Chapter Four when each of these first two patterns is highly represented in the data. The subjective analysis of the process mechanisms (Chapter Four) for each of the key synoptic features in these patterns is similar to the results of the statistical analysis of the entire sample. It is also found that, despite the abstract nature of eigenvectors, the patterns can be easily recognized in the raw data if the weights are high.

W_T eigenvector one includes a synoptic feature over Baffin Bay which is closely related to the orographic influence of Greenland on the flow which, for negative weights, induces uplift and latent heat release. A system of opposite vertical circulation is found over Foxe Basin. For average conditions it is related to advective influences, but during the summer months the local effects of latent heat release and the surface enthalpy flux are significant. There is an increase in importance of this pattern beginning in mid-May. For the case examined in detail (July 26, 1973) this pattern was predominant when an arctic low decayed and drifted south along the west Greenland coast forcing a trough

circulation with the west limb over Foxe Basin (which normally would be associated with negative vorticity and thickness advection) and the east limb was over Greenland with strong topographic forcing.

In eigenvector two there is a major synoptic vortex over central Davis Strait. As a feature of ascent (with a frequency maximum in March - April) it is in advance of a large depression over north Quebec and is controlled by positive vorticity and thickness advection, latent heat release, and frictional convergence. At the same time the advective terms are negative to the north of the low over Foxe Basin and Melville Peninsula producing a region of descent which may be intensified by orographic descent over the lee (west) side of Baffin Island. With the opposite vertical circulation the vertical velocity is less intense and there are two frequency maxima - one in March - April and another in July - August.

There are three important features in eigenvector three - over southeast Davis Strait, northwest Baffin Island, and a system of opposite vertical circulation over Hudson Bay. For all features thickness and vorticity advection are significant processes. For instances of positive weights, which have a frequency maximum during March - April, there is ascent over Davis Strait and northwest Baffin Island within low pressure cells which flank a central high pressure ridge orientated northeast-southwest. The most common case is with negative weights and mild descent of -0.3 to -0.4 cm s^{-1} over Davis Strait. There are large frequencies from January through June.

Eigenvector four illustrates a broad synoptic feature orientated along the northeast coast of Baffin Island which, with positive weights, is a zone of ascent related to a widespread low pressure cell. These cases are biased towards the winter and both advective terms are significant. Ascent is in the range of 0.5 to 0.8 cm s^{-1}. Cases with negative weights are biased towards the summer with moderate descent of -0.4 to -0.9 cm s^{-1} governed almost entirely by negative vorticity advection.

Eigenvector five is the only pattern related in spatial configuration to the surface thermal effects. Over central Baffin Island these effects are insignificant in terms of the contribution to the variance of the total vertical velocity for the entire sample, however during the summer months the contribution to the total ascent by surface heating is 38 per cent. Frictional influences are significant at all times for this feature. Over Davis Strait and Hudson Bay the synoptic systems in this pattern are of opposite vertical circulation and are dominated by vorticity and thickness advection.

The empirical techniques used in this study have been reasonably successful in the identification of major synoptic features, their seasonal bias and process linkages. It is probable that the results would be more reliable if a 'key' day type of classification were used for all fields. A pattern could then be associated with a unique set of data for statistical tests. With eigenvector classification a set of data may be realistically associated with several patterns.

For a 'key' day classification, however, a much larger sample would be required since there would be many more patterns to be analyzed, each with its own unique set of data for the component vertical velocity fields.

In this type of 'static' classification it is impossible to trace the changes in process linkages during the history of a synoptic event and there does not seem to be a well defined repetitive sequence of dominant patterns that could be studied in terms of the evolution of a system. Such a study would be of major interest especially in light of the alternation between advective and local influences found during the course of the system examined in Chapter Four. It would be possible to produce a modified static classification by moving the grid with reference to the center of a depression system. Klein et al (1968) have used this approach to classify the probability and amount of precipitation in various quadrants of a depression system for different cyclone intensities. The techniques used in this chapter could still be applied but instead of identification of mean features and processes at a location the characteristic pattern and assemblage of mechanistic linkages would be related to a certain stage in the evolution of the system. This would certainly lead to a greater understanding of the influence of the Arctic surface on synoptic systems. It would be necessary, however, to consider a much larger grid system to include the entire vortex as it drifts in and out of the region of interest.

CHAPTER SIX

CONCLUSIONS

In 1932 Hesselberg defined dynamic climatology as the "...quantitative application of the laws of hydrodynamics and thermodynamics ... to investigate the general circulation and state of the atmosphere, as well as the average state and motion for shorter time intervals" (Barry and Perry, 1973). Hare (1957) adds that dynamic climatology is "... the explanatory description of world climates in terms of the circulation or disturbances of the atmosphere". These are apt descriptions of this study in the eastern Canadian Arctic. A three-dimensional diagnostic model of atmospheric dynamics is used to determine the physical mechanisms responsible for the major synoptic features of this region. The mechanisms considered are of advected and local origin: differential advection of vorticity, horizontal thickness (thermal) advection, release of latent heat, surface thermal effects, and frictional and orographic influences at the surface. Each acts in combination with the others to produce a vertical circulation and attendant pressure rise or fall. With the aid of the diagnostic model we can calculate the magnitude of each mechanism and the relative contribution to the total intensity of the vertical circulation, and thus examine its effect on synoptic activity. In this manner we relate, quantitatively, the occurrence of low and high pressure features on the regional map to the dynamics of the large scale

flow (the advected mechanisms) and to the processes of local origin.

We examine these relationships with two different approaches. In the first the history of a mid-latitude depression system in July, 1973, is traced through the eastern Canadian Arctic. This system is a common feature of the summer synoptic map. A mature vortex is deflected north towards Davis Strait by strong North Atlantic blocking. For this example it leaves south of Greenland as a decaying system. From qualitative analysis of the products of the diagnostic model we interpret the evolution of this system, within the region, in terms of the shifts in the imbalance of the advected and local mechanisms.

The second approach is a static view in contrast to this case study of development and decay, however, a large sample (234 days) can be evaluated conveniently and general conclusions may be made. The data include the winter and summer of 1973. For average conditions the major centers of synoptic activity in the eastern Canadian Arctic are defined by classifying the field of the total vertical velocity into characteristic patterns. Using empirical techniques to compare both magnitudes and spatial configurations of the total vertical velocity and the component vertical velocities, the prominent mechanisms responsible for each synoptic center are identified. Seasonal changes in both the intensity of these centers and the proposed mechanisms are also discussed.

For the case study of a mid-latitude depression center entering the region of interest we may make the following observations:

1. Upon entering the grid region from the south over central Quebec (July 13) the vortex exhibits the signs of a developing mid-latitude depression. Patterns of vorticity and thickness advection are in phase promoting intense uplift (4 cm s^{-1}) and pressure fall in advance of the system. This uplift is augmented by diabatic effects (latent heat release) which, in mid-latitude systems, commonly acts to prolong the life of the depression.

2. The abrupt shift from zonal to meridional flow as this system enters the Arctic results in a deformation of the isotherms with the development of a cold tongue in the Hudson Bay - Davis Strait area. This alters thickness advection features such that on July 15, 48 hrs after the mature vortex stage, the vorticity and thickness advection act to self cancel within the low. The system would fill and decay rapidly since surface frictional convergence and zero uplift at 85 cb results in mass accumulation in the lower troposphere. However, the southeasterly cyclonic flow at the southeast coast of Baffin Island promotes frictional onshore convergence, orographic uplift, latent heat release, and, coupled with surface heating over the Island, these factors result in local uplift of 1.5 cm s^{-1} and surface pressure fall. The vortex moves over

this area (July 17) and is stabilized there until July 19 by these local mechanisms.

3. A Polar low over the Queen Elizabeth Islands intensifies and the cyclonic circulation combines with that of the Baffin Island low in a trough in the grid area (July 21). The enhanced vorticity advection along the east limb of this trough is combined with thickness advection into a cold dome in this sector resulting in uplift of 1.3 cm s^{-1} over Davis Strait. This rejuvination of the advective terms prompts movement of the Baffin Island low towards Davis Strait and out of the grid area towards the south of Greenland on July 22, nine days after it entered the region.

4. The intensification of this Polar low results in increased westerly flow over Baffin Island with warm air advection of approximately 8 x 10^{-5} kj kg^{-1} s^{-1} at 85 cb on July 22 into the cold dome which is now situated over Davis Strait. This is coupled with adiabatic compression in the lee (east) side of Baffin Island (4 x 10^{-5} kj kg^{-1} s^{-1}). The resultant warming episode is coincident with a major ice melt of 25 cm in 48 hr along the east coast of Baffin Island.

5. On July 24 the Polar low abruptly decays (85 cb height of 129 decameters as compared to 120 decameters on July 23) and moves into Baffin Bay as the mid-latitude system leaves the grid. The movement of this weakened low into Baffin Bay and south along the west coast of Greenland is prompted by strong (3 cm s^{-1}) orographic uplift as the flow of the trough around

this low ascends the west coast.

6. The creation of the cold tongue over Hudson Bay and Davis Strait by deformation of the isotherms as the flow changes from zonal to meridional at the beginning of the study period sets the stage for the development of the classical Arctic 'cold low'. This develops as the isobars coincide with the isotherms of this tongue on July 17, when local effects dominate the vortex circulation. Note that the mid-tropospheric cold center does not form in situ within the low due to adiabatic expansion, as previously suggested, but is rather a feature of the large scale flow. The maintenance and intensification in any direction may be a result of adiabatic expansion. However, depending on flow and surface characteristics, it may also be a result of horizontal advection (cooling in the direction of flow) or surface thermal influences (cooling from below). This latter factor causes the cold center to be stabilized over Davis Strait as the low drifts out of the region on July 21. The uplift and adiabatic cooling within the low at this stage is still intense, however the cold low formation is broken because of this dominance of the local surface thermal effect. These complex mechanistic interactions between the flow and local features may not provide a general explanation for the cold low, which has a high frequency in many sectors of the Arctic. A systematic diagnostic examination of many more cases is required for different locations.

This detailed study of an actual synoptic event lends

confidence to the suitability of the diagnostic model for the identification of physical processes involved in a vortex circulation. The observed development and decay follows closely that expected from analysis of the computed vertical velocity field. The vorticity and thickness advection effects are consistent with the observed flow and isotherm configuration. The reliability of the magnitudes of the local effects is unknown, however, their combined intensity can be appreciable (1.5 cm s^{-1} at 85 cb) and may account for the observed synoptic development when the advective processes are insignificant. Throughout this synoptic episode dominance of advective and local effects alternate. Upon entering the region advective influences are important. Once the system is over Baffin Island, advective influences self cancel and local effects stabilize the circulation. The depression leaves the area when advective effects once more predominate, but at this point they result from the circulation of the Polar low.

In the second type of analysis, the total vertical velocity field at 85 cb for a sample of 234 days (January 2 to August 24, 1973) is decomposed into characteristic patterns or eigenvectors. The first eight patterns have some physical significance and account for 83 per cent of the variance in the original data. The physical mechanisms for the synoptic featuers in the first five eigenvectors (66 per cent of the variance) are well documented using two independent statistical tests and subjective verification with the detailed case study

analysis for July 15 and 25. We make the following observations.

1. The most prominent pattern of vertical circulation accounts for 18 per cent of the variance. This includes a system over Baffin Bay which is closely related to the orographic influence of Greenland. With ascent there is also significant latent heat release. A vertical circulation of opposite sign is found over Foxe Basin for these cases. It is dominated by advective processes, but during the summer months latent heat release and effects of the surface enthalpy flux may also be significant. This pattern increases in importance for both positive and negative weights during the June through August interval of the sample. For the case studied in detail, this pattern occurred when a polar low decayed and drifted south along the west Greenland coast. Here the orographic influences were apparent. The large scale flow was a deep trough around this low which would normally be associated with negative vorticity and thickness advection and attendant subsidence along the west limb over Foxe Basin.

2. In eigenvector two (16 per cent of the variance) are two major synoptic features associated with a low pressure cell (for negative weights) over north Quebec. To the north east of this depression positive advection of vorticity and thickness, combined with latent heat release and surface frictional convergence, produce a zone of ascent over central Davis Strait with vertical velocities in the range of 0.8 to 1.6 cm s^{-1}.

To the north and northwest over Foxe Basin and Melville Peninsula the advective terms are negative and there is a region of descent in the range of -0.5 to -0.9 cm s^{-1}. This may be augmented by orographic descent over the lee (west) coast of Baffin Island. There is a frequency maximum of this situation in March-April. With reverse signs of vertical velocity (positive weights) the vertical circulations are less intense and the frequency maxima are in March-April and July-August.

The Davis Strait low is found in the mean pressure maps of Petterssen (1950) who used U. S. Weather Bureau historical maps from 1899 to 1939, and is also found in the July-September cyclone frequency maps of Reed and Kunkel (1960) for the 1952-1956 period. On this same map there is a maximum of anticyclonic frequency over Foxe Basin. This configuration corresponds to eigenvector two with negative weights.

3. The third eigenvector includes 13 per cent of the variance in the data and illustrates three centers over Davis Strait, northwest Baffin Island (both with ascent for cases of positive vector weights) and Hudson Bay (with descent for positive weights). All of these synoptic features are dominated by the advective processes. There is a maximum frequency of instances with positive weights during the March-April interval. For these cases there is a central high pressure ridge orientated northeast-southwest flanked by low pressure cells over Davis Strait and northwest Baffin Island. Over Davis Strait ascent is

moderate (0.5 cm s^{-1}). However, the most common case is with negative weights and mild descent of -0.3 to -0.4 cm s^{-1} over Davis Strait. There are large frequencies from January through June. The pressure pattern is reversed with low pressure replacing high pressure.

4. The fourth pattern (11 per cent of the variance) represents a zone over the east coast of Baffin Island. With positive eigenvector weights there is ascent of 0.2 to 0.8 cm s^{-1} associated with a widespread depression system over Baffin Island. These cases are biased towards the winter and both advective terms are significant. For cases of negative weights the bias is towards the summer with descent of -0.4 to -0.9 cm s^{-1}. Negative vorticity advection dominates the vertical circulation under the high pressure dome.

5. The spatial configuration of eigenvector five is very similar to a pattern of the surface thermal effects. Weights of the two patterns are highly correlated throughout the sample; however, this process is insignificant in terms of the magnitude of the total vertical circulation for the synoptic feature over south Baffin Island, except for the summer months. For the entire sample interval, most of the variance in the total vertical velocity is explained by the frictional processes over the Island. In this pattern there are two other synoptic systems over Davis Strait and Baffin Bay. These features are dominated by thickness and vorticity advection.

In this static analysis the emphasis is on the average location and morphology of the major synoptic systems. By comparing patterns and magnitudes of the total vertical velocity and the component vertical velocities, we can adequately define the mechanistic linkages for these systems - for mean conditions. However, we do not know the geographical origin of these systems, except for a historical study of one episode, nor the dominant processes at different stages of the average development of a system through the region. An attempt is made to find significant sequences in the occurrence of the patterns of total vertical velocity which could be interpreted in evolutionary terms. The results are negative.

For both the historical and static analyses it is emphasized that the present grid format is not ideal. Often a vortex is only partially in the grid, and major events in this circulation may be off the grid entirely. In future work it would be advisable to base the calculations of the diagnostic model on a much larger grid and analyse the derived data for a reduced grid referenced with respect to the depression center. The grid would move with the system and encompass the entire vortex. The processes could be examined with reference to their location in the system. A classification and study of the process linkages could be made so that each category represented one stage in the evolution of the low, which would have its own average characteristic pattern, rather than for average geographical locations. This design would be more suitable for

the study of depression development and decay.

The methods used in this study to investigate the regional dynamic climatology are new and previously untested. Diagnostic models of atmospheric dynamics have been used extensively in the middle latitudes to investigate the properties of individual systems. The purpose of these theoretical models has been to verify or refine dynamic concepts derived from forecast experience or statistical studies of readily available climatological data. But these models have not been used to generate a large sample of derived data which may be interpreted directly with respect to the prominent or average mechanistic linkages involved in the major synoptic systems of a region. Whereas the magnitudes and importance of each process involved may be examined easily by manual analysis of the model generated data throughout the evolution of one system, it is much more difficult to handle and interpret a large sample of data - data which are several steps removed from the observations. The empirical analysis of Chapter Five only applies to two levels and is based on 46,000 data values from the model calculations and the regional pressure field. In these original calculations there are six levels in the model with approximately 160,000 values of vertical velocity alone. Computer requirements for data analysis and storage are expensive. A major proportion of the effort in this study was directed towards the development and verification of an experimental design that would satisfy

the objectives with a minimum of operator bias in the analysis yet be relatively efficient in terms of computer demands.

BIBLIOGRAPHY

Allis, J.A., B. Harris, A.L. Sharpe, 1963, A COMPARISON OF PERFORMANCE OF FIVE RAINGAUGE INSTALLATIONS, J. Geophys. Res., 68:4723-4730

Anthes, R.A., S.L. Rosenthal, J.W. Trout, 1971, PRELIMINARY RESULTS FROM AN ASYMMETRIC MODEL OF THE TROPICAL CYCLONE, Mon. Weath. Rev., 99:744-758

Asnani, G.C., S.K. Mishra, 1975, DIABATIC HEATING MODEL OF THE INDIAN MONSOON, Mon. Weath. Rev., 103:115-130

Barry, R.G., 1967, SEASONAL LOCATION OF THE ARCTIC FRONT OVER NORTH AMERICA, Geog. Bull, 9:79-95

Barry, R.G., A.H. Perry, 1973, SYNOPTIC CLIMATOLOGY, Methuen and Co. Ltd., London, 555 pp.

Barry, R.G., 1974,FURTHUR CLIMATOLOGICAL STUDIES OF BAFFIN ISLAND, NORTHWEST TERRITORIES, Environment Canada, Inland Waters Directorate, Tech. Bull., 65, 54 pp.

Barry, R.G., R.S. Bradley, J.D. Jacobs, 1975, SYNOPTIC CLIMATOLOGICAL STUDIES OF THE BAFFIN ISLAND AREA, in CLIMATE OF THE ARCTIC, ed. G. Weller and S.A. Bowling, pp 82 - 90

Baumhefner,D.,1968, APPLICATION OF A DIAGNOSTIC NUMERICAL MODEL TO THE TROPICAL ATMOSPHERE, Mon. Weath. Rev., 96:218-228

Bjerknes, J., J. Holmboe, 1944, ON THE THEORY OF CYCLONES, J. Meteorol.,1:1-22

Bosart, L.F., 1973, DETAILED ANALYSIS OF PRECIPITATION PATTERNS ASSOCIATED WITH MESOSCALE FEATURES ACCOMPANYING UNITED STATES EAST COAST CYCLOGENESIS, Mon. Weath. Rev., 101:1-12

Browning, K.A., M.E. Hardman, T.W. Harrold, C.W. Pardoe, 1973, THE STRUCTURE OF RAINBANDS WITHIN A MID-LATITUDE DEPRESSION, Q. J. Roy. Meteorol, Soc., 99:215-231

Bryson, R.A., 1966, AIR MASSES, STREAMLINES AND THE BOREAL FOREST, Geogr. Bull., 8:228-269

Bryson, R.A., P.M. Kuhn, 1961, STRESS-DIFFERENTIAL INDUCED DIVERGENCE WITH APPLICATION TO LITTORAL PRECIPITATION, Erdkunde, 15:287-294

Caffey, J.E., 1965, INTERSTATION CORRELATIONS IN ANNUAL PRECIPITATION AND IN ANNUAL EFFECTIVE PRECIPITATION, Hydrology Paper 6, Colorado State University

Carnahan, B., H.A. Luther, J.O. Wilkes, 1969, APPLIED NUMERICAL METHODS, John Wiley and Sons, New York, 604 pp.

Chang, J.H., 1972, ATMOSPHERIC CIRCULATION SYSTEMS AND CLIMATES, The Oriental Publishing Company, Honolulu, 328 pp.

Charney, J.G., A. Eliassen, 1949, A NUMERICAL METHOD FOR PREDICTING THE PERTURBATIONS IN THE MIDDLE-LATITUDE WESTERLIES, Tellus, 1:38-54

Clark, D., 1975, UNDERSTANDING CANONICAL CORRELATION ANALYSIS, Concepts and Techniques in Modern Geography No. 3, Geo. Abstracts Ltd. Norwich, 36 pp.

Cooley, W.W., P.R. Lohnes, 1971,MULTIVARIATE DATA ANALYSIS, J. Wiley and Sons, New York, 364 pp.

Court, A.D., 1960, RELIABILITY OF HOURLY PRECIPITATION DATA, J. Geophys, Res., 65:4017-4024

Craddock, J.M., 1956, THE REPRESENTATION OF THE ANNUAL TEMPERATURE VARIATION OVER CENTRAL AND NORTHERN EUROPE BY A TWO TERM HARMONIC FORM, Q. J. Roy. Meteorol. Soc., 82:275-288

Craddock, J.M., 1965, A METEOROLOGICAL APPLICATION OF PRINCIPAL COMPONENT ANALYSIS, The Statistician, London, 15:143-156

Craddock. J.M., C.R. Flood, 1969, EIGENVECTORS FOR REPRESENTING THE 500 MB GEOPOTENTIAL SURFACE OVER THE NORTHERN HEMISPHERE, Q. J. Roy. Meteorol. Soc., 95:574-593

Craddock, J.M., S. Flintoff, 1970, EIGENVECTOR REPRESENTATIONS OF NORTHERN HEMISPHERIC FIELDS, Q. J. Roy. Meteorol. Soc., 96:124-129

Csanady, G.T., 1972, GEOSTROPHIC DRAG, HEAT AND MASS TRANSFER COEFFICIENTS FOR THE DIABATIC EKMAN LAYER, J. Atmos. Sci., 29:488-496

Danard, M.B., 1964, ON THE INFLUENCE OF RELEASED LATENT HEAT ON CYCLONE DEVELOPMENT, J. Appl. Meteorol., 3:27-37

Danard, M.B., 1969. A SIMPLE METHOD OF INCLUDING LONGWAVE RADIATION IN A TROPOSPHERIC NUMERICAL PREDICTION MODEL, Mon. Weath. Rev., 97:77

Danard, M.B., G.V. Rao, 1972, NUMERICAL STUDY OF THE EFFECTS OF THE GREAT LAKES ON A WINTER CYCLONE, Mon. Weath. Rev., 100:374-382

Davis, J.C., 1973, STATISTICS AND DATA ANALYSIS IN GEOLOGY, John Wiley and Sons Inc., New York, 550 pp.

Derome, J., A. Winn-Nielsen, 1971, THE RESPONSE OF A MID-LATITUDE MODEL ATMOSPHERE TO FORCING BY TOPOGRAPHY AND STATIONARY HEAT SINKS, Mon. Weath. Rev., 99:564-576

Dickson, R.R., H.H. Lamb, S.A. Malmberg, J.M. Colebrook, 1975, CLIMATIC REVERSAL IN NORTHERN NORTH ATLANTIC, Nature, 256:479-481

Dzerdzeevskii, B.L., 1945, TSIRKULIATSIONNYE SKHEMY V TROPOSFERE TSENTRAL' NOI ARKTIKI, in ISDATEL' STRO AKAD. NAUK. (Eng. trans. in Sci. Rep. No. 3 Contract AF 19 (122)-228 UCLA) cited in Reed and Kunkel, 1960

Dzerdzeevskii, B.L., 1968, CIRCULATION OF THE ATMOSPHERE, CIRCULATION MECHANISMS OF THE ATMOSPHERE IN THE NORTHERN HEMISPHERE IN THE TWENTIETH CENTURY, Results of Meteorological Investigations, IGY Committee, Moscow, 240 pp.

Fankhauser, J.C., 1969, CONVECTIVE PROCESSES RESOLVED BY A MESOSCALE RAWINSONDE NETWORK, J. Appl. Meteorol., 8:778-798

Flohn, H., 1954, WITTERUNG UND KLIMA IN MITTELEUROPA. FORSCH. DT. LANDESKUNDE 78, Stuttgart, 214 pp.

Fogarasi, S., 1972, WEATHER SYSTEMS AND PRECIPITATION CHARACTERISTICS OVER THE ARCTIC ARCHIPELAGO IN THE SUMMER OF 1968, Inland Waters Directorate, Environment Canada, Scientific Series No. 16, 116 pp.

Fritts, H.C., T.J. Blasing, B.P. Hayden, J.E. Kutzbach, 1971, MULTIVARIATE TECHNIQUES FOR SPECIFYING TREE GROWTH AND CLIMATE RELATIONSHIPS AND FOR RECONSTRUCTING ANOMALIES IN PALEOCLIMATE, J. Appl. Meteorol., 10:845-864

Glahn, H.R., 1968, CANONICAL CORRELATION AND ITS RELATIONSHIP TO DISCRIMINANT ANALYSIS AND MULTIPLE REGRESSION, J. Atmos. Sci., 25:23-31

Gould, P.R., 1967, ON THE GEOGRAPHICAL INTERPRETATION OF EIGENVALUES, Trans. Inst. Brit. Geogr., 42:53-86

Green, M.J., 1970, EFFECTS OF EXPOSURE ON THE CATCH OF RAIN GAUGES, J. Hydrol., New Zealand, 9(2):55

Grimmer, M., 1963, THE SPACE FILTERING OF MONTHLY SURFACE TEMPERATURE ANOMALY DATA IN TERMS OF PATTERN, USING EMPIRICAL ORTHOGONAL FUNCTIONS, Q. J. Roy. Meteorol. Soc., 89:395-408

Haltiner, G.J., F.L. Martin, 1957, DYNAMICAL AND PHYSICAL METEOROLOGY, McGraw-Hill, New York, 470 pp.

Hare, F.K., 1957, THE DYNAMIC ASPECTS OF CLIMATOLOGY, Geogr. Annal., 39:87-104

Hare, F.K., 1968, THE ARCTIC, Q. J. Roy. Meteorol. Soc., 94:439-459

Hare, F.K., S. Orvig, 1958, THE ARCTIC CIRCULATION, A PRELIMINARY REVIEW, Arctic Meteorology Research Group, Publication in Meteorology, no. 12, McGill University, Montreal, 211 pp.

Harley, W.S., 1964, USE OF THE ADVECTION SCALE IN THE DETERMINATION OF VERTICAL VELOCITY, Canada Dept. of Transport, Meteorol. Branch, 5 pp.

Harley, W.S., 1965, DETERMINATION OF SPOT VALUES OF VERTICAL VELOCITY AND PRECIPITATION RATE FROM VALUES OF ABSOLUTE VORTICITY ADVECTION, 1000-500 MB THICKNESS ADVECTION AND PRECIPITABLE WATER, Canada Dept. of Transport, Meteorol. Branch, 4 pp.

Harold, T.W., 1973, MECHANISMS INFLUENCING THE DISTRIBUTION OF PRECIPITATION WITHIN BAROCLINIC DISTURBANCES, Q. J. Roy. Meteorol. Soc., 99:232-251

Hendrick, R.L., G.H. Comer, 1970, SPACE VARIATIONS OF PRECIPITATION AND IMPLICATIONS FOR RAINGAUGE NETWORK DESIGN, J. Hydrol., 10:151-163

Hershfield, 1965, ON THE SPACING OF RAINGAUGES, Int. Ass. Sci. Hydrology Symposium, Quebec, Pub. 67:72-81

Hicks, B.B., 1972, SOME EVALUATIONS OF DRAG AND BULK TRANSFER COEFFICIENTS OVER WATER BODIES OF DIFFERENT SIZES, Bound. Layer Meteorol., 3:201-213

Holton, J.R., 1972, AN INTRODUCTION TO DYNAMIC METEOROLOGY, Academic Press, New York, 319 pp.

Hutchinson, P., 1968, AN ANALYSIS OF THE EFFECT OF TOPOGRAPHY IN THE TAIER CATCHMENT AREA, O'TAGO, Earth Sci. J. 2:51-68

Hutchinson, P., 1970, A CONTRIBUTION TO THE PROBLEM OF SPACING RAINGAUGES IN RUGGED TERRAIN, J. Hydrol., 12:1-14

Jacobs, J.D., 1974, SOLAR AND ATMOSPHERIC RADIATION DATA FOR BROUGHTON ISLAND, EASTERN CANADIAN ARCTIC, CANADA, 1971-73, INSTAAR Occasional Paper No. 11

Kaiser, H.F., 1960, THE APPLICATION OF ELECTRONIC COMPUTERS TO FACTOR ANALYSIS, Educational and Psychological Measurement, 20:141-151

Keegan, T.J., 1958, THE WINTERTIME CIRCULATION IN THE ARCTIC TROPOSPHERE, in CONTRIBUTION TO THE STUDY OF THE ARCTIC CIRCULATION, Sci. Rept. 7:22-47, Arctic Meteorology Research Group, McGill University

Kirchhofer, W., 1974, CLASSIFICATION OF EUROPEAN 500 MB PATTERNS, Swiss Meteorol. Inst., Zurich, Arbeits No. 43, 16 pp.

Klein, W.H., D.L. Jorgensen, A.F. Korte, 1968, RELATION BETWEEN UPPER AIRFLOWS AND WINTER PRECIPITATION IN THE WESTERN PLATEAU STATES, Mon. Weath. Rev., 96:162-168

Knighting, E.K., 1969, THREE-DIMENSIONAL WEATHER PREDICTION, in, LECTURES ON NUMERICAL SHORT RANGE WEATHER PREDICTION, WMO Regional Training Seminar, Moscow, 1965, 706 pp.

Krishnamurti, T.N., 1968, A DIAGNOSTIC BALANCE MODEL FOR STUDIES OF WEATHER SYSTEMS OF LOW AND HIGH LATITUDES, ROSSBY NUMBER LESS THAN 1, Mon., Weath. Rev., 96, 197-207

Krishnamurti, T.N., 1968, A STUDY OF A DEVELOPING WAVE CYCLONE, Mon. Weath. Rev., 96:208-217

Krishnamurti, T.N., W.J. Moxim, 1971, ON PARAMETERIZATION OF CONVECTIVE AND NON CONVECTIVE LATENT HEAT RELEASE, J. App. Meteorol., 10:3-13

Kung, E.C., 1972, A SCHEME FOR KINEMATIC ESTIMATE OF LARGE SCALE VERTICAL MOTION WITH AN UPPER AIR NETWORK, Q. J. Roy. Meteorol. Soc., 98:402-411

Kuo, H.L., 1965, ON FORMATION AND INTENSIFICATION OF TROPICAL CYCLONES THROUGH LATENT HEAT RELEASE BY CUMULUS CONVECTION, J. Atmos. Sci., 22:40-63

LaMarche, V.C., H.C. Fritts, 1971, ANOMALY PATTERNS OF CLIMATE OVER THE WESTERN UNITED STATES, 1700-1930, DERIVED FROM PRINCIPAL COMPONENT ANALYSIS OF TREE RING DATA, Mon. Weath. Rev., 99:138-142

Lamb, H.H., 1964, THE ENGLISH CLIMATE, English Universities Press, London, 212 pp.

Lansing, L., 1965, AIR MASS MODIFICATION BY LAKE ONTARIO DURING THE APRIL NOVEMBER PERIOD, Proc. Eighth Conf. Great Lakes, Res., Great Lakes Res. Div., Univ. of Michigan, 257-261

Lateef, M.A., 1967, VERTICAL MOTION, DIVERGENCE, AND VORTICITY IN THE TROPOSPHERE OVER THE CARRIBEAN, AUGUST 3-5, 1963, Mon. Weath. Rev., 95:778-790

Lavoie, R.L., 1972, A MESOSCALE NUMERICAL MODEL OF LAKE EFFECT STORMS, J. Atmos. Sci., 29:1025-1040

Lorenz, E.N., 1956, EMPIRICAL ORTHOGONAL FUNCTIONS AND STATISTICAL WEATHER PREDICTION, M.I.T. Dept. of Meteorology, Sci. Rept. No. 1, Contract AF 19(604)-1566, 49 pp.

McPherson, G.A., F.D. Thompson, L.G. Tibbles, R.A. Treidl, 1969, THE MEANING AND APPLICATION OF ADVECTION FIELDS IN ANALYSIS AND FORECASTING, Canada Dept. of Transport, Meteorol. Branch, 20 pp.

Mansfield, D.A., 1974, POLAR LOWS: THE DEVELOPMENT OF BAROCLINIC DISTURBANCES IN COLD AIR OUTBREAKS, Q. J. Roy. Meteorol. Soc., 100:541-555

Namias, T.J., 1958, SYNOPTIC AND CLIMATOLOGICAL PROBLEMS ASSOCIATED WITH THE GENERAL CIRCULATION OF THE ARCTIC, Trans. Amer. Geophys. Union, 39:40-51

O'Brien, J.L., 1970, ALTERNATIVE SOLUTIONS TO THE CLASSICAL VERTICAL VELOCITY PROBLEM, J. Appl. Meteorol., 9:197-203

O'Connor, J.F., 1961, MEAN CIRCULATION PATTERNS BASED ON TWELVE YEARS OF RECENT NORTHERN HEMISPHERE DATA, Mon. Weath. Rev., 89:211-228

Palmen, E., C.W. Newton, 1969, ATMOSPHERIC CIRCULATION SYSTEMS, Academic Press, New York, 603 pp.

Pedersen, K., 1963, ON QUANTITATIVE PRECIPITATION FORECASTING WITH A QUASI-GEOSTROPHIC MODEL, Geofysiske Pub. 25(1), 25pp.

Penner, C.M., 1963, AN OPERATIONAL METHOD FOR THE DETERMINATION OF VERTICAL VELOCITIES, J. Appl. Meteorol. 2:235-241

Peterson, J.T., 1970, DISTRIBUTION OF SULFUR DIOXIDE OVER METROPOLITAN ST. LOUIS, AS DESCRIBED BY EMPIRICAL EIGENVECTORS, AND ITS RELATION TO METEOROLOGICAL PARAMETERS, Atmos. Environ., 4:501-518

Petterssen, S., 1950, SOME ASPECTS OF THE GENERAL CIRCULATION OF THE ATMOSPHERE, Centenerary Proceedings of the Royal Meteorological Society, London, pp. 120-155

Petterssen, S., 1955, A GENERAL SURVEY OF FACTORS INFLUENCING DEVELOPMENT AT SEA LEVEL, J. Meteorol., 12:36-42

Petterssen, S., P.A. Călabrese, 1959, ON SOME WEATHER INFLUENCES DUE TO WARMING OF THE AIR BY THE GREAT LAKES IN WINTER, J. Meteorol., 16:646-652

Petterssen, S., D.L. Bradbury, K. Pedersen, 1962, THE NORWEGIAN CYCLONE MODELS IN RELATION TO HEAT AND COLD SOURCES, Geogys. Pub. 24:243-280

Pielke, R.A., 1974, A COMPARISON OF THREE-DIMENSIONAL AND TWO-DIMENSIONAL NUMERICAL PREDICTIONS OF SEA BREEZE, J. Atmos. Sci., 31:1577-1585

Rao, G.V., 1966, ON THE INFLUENCES OF FIELDS OF MOTION, BAROCLINICITY AND LATENT HEAT SOURCE ON FRONTOGENESIS, J. App. Meteorol., 5:377-387

Reed, R.J., 1958, ARCTIC SYNOPTIC ANALYSIS, in CONTRIBUTIONS TO THE STUDY OF THE ARCTIC CIRCULATION, Arctic Meteorology Research Group, McGill University, pp. 48-59

Reed, R.J., B.A. Kunkel, 1960, THE ARCTIC CIRCULATION IN SUMMER, J. Meteorol., 17:489-506

Reed, R.J., W.G. Tank, 1956, MISCELLANEOUS STUDIES OF POLAR VORTICES, Sci. Rept. 1. Department of Meteorology and Climatology, University of Washington, Seattle, 21 pp.

Reitan, C.H., 1974, FREQUENCIES OF CYCLONES AND CYCLOGENESIS FOR NORTH AMERICA, 1951-1970, Mon. Weath. Rev., 102:861-868

Robinson, G.D., 1966, ANOTHER LOOK AT SOME PROBLEMS OF THE AIR-SEA INTERFACE, Q. J. Roy. Meteorol. Soc., 92:451-465

Roll, H.U., 1965, PHYSICS OF THE MARINE ATMOSPHERE, Academic Press, New York, 424 pp.

Sanderson, R.M., 1975, CHANGES IN AREA OF ARCTIC SEA ICE, 1966 to 1974, Meteorol. Mag., 104:313-326

Sasamori, T., 1968, A RADIATIVE COOLING CALCULATION FOR APPLICATION TO GENERAL CIRCULATION EXPERIMENTS, J. Appl. Meteorol., 7:721-729

Sasamori, T., 1975, A STATISTICAL MODEL FOR STATIONARY ATMOSPHERIC CLOUDINESS, LIQUID WATER CONTENT, AND RATE OF PRECIPITATION, Mon. Weath. Rev., 103:1037-1049

Scherhag, R., 1957, THE ROLE OF TROPOSPHERIC COLD AIR POLES AND OF STRATOSPHERIC HIGH PRESSURE CENTERS IN THE ARCTIC WEATHER, in POLAR ATMOSPHERE SYMPOSIUM, PART 1, METEOROLOGY SECTION, R.C. Sutcliffe, ed. London, Pergamon Press, pp. 101-117

Schmidt, F., 1975, ON THE ROLE OF TRUNCATION PROCESSES FOR NUMERICAL MODELING, J. Atmos. Sci., 32:1755-1778

Sellers, W.D., 1968, CLIMATOLOGY OF MONTHLY PRECIPITATION PATTERNS IN THE WESTERN UNITED STATES, 1931-1966, Mon. Weath. Rev., 96:585-595

Smith, P.J., 1971, AN ANALYSIS OF KINEMATIC VERTICAL MOTIONS, Mon. Weath. Rev., 99:715-724

Smith, P.J., 1973, THE KINETIC ENERGY BUDGET OVER NORTH AMERICA DURING A PERIOD OF MAJOR CYCLONE DEVELOPMENT, Tellus, 25:411-423

Smith, W., R.J. Younkin, 1972, AN OPERATIONALLY USEFUL RELATIONSHIP BETWEEN THE POLAR JET STREAM AND HEAVY PRECIPITATION, Mon. Weath. Rev., 100:434-440

Stringer, E.T., 1972, FOUNDATIONS OF CLIMATOLOGY, VOL. 1, W. H. Freemand and Co., San Francisco, 586 pp.

Stuart, D.W., 1964, A DIAGNOSTIC CASE STUDY OF THE SYNOPTIC SCALE VERTICAL MOTION AND ITS CONTRIBUTION TO MID-TROPOSPHERIC DEVELOPMENT, J. Appl. Meteorol., 3:669-684

Stuart, D.W., 1970, SPECIFICATIONS OF MESO-SCALE WEATHER FROM LARGE-SCALE DYNAMICAL CALCULATIONS, Final report No. 70-5, Florida State University, pp. 1-79

Stuart, D.W., 1974, A COMPARISON OF QUASI-GEOSTROPHIC VERTICAL MOTIONS USING VARIOUS ANALYSES, Mon. Weath. Rev., 102:363-374

Sutcliffe, R.C., 1951, MEAN UPPER CONTOUR PATTERNS OF THE NORTHERN HEMISPHERE - THE THERMAL SYNOPTIC VIEW POINT, Q. J. Roy. Meteorol. Soc., 77:435-440

Sutcliffe, R.C., A.G. Forsdyke, 1950, THE THEORY AND USE OF UPPER AIR THICKNESS PATTERNS IN FORECASTING, Q. J. Roy. Meteorol. Soc., 76:194-217

Thompson, P.D., 1969, NUMERICAL WEATHER ANALYSIS AND PREDICTION, in LECTURES ON NUMERICAL SHORT RANGE WEATHER PREDICTION, Regional Training Seminar on Numerical Weather Prediction, Moscow, 1965, pp. 11-91

Tracton, M.S., 1975, THE ROLE OF CUMULUS CONVECTION IN EXTRATROPICAL CYCLOGENESIS, in SUBSYNOPTIC EXTRATROPICAL WEATHER SYSTEMS, NCAR Notes, co-ordinator M. Shapiro, pp. 301-317

Vowinckel, E., S. Orvig, 1970, THE CLIMATE OF THE NORTH POLAR BASIN, in S. Orvig, ed. CLIMATES OF THE POLAR REGIONS, World Survey of Climatology, Vol. 14, Elsevier, New York, pp. 129-252

Walters, C.D., 1975, DRAG COEFFICIENT AND ROUGHNESS LENGTH DETERMINATIONS ON AN ALASKAN COAST DURING SUMMER, Bound. Layer Meteorol., 8:235-238

Wilson, W.T., 1954, DISCUSSION OF PRECIPITATION AT BARROW ALASKA, Trans. Amer. Geophys. Union, 35:206-207

Wilson, C.W., 1958, SYNOPTIC REGIMES IN THE LOWER ARCTIC TROPOSPHERE DURING 1955, Sci. Rept. 6, Arctic Meteorol. Res. Group, McGill University, 100 pp.

Wagner, A.J., 1973, WEATHER AND CIRCULATION OF JULY, 1973, Mon. Weath. Rev., 101:777-782

Winston, J.S., 1955, PHYSICAL ASPECTS OF RAPID CYCLOGENESIS IN THE GULF OF ALASKA, Tellus, 7:481-500

APPENDIX ONE

LIST OF SYMBOLS

C_H	bulk transfer coefficient	
C_p	specific heat of air	$cm^2\ s^{-2}\ deg^{-1}$
D	divergence of water vapour	$g\ m^{-2}\ s^{-1}$
F	friction coefficient	
F_E	surface enthalpy flux	$kj\ m^{-2}\ s^{-1}$
f	coriolis parameter	s^{-1}
g	acceleration of gravity	$m\ s^{-2}$
H	diabatic heating	$kj\ kg^{-1}\ s^{-1}$
L	latent heat of condensation	$m^2\ s^{-2}$
p	pressure	cb centibars
q	specific humidity	$kg\ kg^{-1}$
R	gas constant	$m^2\ s^{-2}\ deg^{-1}$
T	temperature	deg
t	time	s
V_g	geostrophic wind velocity	$m\ s^{-1}$
w	vertical velocity	$m\ s^{-1}$
z	height	m
Φ	geopotential height	$m^2\ s^{-2}$
σ	static stability	$m^2\ cb^{-2}\ s^{-2}$
ω	omega	$cb\ s^{-1}$
ρ	density of air	$kg\ m^{-3}$
θ	potential temperature	deg
ζ	vorticity	s^{-1}

APPENDIX TWO

ANNOTATED LISTING OF THE COMPUTER ROUTINE FOR THE CALCULATION OF OMEGA AND ASSOCIATED FIELDS DISCUSSED IN THIS STUDY

This programme is designed for the CDC 7600 of the National Center for Atmospheric Research. It takes 79 seconds to run this routine for 234 days with a ten by ten by six grid.

```
*LIMIT,T=2
*LIMIT,PR=160
*LIMIT,PT=4
*LIMIT,PU=2000
*ASSIGN,B5657=1,R
*TLIB,1,RT,BN
*ASSIGN,B5573=8
*TLIB,8,DC,NS,DT
*FORTRAN,FL
      PROGRAM OMEGA
      COMMON VAR5,VAR6,VAR7,VAR8,VAR9,VAR10
      COMMON T,G,RH,     V,W,SST,H,TT,TDE,DENS,PP,UU,VV
      COMMON DG,XDG,YDG,DUM,XDSG,YDSG,DUMM,DSG,DUMI,XDUMM,YDUMM,VAR1,VAR2,VA
     .2,VAR3,VAR4,DPRI
      COMMON/IO/DAG,AG(70,5)
      DIMENSION GOON(8),TOON(8)
      DIMENSION ANG(10,10)
      DIMENSION VAR5(10,10,8),VAR6(10,10,8),VAR7(10,10,8),VAR8(10,10,8),
     .VAR9(10,10,8),VAR10(10,10,8)
      DIMENSION AVH(6),AVT(6),AVRH(6),STH(6)
      DIMENSION FRICT(10,10)
      DIMENSION VAR4(10,10,8)
      DIMENSION SIGMA(8)
      DIMENSION DEN(8)
      DIMENSION PREH(10,10,8),TOPO2(10,10,8),VCONST(4)
      DIMENSION TOPO1(10,10)
      DIMENSION GA(66,40)
      DIMENSION H(10,10,8),TT(10,10,8),TDE(10,10,8),DENS(8),
     .PP(10,10,8),UU(10,10,8),VV(10,10,8)
      DIMENSION T(10,10,8),G(10,10,8),RH(10,10,8),P(10,10,8),U(10,10,8),
     .V(10,10,8),W(10,10,8),SST(10,10)
      DIMENSION DG(10,10,8),XDG(10,10,8),YDG(10,10,8),DUM(10,10
     .,8),XDSG(10,10,8),YDSG(10,10,8),DUMM(10,10,8),DSG(10,10,8),DUMI(10
     .,10,8),XDUMM(10,10,8),YDUMM(10,10,8),VAR1(10,10,8),VAR2(10,10,8),
     .VAR3(10,10,8),DPRI(10,10,8)
      DIMENSION SSH(10,10,8),ASH(10,10,8),SATT(10,10,8)
C  FORMAT STATEMENTS
    1 FORMAT(8A10)
    3 FORMAT(15F5.0)
    8 FORMAT(1X,F4.1,5X,15F8.0)
7     FORMAT(1X,5HIDENT,I5)
15    FORMAT(1H1,2F10.0,4E10.2)
1000  FORMAT(10F1.0)
1011  FORMAT(X,I5)
1199  FORMAT(1X,10F4.0)
1099  FORMAT(10F5.0)
10    FORMAT(1H0,6E10.2)
11    FORMAT(F10.0)
12    FORMAT(6F10.6)
5004  FORMAT(1X,15HWARNING, NO SST)
5005  FORMAT(1X,31HWARNING, CONDITIONALLY UNSTABLE)
5006  FORMAT(1X,I3,2X,I3)
5007  FORMAT(1X,4HDATE,F15.0)
5008  FORMAT(1X,E10.2)
1089  FORMAT(1X,10E10.2)
9     FORMAT(1X,10HI EXCEEDED,I5)
C  ZERO MATRICES
      CALL ZERO(T)
      CALL ZERO(G)
      CALL ZERO(RH)
```

```
      CALL ZERO(V)
      CALL ZERO(H)
      CALL ZERO(TT)
      CALL ZERO(TDE)
      CALL ZERO(PP)
      CALL ZERO(UU)
      CALL ZERO(VV)
      CALL ZERO(DG)
      CALL ZERO(XDG)
      CALL ZERO(YDG)
      CALL ZERO(DUM)
      CALL ZERO(XDSG)
      CALL ZERO(YDSG)
      CALL ZERO(DUMM)
      CALL ZERO(DSG)
      CALL ZERO(DUMI)
      CALL ZERO(XDUMM)
      CALL ZERO(YDUMM)
      CALL ZERO(VAR1)
      CALL ZERO(VAR2)
      CALL ZERO(VAR3)
      CALL ZERO(VAR4)
      CALL ZERO(VAR5)
      CALL ZERO(VAR6)
      CALL ZERO(VAR7)
      CALL ZERO(VAR8)
      CALL ZERO(VAR9)
      CALL ZERO(VAR10)
      CALL ZERO(DPRI)
      CALL ZERO(SST)
C  DEFINE CONSTANTS
C  FOR CONVERSION OF RELATIVE HUMIDITY TO SPECIFIC HUMIDITY
      ALPHA=0.6
      DELT=5600.
      CON=ALOG10(6.1078)
      A=7.567
      B=2066.926
      C=33.45
C  FIRST DAY TO BE READ
      DAY=1.
C  DAY COUNTER
      ITIME=1
      IDENTI=0
C  CORIOLIS PARAMETER
      FO=1.3705E-4
C  HORIZONTAL GRID DIMENSIONS METERS
      XY=3.9E5
      XX=3.9E5
C  SPECIFIC HEAT
      CP=1.004
C  CONVERSION FROM OMEGA TO VERTICAL VELOCITY
      DEN(1)=-8.32E3
      DEN(2)=-9.40E3
      DEN(3)=-11.22E3
      DEN(4)=-14.64E3
      DEN(5)=-21.88E3
      DEN(6)=-61.72E3
C  DENSITY
      DENS(1)=1.275
      DENS(2)=1.1
```

```
      DENS(3)=0.893
      DENS(4)=0.658
      DENS(5)=0.385
      LENS(6)=0.128
      AMASS=DENS(1)*1000.
C  CONSTANTS FOR PRECIPITATION CALCULATIONS
      VCONST(1)=1.14E-6
      VCONST(2)=1.02E-6
      VCONST(3)=0.76E-6
      VCONST(4)=0.51E-6
C  ALL COMPUTATIONS START AT TOP NORTH-WEST CORNER OF GRID
C  K IS LEVEL NUMBER IN THE VERTICAL, I IS ROW DESIGNATION, J IS COLUMN
C  MATRIX FOR THESE COMPUTATIONS IS 10(I) X 10(J) X 6(K)
C  READ CARD DATA FOR LAND-SEA POSITIONS AND TOPOGRAPHIC HEIGHTS (METERS)
      READ(5,1000)((FRICT(I,J),I=1,10),J=1,10)
      READ(5,1099)((TOPO1(I,J),I=1,10),J=1,10)
C  READ ANGULAR DEVIATIONS TO CORRECT WIND FIELD FOR EQUAL AREA CO-ORDINATES
      DO 750 I=2,9
750   READ(5,1099)(ANG(I,J),J=1,10)
      DO 786 I=1,10
      DO 786 J=1,10
      TOPO1(I,J)=(1.E5-(DENS(1)*9.8*TOPO1(I,J)))*1.E-3
786   CONTINUE
C  READ INPUT FIELDS AND TRANSFORM INTO 3-D MATRICES
C  INPUT FIELDS IN NMC FORMAT ON TAPE 1
C  351 WORDS PER RECORD, 1 ID NUMBER AND 5 FIELDS OF 70 WORDS, ORDER-ID NUMBER
C  YEAR, MONTH, DAY, 66 DATA WORDS (6 X 6), PRESSURE LEVEL DATA, ID CODE
96    IF(ITIME.EQ.1)GOTO99
      IDENT1=6-IDENT
      N=IDENT
      DO 97 I=1,IDENT1
      MO=AG(3,N)
      DA=AG(4,N)
      DO 98 J=1,66
98    GA(J,I)=AG(J+4,N)
      N=N+1
97    CONTINUE
99    CONTINUE
      II=IDENT1+1
      III=II+4
94    CONTINUE
      NWDS=351
      CALL RDTAPE(1,1,0,DAG,NWDS)
      CALL IOWAIT(1,NSTATE,KWDS)
      IF(NSTATE.NE.0)GOTO7896
      N=1
      DO 91 I=II,III
      Y=AG(2,N)
      MO=AG(3,N)
      DA=AG(4,N)
      IF(MO.EQ.8.AND.DA.EQ.30)STOP
      IF(DA.NE.DAY)GOTO93
      DYN=DA
      DO 92 J=1,66
92    GA(J,I)=AG(J+4,N)
      DAY=DA
91    N=N+1
      II=II+5
      III=III+5
      IF(I.GT.35)WRITE(6,9)I
```

```
      GOTO94
95    CONTINUE
      DAY=DA
      DA=DYM
      Y=Y*1.E6
      MO=MO*1.E3
      DATE=Y+MO+DA
      IDENT=N
      WRITE(6,7)IDENT
      ITIME=ITIME+1
      IF(ITIME.EQ.2)GOTO96
      IF(DATE.EQ.19750802020)GOTO96
      ICOUNTR=I-1
      IRH=0
      IT=0
      IG=0
      IW=0
      IU=0
      IV=0
C  SORT RAW DATA INTO 3-D MATRICES AND CHECK FOR DUPLICATE RECORDS
      DO 80 I=1,ICOUNTR
      J=66
      IF(GA(65,I).NE.1000.)GOTO81
      IF(GA(J,I).NE.1)GOTO81
      IF(GA(J,I+1).EQ.1.OR.GA(J,I-1).EQ.1)GOTO85
      GOTO81
85    CONTINUE
      DMAX=GA(1,I)
      DO 82 J=1,64
82    DMAX=AMAX1(DMAX,GA(J,I))
      IF(DMAX.LE.40)GA(66,I)=30
81    CONTINUE
      J=66
      IF(GA(65,I).EQ.GA(65,I-1).AND.GA(66,I).EQ.GA(66,I-1))GOTO80
      IF(GA(J,I).EQ. 1)CALL STACK(GA,I,J,IG,G)
      IF(GA(J,I).EQ.10)CALL STACK(GA,I,J,IT,T)
      IF(GA(J,I).EQ.30)CALL STACK(GA,I,J,IU,U)
      IF(GA(J,I).EQ.31)CALL STACK(GA,I,J,IV,V)
      IF(GA(J,I).EQ.44)CALL STACK(GA,I,J,IRH,RH)
      IF(GA(J,I).EQ.47)CALL STACKI(GA,I,J,SST)
80    CONTINUE
90    CONTINUE
C  SPECIFY PRESSURE LEVELS IN CENTIBARS
      DO 89 II=1,10
      DO 89 JJ=1,10
      P(II,JJ,1)=100.
      P(II,JJ,2)=85.
      P(II,JJ,3)=70.
      P(II,JJ,4)=50.
      P(II,JJ,5)=30.
      P(II,JJ,6)=10.
      P(II,JJ,7)=0.0
89    CONTINUE
C  CORRECT WIND FIELD FOR GRID SHIFT
C  COMPUTE FOR ALL POINTS
      DO 775 I=2,9
      DO 775 J=2,9
C  CONVERT ANG DEV TO RADIANS
      ANGR=ANG(I,J)/57.3
      DO 775 K=1,6
```

```
C  COMPUTE GEOSTROPHIC VECTOR
      R=(V(I,J,K)**2)+(U(I,J,K)**2)
      R=ABS(R)
      R=SQRT(R)
      DUMM(I,J,K)=R
C  COMPUTE ANGLE IN RADIANS
      TANG=V(I,J,K)/U(I,J,K)
      TANG=ABS(TANG)
      TANG=ATAN(TANG)
C  CORRECT SURFACE WINDS FOR EKMAN SPIRAL
       IF(K.EQ.1.AND.FRICT(I,J).LT.0.5.AND.U(I,J,1).GE.0.
     .AND.V(I,J,1).GE.0)TANG=TANG+0.35
       IF(K.EQ.1.AND.FRICT(I,J).LT.0.5.AND.U(I,J,1).GE.0.
     .AND.V(I,J,1).LT.0)TANG=TANG-0.35
       IF(K.EQ.1.AND.FRICT(I,J).LT.0.5.AND.U(I,J,1).LT.0.
     .AND.V(I,J,1).LT.0)TANG=TANG+0.35
       IF(K.EQ.1.AND.FRICT(I,J).LT.0.5.AND.U(I,J,1).LT.0.
     .AND.V(I,J,1).GE.0)TANG=TANG-0.35
       IF(K.EQ.1.AND.FRICT(I,J).GE.1.0.AND.U(I,J,1).GE.0.
     .AND.V(I,J,1).GE.0)TANG=TANG+0.07
       IF(K.EQ.1.AND.FRICT(I,J).GE.1.0.AND.U(I,J,1).GE.0.
     .AND.V(I,J,1).LT.0)TANG=TANG-0.07
       IF(K.EQ.1.AND.FRICT(I,J).GE.1.0.AND.U(I,J,1).LT.0.
     .AND.V(I,J,1).LT.0)TANG=TANG+0.07
       IF(K.EQ.1.AND.FRICT(I,J).GE.1.0.AND.U(I,J,1).LT.0.
     .AND.V(I,J,1).GE.0)TANG=TANG-0.07
C  CHECK QUADRANT
      IF(V(I,J,K).GT.0)GOTO752
C LOWER HALF
      IF(U(I,J,K).GT.0)GOTO751
C QUADRANT III
      IF(J.LT.5)TANG=TANG-ANGR
      IF(J.GT.5)TANG=TANG+ANGR
      IT=0
      IF(J.LT.5.AND.TANG.LE.0)IT=1
      IF(J.GT.5.AND.TANG.GE.1.5706)IT=2
      IF(IT.EQ.1)TANG=-TANG
      IF(IT.EQ.2)TANG=(22./7.)-TANG
      IF(IT.EQ.1)GOTO762
      IF(IT.EQ.2)GOTO761
760   CONTINUE
      U(I,J,K)=-R*COS(TANG)
      V(I,J,K)=-R*SIN(TANG)
      GOTO775
C QUADRANT IV
751   CONTINUE
      IF(J.LT.5)TANG=TANG+ANGR
      IF(J.GT.5)TANG=TANG-ANGR
      IT=0
      IF(J.LT.5.AND.TANG.GE.1.5706)IT=1
      IF(J.GT.5.AND.TANG.LE.0)IT=2
      IF(IT.EQ.1)TANG=(22./7.)-TANG
      IF(IT.EQ.2)TANG=-TANG
      IF(IT.EQ.1)GOTO760
      IF(IT.EQ.2)GOTO763
761   CONTINUE
      U(I,J,K)=R*COS(TANG)
      V(I,J,K)=-R*SIN(TANG)
      GOTO775
752   CONTINUE
```

```
C UPPER HALF
      IF(U(I,J,K).GT.0)GOTO755
C QUADRANT II
      IF(J.LT.5)TANG=TANG+ANGR
      IF(J.GT.5)TANG=TANG-ANGR
      IT=0
      IF(J.LT.5.AND.TANG.GE.1.5706)IT=1
      IF(J.GT.5.AND.TANG.LE.0)IT=2
      IF(IT.EQ.1)TANG=(22./7.)-TANG
      IF(IT.EQ.2)TANG=-TANG
      IF(IT.EQ.1)GOTO763
      IF(IT.EQ.2)GOTO760
762   CONTINUE
      U(I,J,K)=-R*COS(TANG)
      V(I,J,K)=R*SIN(TANG)
      GOTO775
C   QUADRANT I
755   CONTINUE
      IF(J.LT.5)TANG=TANG-ANGR
      IF(J.GT.5)TANG=TANG+ANGR
      IT=0
      IF(J.LT.5.AND.TANG.LE.0)IT=1
      IF(J.GT.5.AND.TANG.GE.1.5706)IT=2
      IF(IT.EQ.1)TANG=-TANG
      IF(IT.EQ.2)TANG=(22./7.)-TANG
      IF(IT.EQ.1)GOTO761
      IF(IT.EQ.2)GOTO762
763   CONTINUE
      U(I,J,K)=R*COS(TANG)
      V(I,J,K)=R*SIN(TANG)
775   CONTINUE
      DO 351 K=1,6
      DO 351 J=1,10
      DO 351 I=1,10
      V(I,J,K)=-V(I,J,K)
351   G(I,J,K)=G(I,J,K)*9.8
      R=0.287
C  CHECK FOR MISSING SURFACE TEMPERATURES
      TOTAL=0.0
      DO 5000 I=1,10
      DO 5000 J=1,10
      TOTALT=SST(I,J)
5000  TOTAL=TOTAL+TOTALT
      TOTAL=ABS(TOTAL)
      IF(TOTAL.GT.0.1)GOTO5002
      DO 5001 I=1,10
      DO 5001 J=1,10
      SST(I,J)=PP(I,J,1)
5001  CONTINUE
      WRITE(6,5004)
5002  CONTINUE
      DO 5013 I=1,10
      DO 5013 J=1,10
      PP(I,J,1)=SST(I,J)
5013   CONTINUE
      N=6
      L=10
      M=10
C  CONVERT RELATIVE HUMIDITY TO SPECIFIC HUMIDITY
      DO 649 I=1,L
```

```
      DO 649 J=1,M
      RH(I,J,1)=RH(I,J,2)
      RH(I,J,2)=(RH(I,J,3)+RH(I,J,2))/2.
      RH(I,J,3)=RH(I,J,3)
      RH(I,J,6)=(RH(I,J,6)+RH(I,J,3))/2.
      IF(RH(I,J,6).LE.RH(I,J,3))RH(I,J,5)=RH(I,J,6)-(RH(I,J,3)-RH(I,J,6)
     .)
      IF(RH(I,J,6).GT.RH(I,J,3))RH(I,J,5)=RH(I,J,6)-((RH(I,J,2)-RH(I,J,6))/2.
     .)/2.)
      DO 649 K=1,6
      RH(I,J,K)=RH(I,J,K)/100.
649   CONTINUE
      DO 650 I=2,9
      DO 650 J=2,9
      DO 650 K=1,6
      SE=CON*(A*(T(I,J,K)+273.16)-B)/(T(I,J,K)+273.16-C)
      SE=10.**SE
      ASE=RH(I,J,K)*SE
      ASH(I,J,K)=(0.621*ASE)/(P(I,J,K)*10.-(0.379*ASE))*1.E3
      SSH(I,J,K)=(0.621* SE)/(P(I,J,K)*10.-(0.379* SE))*1.E3
      SATT(I,J,K)=((ALOG10(ASE)-CON)*C-B)/((ALOG10(ASE)-CON-A))
      SATT(I,J,K)=SATT(I,J,K)-273.16
650   CONTINUE
505   CONTINUE
      WRITE(6,5007)DATE
      WRITE(8,5007)DATE
      CALL DMAXX(U,1)
C  COMPUTE STATIC STABILITY FOR EACH LEVEL, AVERAGED FOR ALL GRID POINTS
      DO 9887 K=1,6
      AVTO=0.
      AVGO=0.
      DO 987 I=1,10
      DO 987 J=1,10
      AVTO=AVTO+T(I,J,K)
987   AVGO=AVGO+G(I,J,K)
      GOON(K)=AVGO/100.
      AVTO=AVTO/100.
9887  TOON(K)=(AVTO+275.16)*((1000./(P(I,J,K)*10.))**(2./7.))
      DO 9889 K=2,6
      PDIF=P(I,J,K)-P(I,J,K-1)
      SIGMA(K)=(((GOON(K)-GOON(K-1))/PDIF)/TOON(K))*((TOON(K)-TOON(K-1))
     ./PDIF)
9889  CONTINUE
C  COMPUTE ENTHALPY FLUX, KJ KG-1 S-1 AND CB M S-1
      CALL ZERO(DUM)
      CALL ZERO(DUM1)
      CALL ZERO(VARS)
      DO 610 I=1,L
      DO 610 J=1,M
      IF(DATE.LT.19730906015)GOTO600
      SST(I,J)=0.
      IF(FRICT(I,J).LT.0.5)SST(I,J)=5.
      IF(FRICT(I,J).LT.0.5.AND.J.GE.7.AND.I.LE.6)SST(I,J)=-5.
600   CONTINUE
      VG=ABS((U(I,J,1)**2)+(V(I,J,1)**2))
      VG=SQRT(VG)
      IF(FRICT(I,J).LT.0.5)CH=2.E-3                                    CONT
      IF(FRICT(I,J).GE.1.0)CH=1.E-3                                    OCEAN
      IF( T(I,J,1)-SST(I,J))601,602,603
601   CH=CH*3.                                                         USTABLE
```

```
      GOTO604
602   CH=CH*2.                                                    NEUT
      GOTO604
605   CONTINUE
604   CONTINUE
      DUM(I,J,2)=(T(I,J,1)-SST(I,J))*V6*CH
      DUM(I,J,2)=((DUM(I,J,2)/60.)*61.868)/ANASS
610   CONTINUE
      DO 611 I=1,L
      DO 611 J=1,M
611   VARS(I,J,2)=(DUM(I,J,2)*0.7)*(18.8/15.)
      DO 613 I=3,8
613   WRITE(8,10)(DUM(I,J,2),J=3,8)
      CALL MDELSQ(DUM,DUM),VARS,L,M,N,XX,XY)
      CALL ZERO(DUM)
      CALL ZERO(DUM)
      DO 614 J=1,M
      DO 614 I=1,L
      VARS(I,J,2)=-VARS(I,J,2)
614   VARS(I,J,2)=VARS(I,J,2)*(R/(CP*P(I,J,2)))
      CALL ZERO(W)
C  COMPUTE OMEGA FORCING FUNCTIONS FOR ENTIRE MATRIX
      CALL VERDER(G,P,DG,L,M,N)
      DO 615 I=1,L
      DO 615 J=1,M
      DO 615 K=1,N
615   DG(I,J,K)=-DG(I,J,K)
      CALL MDEL(DG,DUM,XDG,YDG,L,M,N,XX,XY)
      CALL MDELSQ(G,DUM,DSG,L,M,N,XX,XY)
C  COMPUTE LAYER 1 OMEGA INCLUDING EKMAN LAYER PUMPING - WINN-NIELSEN
      DO 900 I=1,L
      DO 900 J=1,M
      IF(FRICT(I,J).LT.0.5)DENN=0.E-6
      IF(FRICT(I,J).GE.1.)DENN=4.E-6
      W(I,J,1)=-1.*((DSG(I,J,1)/FO)/(2.*FO))*P(I,J,1)*DENN+W(I,J,1)
      UU(I,J,1)=W(I,J,1)*DEN(1)
900   CONTINUE
C  COMPUTE LAYER 1 OMEGA INCLUDING TOPO FORCING
      L1=L-1
      M1=M-1
      DO 710 I=2,L1
      DO 710 J=2,M1
      W(I,J,1)=W(I,J,1)+(((TOPO1(I+1,J)-TOPO1(I,J))/(XX))*V(I,J,1))
     .+(((TOPO1(I,J+1)-TOPO1(I,J))/(XY))*U(I,J,1))
      VV(I,J,1)=(W(I,J,1)*DEN(1))-UU(I,J,1)
710   CONTINUE
      DO 720 J=1,M
      W(1,J,1)=0.0
720   W(10,J,1)=0.0
      DO 730 I=1,10
      W(I,1,1)=0.0
730   W(I,10,1)=0.0
      DO 700I=1,L
      DO 700J=1,M
      DO 700K=1,N
      DUMM(I,J,K)=(1./FO)*DSG(I,J,K)
700   CONTINUE
      CALL MDEL(DUMM,DUM,XDUMM,YDUMM,L,M,N,XX,XY)
      CALL DOT(XDUMM,YDUMM,DUM),U,V,L,M,N)
      DO 17 I=1,L
```

```
      DO 17 J=1,M
      DO 17 K=1,N
17    DUM1(I,J,K)=DUM1(I,J,K)+V(I,J,K)*7.8288E-12
      CALL VERSER(DUM1,P,DUM,L,M,N)
      DO 75 I=1,L
      DO 75 J=1,M
      DO 75 K=1,N
      VAR1(I,J,K)=FO*DUM(I,J,K)
75    CONTINUE
      CALL ZERO(DUM1)
      CALL DOT(XD6,YD6,DUM1,U,V,L,M,N)
      CALL MDELSQ(DUM1,DUM,VAR2,L,M,N,XX,XY)
      DO 800I=1,L
      DO 800J=1,M
      DO 800K=1,N
      VAR3(I,J,K)=VAR1(I,J,K)+VAR2(I,J,K)+VAR5(I,J,K)
800   CONTINUE
C  COMPUTE INITIAL OMEGA, MINUS LATENT HEAT  FUNCTION
      CALL RELAX(VAR3,N,L,M,N,XX,XY,P,SIGMA)
      CALL ZERO(DUM)
      CALL ZERO(DUM1)
      CALL ZERO(DUMM)
C  COMPUTE VAPOUR FLUX DIVERGENCE IN MM CM-2 HR-1
      DO 850 I=2,9
      DO 850 J=2,9
      DO 811 K=1,4
      TOPO2(I,J,K)=(((V(I+1,J,K)*100.)*(ASH(I+1,J,K+1)*VCONST(KE)-
     .(V(I,J,K)*100.)*(ASH(I,J,K+1)*VCONST(K)))/(XX*100.))+(((U(I,J+1,KE
     .*100.)*(ASH(I,J+1,K+1)*VCONST(K))-(U(I,J,K)*100.)*(ASH(I,J,K+1)*
     .VCONST(K)))/(XY*100.))
      PREW(I,J,K)=ASH(I,J,K+1)*VCONST(K)
811   CONTINUE
      TOPO2(I,J,1)=TOPO2(I,J,1)*3.6E4*1.5E5
      TOPO2(I,J,2)=TOPO2(I,J,2)*3.6E4*1.5E5
      TOPO2(I,J,3)=TOPO2(I,J,3)*3.6E4*2.5E5
      TOPO2(I,J,4)=TOPO2(I,J,4)*3.6E4*3.5E5
      PREW(I,J,1)=PREW(I,J,1)*1.5E5+PREW(I,J,2)*1.5E5+PREW(I,J,3)*2.5E5+
     .PREW(I,J,4)*3.5E5
      PREW(I,J,1)=PREW(I,J,1)*10.
C TEST FOR CONDITIONAL INSTABILITY
      TE=((T(I,J,2)+273.)*(1.176**0.285))*EXP(2488.*((SSH(I,J,2)*1.E-3)/
     .(T(I,J,2)+273.)))
      TEE=(T(I,J,1)+273.)*EXP(2488.*((SSH(I,J,1)*1.E-3)/(T(I,J,1)+273.))
     .)
      TEST1=(TEE-TE)/(G(I,J,1)*100.-G(I,J,2)*100.)
C  COMPUTE LATENT HEAT FUNCTION
      IF(TEST1.LT.0)GOTO804
      DO 809 K=1,3
      IF(W(I,J,K).GE.0)GOTO 802
      IF(W(I,J,K).LT.0)GOTO803
C  ABSOLUTELY STABLE - NO PRECIPITATION
802   DUMM(I,J,K)=0.0
      GOTO809
C  ABSOLUTELY STABLE - PRECIP POSSIBLE
803   IF(RH(I,J,K).LT.0.7)GOTO802                                          C
      DUMM(I,J,K)=-598.*W(I,J,K)*((SSH(I,J,K+1)*1.E-3-SSH(I,J,K)*1.E-3)/
     .(P(I,J,K+1)-P(I,J,K)))
      DUMM(I,J,K)=DUMM(I,J,K)*4.1855
      IF(DUMM(I,J,K).LT.0)DUMM(I,J,K)=0.0
809   CONTINUE
```

```
      GOTO810
C  CONDITIONALLY UNSTABLE
804   CONTINUE
C  TEST FOR CONVERGENCE
      IF(TOPO2(I,J,1).LT.0)GOTO805
      IF(TOPO2(I,J,1).GE.0)GOTO806
805   CONTINUE
      DUMM(I,J,1)=(CP*ALPHA*(SATT(I,J,1)-T(I,J,1)))/DELT
      DUMM(I,J,1)=-DUMM(I,J,1)
      IF(DUMM(I,J,1).LT.0)DUMM(I,J,1)=0.0
      WRITE(6,5005)
      WRITE(6,5006)I,J
      DUM(I,J,1)=1.0
      GOTO806
806   CONTINUE
      DO 810 K=2,5
      IF(W(I,J,K).GE.0)GOTO808
      IF(W(I,J,K).LT.0)GOTO807
807   CONTINUE
      IF(RH(I,J,K).LT.0.7)GOTO808                                          C
      DUMM(I,J,K)=-590.*W(I,J,K)*((SSH(I,J,K+1)*1.E-3-SSH(I,J,K)*1.E-3)/
     .(P(I,J,K+1)-P(I,J,K)))
      DUMM(I,J,K)=DUMM(I,J,K)*6.1655
      IF(DUMM(I,J,K).LT.0)DUMM(I,J,K)=0.0
      GOTO810
808   DUMM(I,J,K)=0.0
810   CONTINUE
850   CONTINUE
      DO 12345 I=2,9
      DO 12345 J=2,9
12345 TOPO2(I,J,1)=TOPO2(I,J,1)+TOPO2(I,J,2)+TOPO2(I,J,3)+TOPO2(I,J,4)
      DO 815 K=1,5
      DO 815 I=2,9
      DO 815 J=2,9
815   DUMM(I,J,K)=(DUMM(I,J,K)/2469.4)*2.5E6
C  RECOMPUTE W INCLUDING LATENT HEAT RELEASE
      CALL MDELSQ(DUMM,DUM,DUM1,L,M,N,XX,XY)
      DO 311 I=1,L
      DO 311 J=1,M
      DO 311 K=2,4
      VAR6(I,J,K)=(R/(CP*P(I,J,K)))*DUM1(I,J,K-1)
      VAR6(I,J,K)=-VAR6(I,J,K)
311   VAR5(I,J,K)=VAR5(I,J,K)+VAR6(I,J,K)
      CALL RELAX(VAR5,N,L,M,N,XX,XY,P,SIGMA)
C  CALCULATE PRECIPITATION
      DO 860 I=2,9
      DO 860 J=2,9
      DO 859 K=1,5
859   DUMM(I,J,K)=DUMM(I,J,K)/2.5E6
      DUMM(I,J,1)=DUMM(I,J,1)*DENS(1)*1.E2*1.5
      DUMM(I,J,2)=DUMM(I,J,2)*DENS(2)*1.E2*1.5
      DUMM(I,J,3)=DUMM(I,J,3)*DENS(3)*1.E2*2.5
      DUMM(I,J,4)=DUMM(I,J,1)+DUMM(I,J,2)+DUMM(I,J,3)
      DUMM(I,J,4)=DUMM(I,J,4)*3600.*10.
860   CONTINUE
      DO 861 I=3,8
861   WRITE(8,10)(DUMM(I,J,4),J=3,8)
C  COMPUTE PER CENT CONTRIBUTION AT 850 MB
C  COMPUTE WITHOUT BOUNDARY
      CALL ZERO(VAR6)
```

```
      CALL ZERO(VAR7)
      CALL ZERO(VAR8)
      CALL ZERO(VAR9)
      CALL ZERO(VAR10)
      CALL RELAX(VAR1,VAR6 ,L,M,N,XX,XY,P,SIGMA)
      CALL RELAX(VAR2,VAR7 ,L,M,N,XX,XY,P,SIGMA)
      CALL RELAX(VAR4,VAR8 ,L,M,N,XX,XY,P,SIGMA)
      CALL RELAX(VAR5,VAR10,L,M,N,XX,XY,P,SIGMA)
C  COMPUTE ADVECTIVE HEATING AT 850 MB
      CALL ZERO(DUM1)
      CALL ZERO(DUM)
      CALL ZERO(DUMM)
      DO 350 I=2,9
      DO 350 J=2,9
      DUM1(I,J,2)=((T(I,J,2)-T(I,J+1,2))/(XY))*U(I,J,2)
      DUM(I,J,2)=((T(I,J,2)-T(I+1,J,2))/(XX))*V(I,J,2)
      DUMM(I,J,2)=W(I,J,2)*(((T(I,J,3)-T(I,J,2))/(P(I,J,3)-P(I,J,2)))-((
     .R/P(I,J,2))/CP))
C  VERTICAL
      DUMM(I,J,1)=DUMM(I,J,2)*CP
C  HORIZONTAL
      DUMM(I,J,2)=(DUM1(I,J,2)+DUM(I,J,2))*CP
350   CONTINUE
C  ALL DATA WRITTEN ONTO TAPE 8
      DO 354 I=3,8
354   WRITE(8,10)(DUMM(I,J,2),J=3,8)
      DO 355 I=3,8
355   WRITE(8,10)(DUMM(I,J,1),J=3,8)
C  CONVERT OMEGA INTO VERTICAL VELOCITY
      DO 502 I=1,L
      DO 502 J=1,M
      DO 502 K=1,N
502   W(I,J,K)=W(I,J,K)*DEN(K)
      CALL WRITR(W)
      DO 952 I=2,9
      DO 952 J=2,9
      VAR1(I,J,2)=VAR6(I,J,2)*DEN(2)
      VAR2(I,J,2)=VAR7(I,J,2)*DEN(2)
      VAR4(I,J,2)=VAR8(I,J,2)*DEN(2)
      IF(VAR4(I,J,2).LE.0)VAR4(I,J,2)=0.0
      VAR5(I,J,2)=VAR10(I,J,2)*DEN(2)
952   CONTINUE
      DO 953 I=3,8
953   WRITE(8,10)(VAR1(I,J,2),J=3,8)
      DO 954 I=3,8
954   WRITE(8,10)(VAR2(I,J,2),J=3,8 )
      DO 955 I=3,8
955   WRITE(8,10)(VAR4(I,J,2),J=3,8 )
      DO 956 I=3,8
956   WRITE(8,10)(VAR5(I,J,2),J=3,8 )
      CALL DMAXX(W ,2)
C  REDUCE MATRIX INTO CENTRE CORE - REMOVE EDGE EFFECTS
C  CENTER CORE IS 6 X 6
      L=L-4
      M=M-4
      DO 400 K=1,N
      DO 401 I=1,L
      DO 401 J=1,M
      T(I,J,K)=T(I+2,J+2,K)
      RH(I,J,K)=RH(I+2,J+2,K)
```

```
601   W(I,J,K)=W(I+2,J+2,K)
600   CONTINUE
      DO 605 I=1,L
      DO 605 J=1,M
      VV(I,J,1)=VV(I+2,J+2,1)
      UU(I,J,1)=UU(I+2,J+2,1)
605   TOPO2(I,J,1)=TOPO2(I+2,J+2,1)
      K=2
      DO 500 I=1,6
      WRITE(8,10)(W(I,J,K),J=1,6)
500   CONTINUE
      DO 503 I=1,6
503   WRITE(8,10)(TOPO2(I,J,1),J=1,6)
      DO 504 I=1,6
504   WRITE(8,10)(UU(I,J,1),J=1,6)
      DO 505 I=1,6
505   WRITE(8,10)(VV(I,J,1),J=1,6)
      DO 669 I=3,8
669   WRITE(8,10)(PREM(I,J,1),J=3,8)
      DO 8971 I=3,8
8971  WRITE(8,10)(G(I,J,2),J=3,8)
C  AVERAGE AND PUNCH FOR SASAMORI PRECIPITATION CALCULATIONS
      DO 670 K=1,5
      AVW(K)=0.0
      AVT(K)=0.0
      AVRH(K)=0.0
      STW(K)=0.0
      DO 671 I=1,6
      DO 671 J=1,6
      AVW(K)=AVW(K)+W(I,J,K)
      AVT(K)=AVT(K)+T(I,J,K)
      AVRH(K)=AVRH(K)+RH(I,J,K)
671   CONTINUE
      AVW(K)=AVW(K)/36.
      AVT(K)=AVT(K)/36.
      AVRH(K)=AVRH(K)/36.
      DO 672 J=1,6
      DO 672 I=1,6
672   STW(K)=STW(K)+((W(I,J,K)-AVW(K))**2)
      STW(K)=STW(K)/36.
      WRITE(8,15)DATE,P(1,1,K),AVW(K),STW(K),AVT(K),AVRH(K)
670   CONTINUE
      GOTO96
  250 CALL EXIT
7896  CONTINUE
      PRINT NSTATE,KNDS
      STOP
      END
      SUBROUTINE VERDER(X,Y,Z,L,M,N)
C  CALCULATE VERTICAL DERIVATIVES
      DIMENSION X(10,10,8),Y(10,10,8),Z(10,10,8)
      NN=N-1
      DO 4 I=1,L
      DO 4 J=1,M
      DO 4 K=2,NN
      Z(I,J,K)=(X(I,J,K+1)-X(I,J,K))/(Y(I,J,K+1)-Y(I,J,K))
4     CONTINUE
      RETURN
      END
      SUBROUTINE MDEL(X,Z,XY,XXX,L,M,N,XX,YY)
```

```
C  CALCULATE HORIZONTAL DERIVATIVES
      DIMENSION X(10,10,8),Z(10,10,8),XXX(10,10,8),XY(10,10,8)
      LL=L-1
      MM=M-1
      DO 4 K=1,N
      DO 4 I=2,LL
      DO 4 J=2,MM
      XXX(I,J,K)=(X(I+1,J,K)-X(I,J,K))/XX
      XY(I,J,K)=(X(I,J+1,K)-X(I,J,K))/YY
      Z(I,J,K)=XXX(I,J,K)+XY(I,J,K)
4     CONTINUE
      RETURN
      END
      SUBROUTINE HDELSQ(X,Y,Z,L,M,N,XX,YY)
C  CALCULATE SQUARE OF HORIZONTAL DERIVATIVES
      DIMENSION X(10,10,8),Y(10,10,8),Z(10,10,8)
      LL=L-1
      MM=M-1
      DO 4 K=1,N
      DO 4 I=2,LL
      DO 4 J=2,MM
      Z(I,J,K)=((X(I-1,J,K)-(2.*X(I,J,K))+X(I+1,J,K))/(XX**2))+
     .((X(I,J-1,K)-(2.*X(I,J,K))+X(I,J+1,K))/(YY**2))
4     CONTINUE
      RETURN
      END
      SUBROUTINE DOT(X,Y,Z,XXX,XY,L,M,N)
C  CALCULATE DOT PRODUCT
      DIMENSION X(10,10,8),Y(10,10,8),Z(10,10,8),XXX(10,10,8),XY(10,10,8
     .)
      LL=L-1
      MM=M-1
      DO 4 K=1,N
      DO 4 I=2,LL
      DO 4 J=2,MM
      Z(I,J,K)=(X(I,J,K)*XXX(I,J,K))+(Y(I,J,K)*XY(I,J,K))
4     CONTINUE
      RETURN
      END
      SUBROUTINE  RELAX(X,U,NX,NY,NZ,XX,Y,P,SIGMA)
C SOLVE POISSON EA IN 3D WITH UNEQUAL MESH SIZE, DELSQ(U)=F(XYZ)
C  TOP AND SIDE BOUNDARIES ARE OMEGA = 0
C  BOTTOM BOUNDARIES ARE OMEGA OF TOPOGRAPHY AND FRICTION
      DIMENSION SIGMA(8)
      DIMENSION P(10,10,8)
      DIMENSION U(10,10,8),X(10,10,8)
C  USE GAUSS-SEIDEL ITERATION TECHNIQUE CF. CARNAHAN ET AL, PP 269
      XS=XX**2
      YS=Y**2
      CP=1.3705E-4
      CP=CP**2
      ITMAX=50
      EPSMAX=1.E-8
      EPSMAX=1.E-7
      EPSMAX=1.E-6
C  CALCULATE APPROXIMATIONS TO U(IJK)
      ITER=0
5     EPS=0
      ITER=ITER+1
      NZZ=NZ
```

```
      MXX=MX-1
      MYY=MY-1
      DO 4 K=2,MZZ
      DO 4 I=2,MXX
      DO 4 J=2,MYY
      X(I,J,6)=0.0
      C=SIGMA(K)
      ZS=(P(I,J,K+1)-P(I,J,K))**2
      DENN=2.*(C/XS+C/YS+CP/ZS)
      HOLDT=U(I,J,K)
      U(I,J,K)=(C*((U(I+1,J,K)+U(I-1,J,K))/XS+(U(I,J+1,K)+U(I,J-1,K))/YS
     .)+CP*((U(I,J,K+1)+U(I,J,K-1))/ZS)-X(I,J,K))/DENN
4     EPS=EPS+ABS(U(I,J,K)-HOLDT)
C
C  STOP ITERATIONS IF COMPUTED VALUES SHOW LITTLE FURTHUR CHANGE
      IF(EPS.LE.EPSMAX)GOTO6
      IF(ITER-ITMAX)5,5,8
C  PRINT VALUES OF THE ITERATION COUNTER AND FINAL FIELD
6     CONTINUE
      RETURN
C  COMMENT IN CASE ITER EXCEEDS ITMAX
8     WRITE(6,205)
      CALL WRITR(U)
      STOP
C
202   FORMAT(X,10E10.2)
205   FORMAT(X,44H NO CONVERGENCE. CURRENT VALUES OF FIELD ARE)
206   FORMAT(X,/)
      END
      SUBROUTINE STACK(GA,I,J,IP,GGG)
      DIMENSION GAG(10,10,8)
      DIMENSION GGG(10,10,8),GA(66,40)
      IP=IP+1
20    FORMAT(1X,16HWARNING, IP GT 8)
      IF(IP.GT.8)WRITE(6,20)
      IF(IP.GT.8)RETURN
      DO 3 II=1,10
      DO 2 JJ=1,10
2     GGG(JJ,II,IP)=0.0
3     CONTINUE
      N=1
      DO 4 JJ=2,9
      DO 5 II=2,9
      GGG(JJ,II,IP)=GA(N,I)
      N=N+1
5     CONTINUE
4     CONTINUE
      DO 8 JJ=1,10
      JJJ=11-JJ
      DO 8 II=1,10
8     GAG(JJJ,II,IP)=GGG(JJ,II,IP)
      DO 9 JJ=1,10
      DO 9 II=1,10
9     GGG(JJ,II,IP)=GAG(JJ,II,IP)
      DO 10 JJ=1,10
      GGG(JJ,1,IP)=GGG(JJ,2,IP)
10    GGG(JJ,10,IP)=GGG(JJ,9,IP)
      DO 11 II=1,10
      GGG(1,II,IP)=GGG(2,II,IP)
11    GGG(10,II,IP)=GGG(9,II,IP)
```

```
      RETURN
      END
      SUBROUTINE STACK1(GA,I,J,GGG)
      DIMENSION GAG(10,10)
      DIMENSION GGG(10,10)
      DIMENSION GA(66,60)
      DO 3 II=1,10
      DO 2 JJ=1,10
    2 GGG(JJ,II)=0.0
    3 CONTINUE
      N=1
      DO 4 JJ=2,9
      DO 5 II=2,9
      GGG(JJ,II)=GA(N,I)
      N=N+1
    5 CONTINUE
    4 CONTINUE
      DO 8 JJ=1,10
      JJJ=11-JJ
      DO 8 II=1,10
    8 GAG(JJJ,II)=GGG(JJ,II)
      DO 9 JJ=1,10
      DO 9 II=1,10
    9 GGG(JJ,II)=GAG(JJ,II)
      DO 10 JJ=1,10
      GGG(JJ,1)=GGG(JJ,2)
   10 GGG(JJ,10)=GGG(JJ,9)
      DO 11 II=1,10
      GGG(1,II)=GGG(2,II)
   11 GGG(10,II)=GGG(9,II)
      RETURN
      END
      SUBROUTINE ZERO(A)
      DIMENSION A(10,10,8)
      DO 2 I=1,10
      DO 2 J=1,10
      DO 2 K=1,8
    2 A(I,J,K)=0.0
      RETURN
      END
      SUBROUTINE WRITR(A)
      DIMENSION A(10,10,8)
 2000 FORMAT(X,10E10.2)
 2001 FORMAT(X,/)
      DO 5 K=1,8
      DO 6 I=1,10
    6 WRITE(6,2000)(A(I,J,K),J=1,10)
      WRITE(6,2001)
    5 CONTINUE
      WRITE(6,2001)
      RETURN
      END
      SUBROUTINE DMAXX(A,K)
      MAX AND MIN OF ONE LEVEL OF A MATRIX
      DIMENSION A(10,10,8)
      DMAX=DMIN=A(3,3,K)
      DO 10 I=3,8
      DO 10 J=3,8
      DMAX=AMAX1(DMAX,A(I,J,K))
   10 DMIN=AMIN1(DMIN,A(I,J,K))
```

```
      WRITE(6,20)DMAX,DMIN
20    FORMAT(1X,4HDMAX,E20.2,8X,4HDMIN,E20.2)
      RETURN
      END
*RUN

11
1111  1
11 1 111
  1 11111
  11
   1 11
    111
1    111 1
1111111111
             3    3    3    3    3    3    3    3
             150  50   3    3    3    3    3    3
                       150  50        25   150  150
             150       100                 25   50
 1200 1200        200                          50
  600 1200             3    3    3    3    3    3
 2500 2500  600         50             420  750  600
 2500 2500 2500  900                    50  550   50
 2500 2500 2500 2500  900                    50
 2500 2500 2500 2500 2500  900
         48   36   18        120   32   48   56
         38   27   14         15   24   36   47
         31   22   10         12   19   29   40
         27   19    9         10   18   25   36
         24   17    8          9   16   21   32
         21   13    7          8   14   19   36
         20   12    6          7   12   18   27
         19   12    5          6   10   16   23
*END
```

APPENDIX THREE

85 CB MODEL GENERATED DATA FOR THE PERIOD FROM JULY 13 - 25, 1973

w total vertical velocity
w_V vertical velocity due to vorticity advection
w_{TH} vertical velocity due to thickness advection
w_H vertical velocity due to surface thermal effects
w_{LP} vertical velocity due to latent heat release

Line 1: 36 grid point averages
Line 2: 36 grid point standard deviations

Date	w cm s^{-1}	w_V cm s^{-1}	w_{TH} cm s^{-1}	w_H cm s^{-1}	w_{LP} cm s^{-1}	Temp ^oC	85 cb Height decameters
13	7.1E-2	1.3E-1	5.1E-2	-1.4E-3	3.2E-2	4.2	141
	9.5E-1	4.4E-1	3.1E-1	1.3E-1	1.0E-1	3.0	4
14	2.3E-1	1.1E-1	1.2E-2	3.2E-2	1.6E-2	3.7	139
	5.9E-1	2.6E-1	3.2E-1	2.0E-1	4.5E-2	3.1	8
15	1.7E-2	8.1E-2	1.6E-2	3.4E-2	1.5E-2	3.5	138
	6.7E-1	2.4E-1	2.7E-1	2.2E-1	3.9E-2	3.4	7
16	1.2E-1	4.3E-2	5.2E-3	7.5E-3	1.5E-2	4.9	136
	6.5E-1	1.3E-1	1.5E-1	2.9E-1	4.0E-2	2.5	5
17	5.3E-2	5.5E-2	-3.7E-3	2.6E-2	1.3E-2	3.4	137
	4.3E-1	1.8E-1	2.0E-1	2.4E-1	2.6E-2	2.6	4
18	1.0E-1	6.1E-2	-2.3E-2	2.3E-2	1.8E-2	3.2	136
	4.8E-1	1.1E-1	1.4E-1	1.5E-1	3.9E-2	2.9	3
19	1.6E-2	7.6E-3	-1.3E-3	-1.4E-3	1.7E-2	3.4	139
	4.3E-1	2.8E-1	1.7E-1	1.1E-1	3.9E-2	3.0	3
20	4.8E-2	-2.0E-2	-4.7E-2	1.4E-2	2.2E-2	2.7	137
	4.7E-1	3.8E-1	2.2E-1	1.5E-1	4.6E-2	3.6	4
21	3.9E-2	-1.0E-1	4.4E-2	-3.2E-4	1.3E-2	5.1	137
	3.6E-1	2.3E-1	1.6E-1	1.6E-1	3.2E-2	4.9	5
22	-1.7E-2	-1.8E-1	3.5E-2	-2.3E-2	1.6E-2	6.7	138
	5.5E-1	2.8E-1	3.4E-1	2.0E-1	2.8E-2	6.1	8
23	2.7E-1	-2.7E-2	2.5E-2	2.9E-2	2.2E-2	5.6	141
	8.2E-1	3.4E-1	2.7E-1	4.8E-1	7.4E-2	7.6	7
24	7.2E-2	7.5E-2	1.8E-3	1.0E-2	8.8E-3	3.9	142
	5.0E-1	5.8E-1	4.0E-1	2.1E-1	2.7E-2	7.5	6
25	3.7E-1	1.3E-1	-2.8E-2	1.4E-2	3.7E-2	2.1	139
	1.1E 0	5.8E-1	3.6E-1	3.9E-1	7.9E-2	5.1	7

APPENDIX THREE (continued)

V. A. Vertical (adiabatic) advection
H. A. Horizontal advection
H. E. Heating by surface thermal effects
L. H. Latent heat release
Vo. A. 50 cb vorticity advection
V. F. Vapour flux divergence, 100 to 30 cb.
Prec. Precipitation

Date	V. A.	H. A.	H. F.	L. H.	Vo. A.	V. F.	Prec.
	kilojoules kilogram^{-1} second^{-1}				s^{-2}	mm cm^{-2} hr^{-1}	mm hr^{-1}
13	-1.6E-6	1.3E-5	-2.3E-5	9.2E-6	9.2E-11	2.0E-2	5.8E-2
	5.4E-5	3.8E-5	2.0E-5	2.6E-5	7.1E-10	5.0E-1	1.4E-1
14	-6.2E-6	3.7E-6	-1.9E-5	1.7E-6	1.5E-10	1.7E-1	2.9E-2
	2.3E-5	7.3E-5	2.0E-5	4.5E-6	6.7E-10	4.7E-1	6.9E-2
15	2.5E-6	7.5E-6	-2.2E-5	3.5E-6	1.3E-10	1.1E-1	3.1E-2
	3.4E-5	4.9E-5	2.3E-5	7.3E-6	7.7E-10	5.5E-1	5.6E-2
16	-6.1E-6	-3.0E-6	-2.6E-5	4.8E-6	6.3E-11	1.5E-1	2.3E-2
	3.9E-5	2.9E-5	3.3E-5	1.0E-5	3.7E-10	3.4E-1	5.1E-2
17	-2.3E-6	-4.0E-6	-2.0E-5	5.5E-6	1.2E-10	-9.3E-3	2.8E-2
	2.4E-5	2.8E-5	2.6E-5	8.8E-6	5.5E-10	3.2E-1	3.3E-2
18	-5.4E-6	-1.1E-6	-1.8E-5	6.3E-6	6.0E-11	1.9E-2	3.6E-2
	3.1E-5	1.9E-5	2.3E-5	1.1E-5	4.7E-10	1.7E-1	5.0E-2
19	-1.0E-6	3.1E-6	-1.3E-5	4.5E-6	1.7E-11	7.5E-2	3.4E-2
	2.8E-5	4.2E-5	1.4E-5	8.7E-6	6.8E-10	2.9E-1	5.6E-2
20	-3.9E-6	1.4E-6	-1.3E-5	5.0E-6	7.3E-11	4.4E-2	3.3E-2
	2.7E-5	4.6E-5	1.7E-5	8.9E-6	1.1E- 9	2.4E-1	4.7E-2
21	-2.3E-6	4.1E-5	-2.0E-5	4.3E-6	-6.2E-11	-5.5E-2	1.9E-2
	2.3E-5	5.0E-5	2.1E-5	7.8E-6	4.3E-10	2.3E-1	3.5E-2
22	3.2E-7	2.5E-5	-2.9E-5	6.6E-6	-9.5E-11	-1.1E-1	2.0E-2
	3.6E-5	7.6E-5	2.9E-5	1.2E-5	4.8E-10	2.5E-1	2.9E-2
23	-1.7E-5	-3.2E-6	-1.8E-5	5.2E-6	-2.8E-11	-1.3E-2	3.5E-2
	4.9E-5	5.3E-5	4.9E-5	1.3E-5	9.0E-10	2.9E-1	8.6E-2
24	-7.8E-6	-1.9E-5	-1.4E-4	2.4E-6	2.5E-10	-1.2E-1	1.4E-2
	2.7E-5	7.5E-5	2.3E-5	8.5E-6	9.6E-10	2.9E-1	2.8E-2
25	-2.5E-5	-3.6E-5	-1.1E-5	1.2E-5	2.5E-10	1.4E-1	7.4E-2
	6.3E-5	6.3E-5	3.7E-5	2.3E-5	1.3E- 9	4.0E-1	1.1E-1